SPECTROSCOPIC STUDIES OF RARE EARTH IONS DOPED GLASSES FOR PHOTONIC APPLICATIONS

Thesis

Submitted to the Delhi Technological University
for the Award of the Degree of

DOCTOR OF PHILOSOPHY

in

APPLIED PHYSICS

Submitted By:

YASHA TAYAL

(2K16/Ph.D/AP/11)

Under the Supervision of

Prof. A.S. RAO

DEPARTMENT OF APPLIED PHYSICS,
DELHI TECHNOLOGICAL UNIVERSITY
DELHI-110042, INDIA

September- 2022.

Delhi Technological University

(Govt. of National Capital Territory of Delhi)
Bawana Road, Delhi-110042

CERTIFICATE

This is to certify that the thesis titled "***Spectroscopic Studies of Rare Earth Ions Doped Glasses for Photonic Applications***" is being submitted by ***Mrs. YASHA TAYAL*** with registration number ***2K16/PHDAP/11*** to the Delhi Technological University for the award of the degree of Doctor of Philosophy in Applied Physics. The work embodied in this thesis is a record of bonafide research work carried out by me in the Microelectronics Research Lab, Applied Physics Department, Delhi Technological University (Formerly Delhi College of Engineering), New Delhi under the guidance of ***Prof. A.S. Rao***. It is further certified that this work is original and has not been submitted in part or fully to any other University or Institute for the award of any degree or diploma.

Yasha Tayal
Candidate
Roll No. 2K16/PHDAP/11

This is to certify that the above statement made by the candidate is correct to the best of our knowledge.

Prof. A.S. Rao
Supervisor (Professor)
Department of Applied Physics
Delhi Technological University
Delhi, India

Prof. A.S. Rao
Head
Department of Applied Physics
Delhi Technological University
Delhi, India

DECLARATION

This to certify that thesis Entitled **"Spectroscopic Studies of Rare Earth Ions Doped Glasses for Photonic Applications",** submitted to Delhi Technological University, Delhi for the award of the degree of Doctor of Philosophy' is based on the original research work carried out by me under the guidance of Prof. A.S. Rao, Department of Applied Physics, Delhi Technological University, Delhi. It further certified that the work embodied in this thesis has neither been partially nor fully submitted to any other University or institutions for award of any degree or diploma.

Yasha Tayal
2K16/PHD/AP/11
Research Scholar
Delhi Technological University

Dedicated

To

My Parents

ACKNOWLEDGEMENTS

Accomplishment of my Ph.D brings an end to the voyage in the form of this thesis. I feel truly grateful to acknowledge all those who have assisted me directly or indirectly for the finalization of my research work. In the rolling up of my doctorate work there are numerous people who are worthy to be recognized. In the first place, I desire to be grateful to almighty GOD, enduring me with strength and motivating throughout this journey towards the research.

I am devoid of appropriate words to express my deep sense of gratitude and esteem for my supervisor, Professor A. S. Rao, Head, Department of Applied Physics, Delhi Technological University, Delhi. He has been consistently supportive and stimulating ideas has helped me with all the supervision that I required. His motivating guidance and encouragement allowed me sufficient freedom in seeking my research interests. There are no words for thanking his valuable amount of time, significant suggestions and the resources provided for successful compliance of this research work. This entire tenure of my Ph. D under his supervision will be adored by me forever.

I am also thankful to Dr. M. Jayasimhadri and Dr. Amrish Panwar and other faculty menbers, Department of Applied Physics, Delhi Technological University, New Delhi for granting their lab facilities to furnish the research work. I am thankful to the DRC chariman, DRC members and SRC members and other teaching and non-teaching staff of the department of Applied Physics.

I am also thanful to Dr. Sk. Mahamuda, Dr. K. Swapna, Dr. M. Venkateswarlu, Dr. Rekha Rani, Dr. Rupesh A. Talwar from K.L. University, A.P. for providing the characterization facilities for my research work and necessary guidance.

Aboveboard I would like to express my gratitude towards Dr. Sumandeep Kaur for her precious time, support, motivation and guidance throughout the tenure my research work. I present my thanks to my seniors Dr. Amit K. Vishwakarma, Dr. Kaushal Jha, Dr. Nisha Deopa, Dr. Aman Prasad, Dr. Arti Yadav, Dr. Kanika Gupta, for their precious suggestions and assistance.

I desire to thank all my friends, colleagues. I thank my fellow researchers Dr. Harpreet Kaur, Dr. Sankar Subramanium, Mr. Mukesh K. Sahu, Mr. Rajat Bajaj, Ms. Pooja Rohilla, Ms. Ravita, Ms. Kartika Maheshwari, Mr. Mohit Tyagi, Mr. Mohit Mann, Mr. Sandeep Sharma, Ms. Shristy, Ms. Anu, Ms. Sheetal, Ms. Shweta, Mr. Videsh, Ms. Deepali, Mr. Vikas, Mr. Indrajeet, Ms. Vartika for the help whenever needed in completing my research work.

I also desire to thank the Head of the department of AS&H ABSES Engineering College and all my colleagues in AS&H department for all the guidance and motivation for pursuing my research work.

Concluding, all above is permissible by the continuing faith, support and love by my family and friends. I thank my parents Mr. Yogendra Kumar Tayal and Mrs. Girija Tayal whose encouragement and determined life facilitated me to reach where I am right now. I desire to reveal my admiration towards my husband Mr. Ankit Gupta, Software Manager, Accenture, my son Aujasya Gupta and my daughter Yanvika who have been supporting me throughout this research work. I am also grateful to my brothers Mr. Vivek Tayal and Mr. Avinash Tayal and my sister Mrs. Ritu Garg for their encouragement and consistent support to attain my goal of completing this research work.

With the compliance of this Ph.D thesis work through examining and questioning of various issues and resulting in the finished work. Hoping to lend better facts in the academics and scientific world. With the further blessing from the almighty, I wish to assist in the technical field and society.

Yasha Tayal

LIST OF PUBLICATIONS (INCLUDED IN THESIS)

1. Orange color emitting Sm^{3+} ions doped borosilicate glasses for optoelectronic device applications

   Yasha Tayal and A.S. Rao.

   Optical Materials 107 (2020) 110070 (Impact factor = 3.08).

2. Spectroscopic analysis of Dy^{3+} ions activated borosilicate glasses for photonic device applications

   Yasha Tayal and A.S. Rao

   Optical Materials 117 (2021) 111112 (Impact factor = 3.08).

3. Photoluminescence characteristics of Sm^{3+}/ Eu^{3+} co-doped LPZABS glasses for solar cell applications

   Yasha Tayal, Sumandeep Kaur and A.S. Rao

   Solid State Sciences 125 (2022) 106834 (Impact factor = 3.059)

ABSTRACT

In this thesis, we have examined the structural, optical and photoluminescence characteristics of rare earth (RE) doped glasses. Glasses are emerging as better candidate for the doping of RE ions for wide range of applications in the fields of white light emitting diode (w-LEDs), solid state lasers, sensors and optical amplifiers, etc. They are sustainable and holds wide emission as well as homogeneous emission characteristics. Glasses can be synthesized by simple technique and they possess high thermal and mechanical sustainability with minimum manufacturing charges. Incorporation of alkali and alkaline metal oxides enhances its durability and emission probabilities of the host glass system. Further addition of RE ions increases utility in photonic applications.

Visualizing these facts, the aim of this research work is to explore the effect of RE ions doping on structural and spectroscopic properties of borosilicate glasses. In the present work lithium lead zinc alumino borosilicate (LPZABS) glasses have been prepared by melt quench technique doped with RE ions like Sm^{3+}, Dy^{3+} and Sm^{3+}/Eu^{3+} through different concentrations of these RE ions and studied their structural and photoluminescence properties to understand their usage in photonic device applications. The glassy nature and functional groups present in the host glass has been confirmed by recording XRD and FT-IR spectral features. The experimentally measured physical properties such as density (Archimedes principle) and refractive index (Brewster's angle method) were used to compute many other physical properties of the titled glasses. Spectroscopic analysis was done on the basis of absorption, excitation, emission and decay recordings. Five chapters of this thesis consists of literature survey, manufacturing technique and characterization of the titled glass samples.

Chapter 1: This chapter consists of brief introduction to origin and history of glasses. Different glasses with its components, formation and properties are studied. Electronic

transitions, optical parameters, energy transfer in RE ions and selection of the host glass system are explained. Along with this, recent developments and encouragement to pursue research in the field of glasses has been discussed in detail.

Chapter 2: In this chapter synthesis and characterization techniques for the present glass system have been incorporated in detail.

Chapter 3: It describes an intense orange color emitting Sm^{3+} activated LPZABS glasses which were propitiously fabricated by using sudden quenching method to study the luminescent potentiality using spectroscopic techniques such as XRD, FT-IR, optical absorption, photoluminescence (PL) and PL decay. XRD and FT-IR reveals the glassy nature and various functional groups present in LPZASB host glass respectively. Judd-Ofelt parameters derived from absorption spectra are used to estimate various radiative parameters for the excited states of Sm^{3+} ions in LPZASB glasses. Under 400nm excitation, the luminescence spectra in the as prepared glasses exhibit three emission bands that corresponds to $^4G_{5/2} \rightarrow {}^6H_{5/2}$ (562 nm), $^4G_{5/2} \rightarrow {}^6H_{7/2}$ (598 nm) and $^4G_{5/2} \rightarrow {}^6H_{9/2}$ (645 nm) transitions of Sm^{3+} ions. Among these three, $^4G_{5/2} \rightarrow {}^6H_{9/2}$ transition observed in orange region (598 nm) is relatively more intense and prominent. The PL decay curves recorded for $^4G_{5/2}$ fluorescent level reveal exponential behavior and single exponential fitting is applied to evaluate the experimental lifetimes (τ_{exp}). The τ_{exp} values are found to be decreasing with Sm^{3+} ion content due to cross-relaxation energy transfer process. The results reveal that the as prepared glasses can be effectively used in fabricating intense visible orange color emitting optoelectronic devices. (Part of this chapter is published in Optical Materials)

Chapter 4: This chapter describes optically translucent borosilicate glasses activated with varying concentrations of Dy^{3+} ions were fabricated by employing melt quenching method. Spectral investigations were conducted by recording the absorption, photoluminescent (PL) excitation and PL emission for Dy^{3+} activated borosilicate glasses. The absorption spectral information was exposed to Judd-Ofelt (J-O) analysis to calculate various radiative properties such as transition probability, total transition probability, branching ratios and radiative lifetimes of the as synthesized glasses. The excitation spectrum recorded under 483 nm emission wavelength possess a sharp peak at 348 nm in 0.1 mol% of Dy^{3+} ions doped borosilicate glass. Emission spectra recorded for all the Dy^{3+} ions activated borosilicate glasses under 348 nm intense excitation wavelength exhibit two potential peaks in visible region at 483 nm ($^4F_{9/2} \rightarrow {}^6H_{15/2}$) and 575 nm ($^4F_{9/2} \rightarrow {}^6H_{13/2}$). The emission centered at 483 nm is most prominent. Radiative properties measured from the absorption spectral feature were correlated with emission spectral information to estimate emission cross-section, gain band width and optical gain parameters to understand the utility of the as synthesized glasses as photonic devices. The CIE coordinates measured for all the titled glasses are in good proximity with the white light coordinates of CIE 1931 diagram. (Part of this chapter is published in Optical Materials)

Chapter 5: In this chapter, a series of Sm^{3+}/Eu^{3+} co-doped LPZABS (lithium lead zinc alumino borosilicate) transparent glasses were synthesized by the melt quench method. Fluorescent characteristics and energy transfer mechanisms were analyzed thoroughly. The amorphous nature of the glasses was confirmed from the observed X-ray diffraction patterns. An expansion in photoluminescence (PL) excitation of Eu^{3+} ions was observed on sensitizing it with Sm^{3+} ions in the title compounds. The PL emission spectra obtained

for different excitations show bands due to Sm^{3+} and Eu^{3+} ions with increment in intensity on increasing Eu^{3+} ion concentration. On implementing the Dexter energy transfer formula & Reisfeld's approximation to PL emission spectra and the Inokuti-Hirayama (I-H) model to PL decay profiles, the dipole-dipole interaction among activator and sensitizer is revealed. Chromaticity coordinates (CIE) relocate from the orange to the red region gradually on increasing Eu^{3+} ion concentration in Sm^{3+}/Eu^{3+} co-doped LPZABS glasses. The Sm^{3+}/Eu^{3+} co-doped LPZABS glasses have the potential for downshifting of n-UV & blue exciting photons into visible red color photons possibly useful for copper phthalocyanine (CuPc) solar cell applications. (Part of this chapter is published in Solid State Sciences)

Chapter 6: This chapter describes the summary of the results obtained in the thesis work along with future scope of work.

****

CONTENTS

LIST OF TABLES

LIST OF FIGURES

CHAPTER 1

INTRODUCTION

Chapter 1 *comprises of initiation and inspiration on working about glasses for photonic applications. Different types of glasses with their formation and properties associated with them are discussed in this chapter. RE ions doped glasses have high importance for various fields of fibers, lasers, w-LEDs, solar cells, etc. Special focus of our study is on photoluminescence characteristics and energy transfer mechanism involved. Exceptional attributes of Lithium Lead Zinc Alumino Borosilicate (LPZABS) glasses in comparison to various host system has prompted us to select the present host which are detailed in this chapter. Significance of chemical elements introduced in the host system are elaborated. Applications of selected host in various photonic devices has been elaborated in the chapter. When the host lattice is doped by RE ions, the emission so generated finds vast usage in optical devices in different technical areas.*

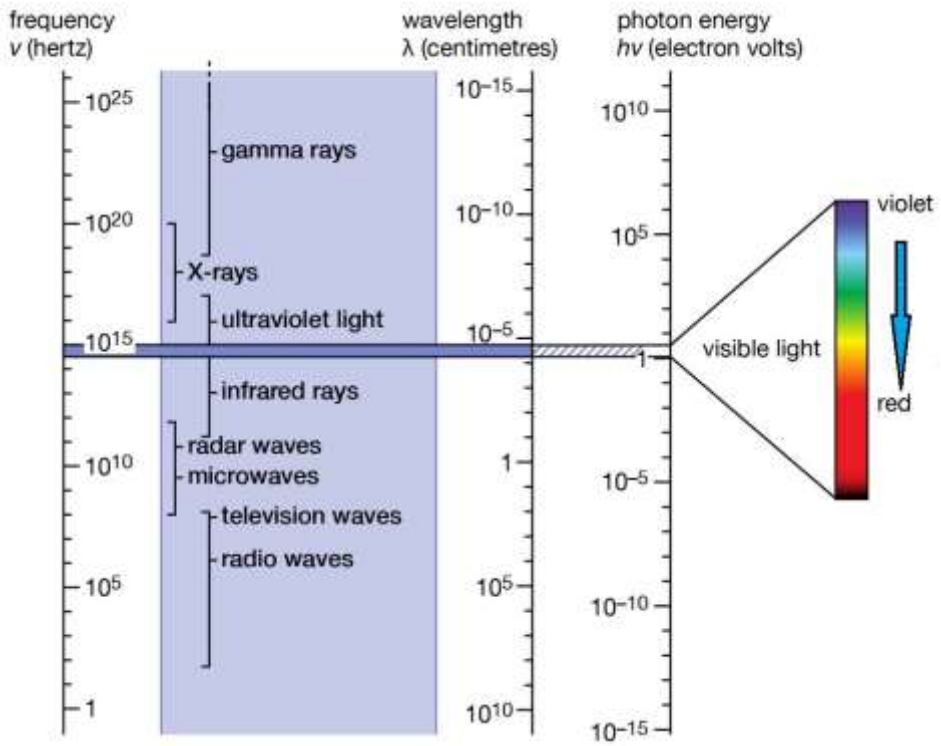

1. Introduction

Interaction of electromagnetic (EM) radiation with matter can be termed as spectroscopy in wider sense. The behavior of atoms and molecules present in a host matrix can be better understood by using spectroscopic techniques. EM radiation vary from gamma rays to radio waves with immense wavelength range. Spectroscopic analysis is classified into numerous types for elaborating different analytical problems. Traditionally, for quantitative and qualitative studies, visible light is subjected to matter and this analysis is termed as spectroscopy. When a specific EM radiation interacts with matter, absorption and emission occurs, which in turn helps in understanding the behavior of molecular structure and its environment by numerous methodologies. The subjected atoms and molecules liberate characteristics wavelengths, which helps in studying the ground state and various excited states for the electron configuration. Strictly speaking about optical spectroscopy, it comprises of optical reflection, refraction, scattering, absorption and emission of EM radiation when it is encountered by matter (atoms or molecules) that may be in any state (solid, liquid or gaseous). With the new advancements in technical arena, there is a huge demand for more progressive luminescent material fitting more appropriate to many new applications. When we analyze the optical spectra for solids, on the basis of theoretical knowledge of electronic and atomic structure, it turns out to be more strenuous than to that of atomic or molecular spectra. As there is an arrangement of atoms or ions in long or short range for crystalline and non-crystalline (glasses) respectively.

In comparison to crystalline materials, glasses hold an edge over them due to numerous characteristics. For spectroscopic analysis, glasses provide better platform than crystals. Glassy host are better candidates for doping with RE ions as they provide better tuning of

wavelength, simple manufacturing techniques for even bigger sizes, simple crafting, high level of doping possibility and nature of glasses is isotropic [1-10]. RE ions doped glasses finds vast usage in optoelectronics and numerous other applications such as googles which provides protection to eyes when subjected to high energy neutrons and to provide active medium for many spectroscopic analysis. RE ions possess $4f^n$ configuration in their electronic energy levels, arising numerous spectral properties paving the way for heavy usage in various fields. For certain applications, optical transitions from $4f^n$ to $4f^n$ are preferred, as the requirement demands of high lifetimes, fine absorption lines and brilliant coherence. On the other hand, if greater oscillator strengths, lower lifetimes and broad absorption transitions are essential, then $4f^n$ to $4f^{n-1}5d$ transition are favored. Previous decades show huge development in the RE^{3+} ions doped substances which finds utility in modern technic, photonics, high power lasers, light converted phosphors, optical amplifiers, memories with large density, color display systems and others as well [11-15]. All RE ions holds key feature in luminescent materials like Nd^{3+} glass for lasers and Dy^{3+} ion based optoelectronic devices are suitable for white light generation. Glasses are famous for easily obtaining bulk specimen and diverse doping range is easily achievable for the particular device implementation. Apart from these, they can be designed into variable shapes and sizes, still they will possess even RE ion distribution that too without crystallization. Glasses have unique property to provide huge optical translucency window wrapping UV, visible and infrared (IR) range of the EM radiation.

For the development of optimized RE ion glass host configuration, RE ion optical characteristics needs to be explored thoroughly in terms of excitation, emission, peak wavelength, emission cross sections, line widths, lifetimes and quantum efficiencies. Surrounding of the RE ion in the host glass matrix and phonon energies of the glass

system commands the aforementioned properties. So, we need to carefully identify a suitable glass host acquiring relatively low phonon energies and large value of quantum efficiency [16-21]. Solid- state materials doped by RE ions are mostly filling the need for optical devices. Huge focus of researchers is seen towards developing crystalline and non-crystalline RE doped substances. When non-crystalline materials like glasses with many components comprising of network formers, modifiers and intermediates are equipped with enormous optical characteristics, finds immense applications in various technical fields. The current work presented in this thesis revolves around the optical spectroscopy shown by LPZABS glasses doped by RE ions like Sm^{3+}, Dy^{3+}, and co-doped by Sm^{3+}/Eu^{3+}. Focus of the research is to explore the influence of the aforementioned RE ions on absorption, emission and decay measurements.

1.1. Classification of Solids

Based on the arrangement of atoms or molecules, the solid state materials can be broadly classified in to two such as crystalline and amorphous. The crystalline and amorphous structure of solids can be verified from each other through X- ray diffraction methodology. Fig. 1.1. represent the two types of solids.

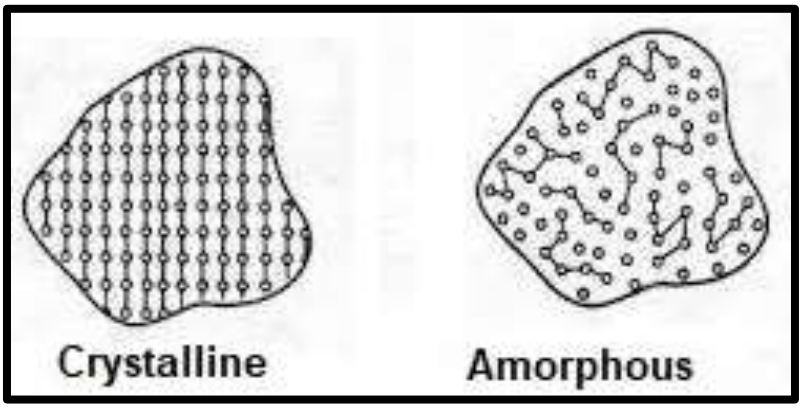

Fig.1.1. Crystalline and amorphous solids

1.1.1. Crystalline Solids

This category of solids comprises of properties like long range order of constituents. Crystalline solids possess definite structure and are majorly anisotropic in characteristics. These are termed as true solids figuring with fixed value of heat of fusion and sharp melting points. Some of the crystalline solids are like diamond, KCl, etc…

1.1.2. Amorphous Solids

This category comprises of solids possessing short range order of its constituents resulting in irregular shape or we can say devoid of any form. Amorphous solids are as well assumed to be pseudo solids (super cooled liquids) and do not possess definite heat of fusion. Amorphous solids can be molded as they tend to get soft over a range of temperature, as they do not have sharp melting and boiling points. In x-ray diffraction methodology of amorphous solids, we can find broad series of peaks with very less angles of scattering, confirming the short-range order. Amorphous solids possess same property in all directions (isotropic in behavior). Some of the examples of amorphous solids are like rubber, glass, plastics etc.

1.2. Glass

The word “glass” is originated from a Latin term ‘glaseum’ which means translucent and lustrous substance. Early civilization used to figure glasses as a symbol of durability and luster. With the rapid development, on account of usage of glasses for various fields, different constituents were added to it to further enhance the desired property. With the awareness on various technical properties of glasses, their definition changed from time to time [22-25]:

- 1930, saw glass termed as amorphous solid (solids without structure).
- 1938, inorganic substance comparable and continuous to its liquid state, but it is considered as rigid for applications point of view, since it acquires a high degree of viscosity due to reversible change in viscosity in the course of cooling.
- 1949, inorganic outcome of fusion, which acquires rigid state when cooled without crystallization (by American society for testing materials).
- 1960, glass was finally termed as non-crystalline solid.

1.2.1. Types of Glass

Glasses are simply categorized into two, firstly upon the contributing components and secondly on their final usage:

Natural glasses: These types of glasses are formed upon cooling of molten lava as it reaches earth's crust like pumice, obsidians etc. Natural glasses also form when strong shock waves encounter the substance under unexpected increase in temperature. Vitreous SiO_2 is founded as a large rod in the skeleton of some deep water sponges.

Artificial Glasses: Man made glasses are possible in diversified types of materials. With practical utility of glasses are quite less in comparison to glasses which have negligible usage. Presence of the type of bond and its chemical composition leads to wide types of artificial glasses like oxide glasses, chalcogenide glasses, metallic glasses and halide glasses.

I. Oxide glasses: Silicates (SiO_2), phosphates (P_2O_5), borates (B_2O_3) glasses etc. play an important part in inorganic glasses by serving as glass formers. These glasses on the structure part are common to liquids while mechanically act like

solids and are translucent to visible range of EM spectrum. Such properties of oxide glasses mark towards the applications in photonics like lasing and in optical fibers for core materials.

(i) Silicate glasses: Most explored glass among all oxide are silicate glasses. Silicate glasses (SiO_2 based) act as a former for the glass structure and examination of properties and structure are quite useful in identifying the complex glasses for this group. It comprises of silicon in the form of SiO_4 tetrahedral structure. Silicate glasses are highly chemically stable which fits it in numerous applications like development of corrosion free laboratory equipment's, thermo resistant cooking equipment's, immobilization of radioactive waste, piping to fiber composites LEDs and LCDs etc.

(ii) Borate glasses: Borate glasses are formed by using H_3BO_3 or $Na_2B_4O_7$. Based upon the composition of the host glass, borate glasses possess BO_3 triangular and BO_4 tetrahedral units. Incorporation of any alkali oxide to borate glasses results in different set of outputs as compared to addition of alkali oxides in other oxide glasses. Borate glasses possess high glass forming ability, optimum bandwidths, high transparency and mechanical strength, etc.

II. Chalcogenide glasses: These glasses are formed by the amalgam of elements of VI (S, Te or Se) and V (P, Sb, As, Ti or Bi) group as well as IV (Ge, Pb, Si) group elements. As these glasses do not contain oxygen, they find utility in optical transmission in infrared (IR) range and electrical switching properties.

Other applications of chalcogenide glasses include detectors and modulators for IR radiations as well as in opto acoustic field.

III. **Metallic glasses**: In new era, metallic glasses find significant spot. Metal-metal alloys and metalloid alloys are the two types of metallic glasses. These glasses are formed by transition metal element and from the border line of metal insulator. These glasses have extremely minimum magnetic losses, large chemical corrosion resistance and nil magnetostriction. Such properties make them useful in being applied as cores of moving magnets, in audio and computer tape recordings as amorphous heads and large frequency power transformers.

IV. **Halide glasses:** Halide glasses are mostly formed by BeF_2. On account of very less refractive index ≈ 1.275 they are highly suitable for high power laser systems for thermonuclear fusion applications. BeF_2 is similar to SiO_2 in terms of structure. BeF_2 glass comprises of 3-D network which is random in nature with BeF_2 tetrahedral acting as building block with neighbors associated by only one corner [26-29]. Other halide compounds which form glasses are GaF_3, BeF_2, PbF_2 and AlF_3.

1.2.2. Glass transition temperature

Transition of solid glass from viscous liquid is termed as glass transition and the temperature at which this occurs is called as glass transition temperature (T_g). However, if the glass temperature is raised above T_g, a reversible process is possible according to which glass is transformed to viscous liquid. When viscosity is increased, glass transition process is observed while the increasing rate of viscosity is influenced by cooling rate, this process leads to variation in glass transition

temperature. This variation can be still observed even if the chemical composition is same as T_g is dependent on cooling rate of the glassy liquid. Fig. 1.2. shows the variation of enthalpy with temperature (V-T graph) for the glass formation:

I. A molten substance (liquid) is raised above its melting temperature (Tm).

II. Cooling of liquid results in changes in its atomic structure.

III. Super cooled liquid is obtained without crystallization, if it is cooled rapidly below Tm. Atoms rearrange themselves on further cooling of the super cooled liquid.

IV. This result in increment of viscosity which prevents total rearrangement and it is in equilibrium liquid structure at the time of experiment.

V. A lag in structure is observed when the liquid is provided enough duration to attain equilibrium condition.

VI. A deviation from equilibrium line is observed for the enthalpy, and obeys a curve of slowly decreasing slope unless it is influenced by heat capacity of frozen liquid.

VII. This results in further increment of viscosity so that establishment of liquid structure takes place and turns out to be independent of time.

VIII. Tg stands in between the region of equilibrium liquid and frozen liquid with respect to enthalpy.

IX. Hence this fast cooling does not allow local atomic arrangements and glass transition is observed at higher temperature. Higher the cooling rate for glass, elimination of nucleation and crystal growing is avoided.

While if the glass is cooled slowly below its Tm, material gets into crystalline state (long range regular atomic arrangement) as viscous liquid will have sufficient time to achieve minimum free energy for the particular temperature to change the local atomic arrangement. Higher free energy is attained for glasses as observed in V-T diagram. It is also observed that quickly cooled glass is more open as freezing of the atomic arrangement is obtained at higher temperature. These aforementioned facts result in characteristics of glass to vary from glasses in accordance with the thermal history, even though chemical composition remains fixed.

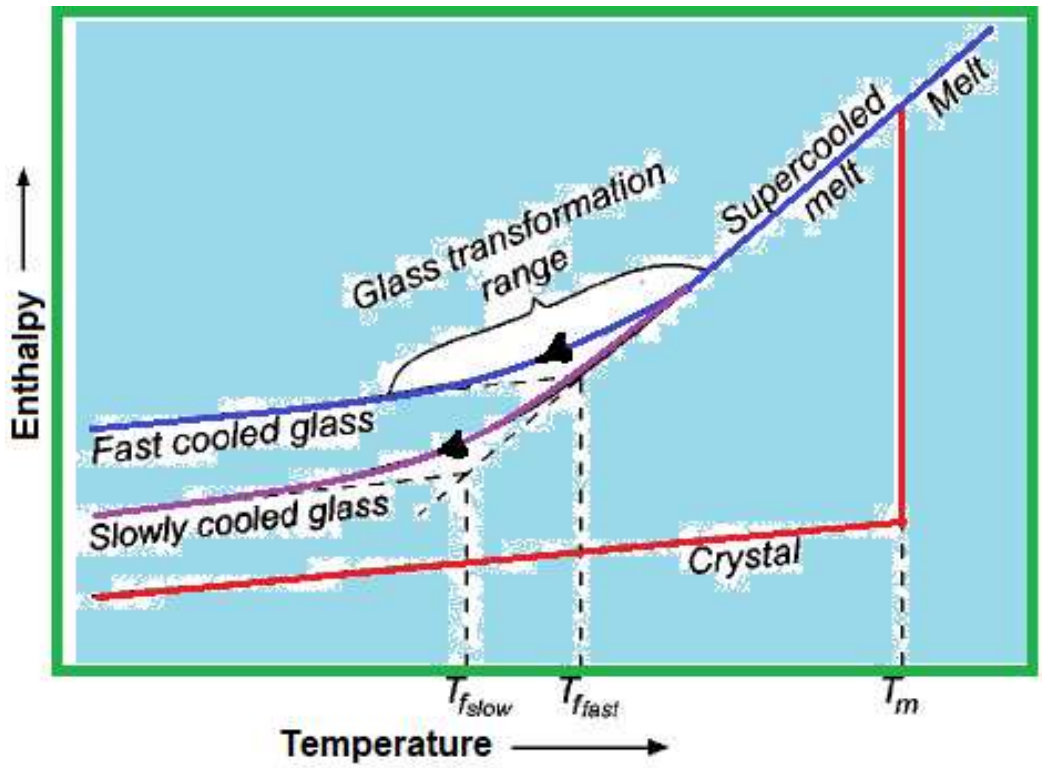

Fig. 1.2. Variation of enthalpy with temperature (V-T graph) for the glass formation.

1.2.3 Constituents of a glass

Selection of appropriate glass constituents leads to defined characteristics and functions. Constituents of glass are distinguished on the basis of bond strength. They

are categorized in three types like network formers, network modifiers and intermediates of the glass.

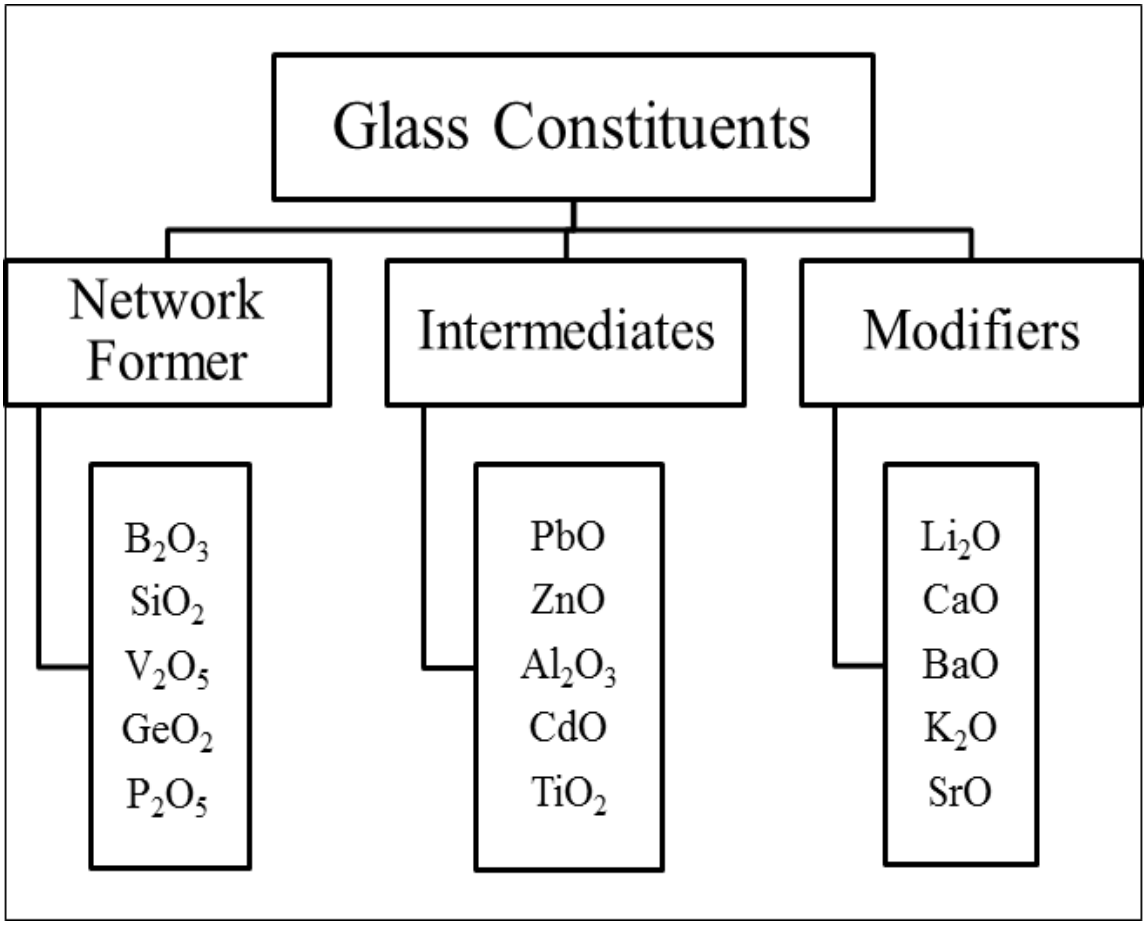

1.2.4. Network formers

Network formers or glass formers act as interconnected backbone for the glass structure, with contributing cation oxygen bond strength > 80 x 10^3 calmol^{-1}. Basic network formers are SiO_2, B_2O_3, GeO_2, P_2O_5, Sb_2O_5, As_2O_5 and V_2O_5. Coordination number for network formers is generally four for all oxides (forming tetrahedral units) except B_2O_3 which possess three coordination number (forming triangular structure). These elements acquire a specific area in periodic table which have intrinsic property

to form glasses on its own when are melted and are cooled very quickly. These can form ionic structures as are adequately electropositive but cannot form covalent bond as are not adequately electronegative.

1.2.5. Network modifiers

Network modifiers are the constituents of a glass which do not form glass under normal condition but results in modification of glass properties. They possess lower bond strength in the range of 10 to 40 x 10^3 calmol^{-1} while coordination number lies in the range of four to ten. With such a low value of bond strength, it cannot acts as a network former; however it is used to enhance the properties of glass marking its significant utility in sensor applications, solid state ionic conductors, optoelectronic device etc. Hence figuring out of a particular modifier as per the need for the particular technique is mandate. Common modifiers used are alkali and alkaline earth elements along with some transition metals and other metals like Na_2O, K_2O, MgO, HgO, CaO, BaO, Li_2O and SrO etc.

1.2.6. Intermediates

Oxides like TiO_2, PbO, ZnO, ZnO_2, Al_2O_3, CdO, etc. serves as intermediates holding position in between network formers and modifiers. Some elements like lead can serve as modifier as well as intermediates according to their coordination number and the selected glass host. These oxides have high bond strength, near about to 80 x 10^3 calmol^{-1}.

1.2.7. Characteristics of glasses

Some of the important characteristics of glasses comprises of:

I. High chemical durability

II. Immense resistance to corrosion as consists of more than two oxides

III. Highly inert, translucent, cheap and homogeneous material with little expansion coefficient

IV. For the same composition glasses hold more internal energy than its crystalline phase

V. Indistinct melting point and on increasing temperature tend to soften and finally turns into molten state

VI. Insulating nature at room temperature and conducting nature at high temperatures

With the selection of glass composition according to the application, there can be variance in its characteristics. Researchers are keen to attain glass with high efficiency and low cost. Further doping them with RE ions marks their utility in lasers, optical fibers, communication systems and more.

1.3. Luminescence

When a radiation is emitted spontaneously by a substance which is not subjected to heat is luminescence and can be termed as cold body radiation. This phenomenon occurs on account of chemical reactions, electrical energy, subatomic motions or stress on a crystal. Luminescence showing materials are termed as luminescent materials. They are of two types: phosphor (crystalline materials) or luminescent glasses (non-crystalline materials). These are generally inorganic materials comprising of host lattice doped with impurities for achieving desired results. The

percentage of dopant is in general kept at relatively low value; at higher dopant content efficiency of luminescence process decreases due to concentration quenching. Under excitation process, the host lattice or impurities added to the host lattice absorbs the energy. As impurity ion absorb excitation energy, it jumps to the excited state. When emission of radiation occurs from impurities ions while returning to their ground state from excited state then these ions are called activator (A) or luminescent center [30-31]. If the absorption of energy by activator ions is weak then another type of impurity is added to the host lattice known as sensitizer (S). Work of sensitizer is to absorb the energy significantly and to transfer it to the activator ions, which show emission process. Generally, impurities added to the luminescent materials are RE ions which show emission in UV-vis-IR range. Fig. 1.3. show the energy transfer process from sensitizer to activator in a host lattice leading to emission of radiation.

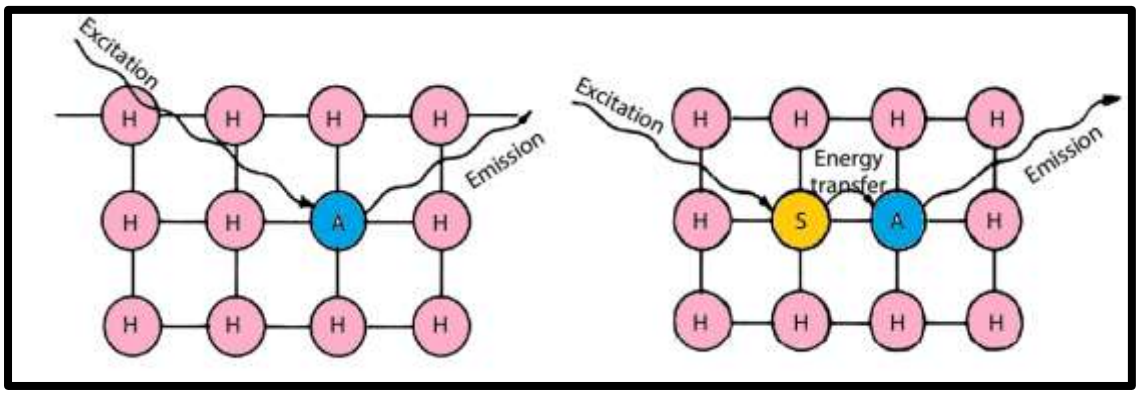

Fig. 1.3. The energy transfer process from sensitizer to activator in a host lattice.

The phenomenon of luminescence can be produced by various methods, which are classified on the basis of their excitation source. Different types of luminescence along with their excitation source and application are shown in flowchart given below:

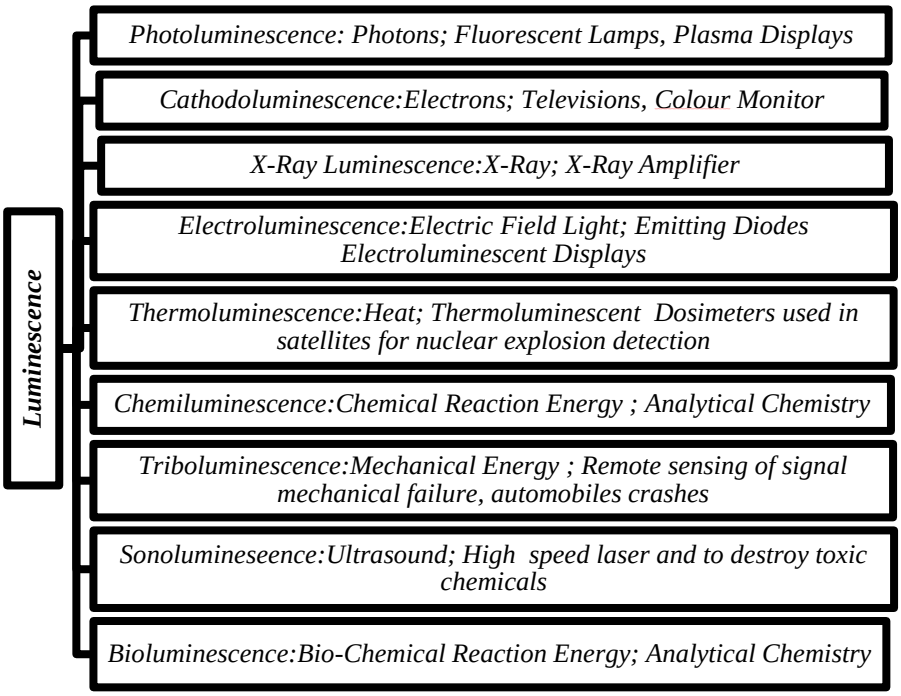

Photoluminescence:

Photoluminescence (PL) is the process in which emission of light takes place from atoms which have absorbed EM radiation. Atoms acquire position in excited state from their ground state when they are pumped by a specific EM radiation. While returning to their original state (ground state) they lose energy by radiation less transition or emitting a radiation. This energy lost value depends upon the two interacting states (ground state and excited state). According to the rate of decay of emitting radiation, PL is further classified as fluorescence and phosphorescence.

Fluorescence:

When the decay of atoms from excited state to ground state gives a photon emission rapidly (at around 10^{-8} seconds) after the removal of the source of excitation, then the emission is called fluorescence.

Phosphorescence:

However, in phosphorescence the emission process is consistent for longer time period (milliseconds to 10 seconds) even after the elimination of pumping source. For this reason, phosphorescence is also called as delayed fluorescence or afterglow. This phenomenon leads to luminosity in phosphorescent materials for longer duration (some minutes to hours) as the excited atoms take their own good time to return to ground state.

1.4. Rare Earth (RE) ions

RE ions are most suitable for photonic device applications, owing to their numerous optical properties like:

I. Emission of RE ions lie in wide range of EM radiation.

II. They acquire small homogeneous line widths

III. High refraction along with low dispersion is observed in RE ions.

IV. Longer emission lifetimes are associated with RE ions.

V. Optical pumping mechanism is possible in numerous excited states possessed by RE ions.

These characteristics of RE ions are used in various technical fields for their usage in the fields such as fibers, glass lasers in communicating areas, LEDs, filters and lenses. Apart from these, RE ions are also used in coloring and decoloring agents, agents as source for glass polishing, pH electrodes and for absorbing radiations like X-ray and gamma- ray incorporated in glassy medium. These unique characteristics and applications are possible on account of their spectroscopic properties.

RE elements are the 15 lanthanides ranging from lanthanum (La) to lutetium (Lu) with atomic number varying from 57 to 71 and are shown in Fig. 1.4. Except La and

Lu, they possess partially occupied *4f* shell as the two elements (La and Lu) are devoid of any *4f* electrons [32, 33].

As a result, these two elements cannot be used for pumping and emission phenomenon in and near the vicinity of visible range. Very less effect is observed on luminescence pattern due to lanthanide contraction, where lanthanide contraction is decrement of ionic radius of lanthanides as atomic number increases. Reduction in ionic radius is due to unsound mutual shielding of 4f electrons. Factors like ionic radius, solubility in various host lattice and oxidation state results in usage of RE ions as sensitizer (S) or activator (A). Number of orbitals for *4f* orbitals is 7 from (*2l +1*) relation, where *l* being the azimuthal quantum number (*l* = 3 for 4f orbitals).

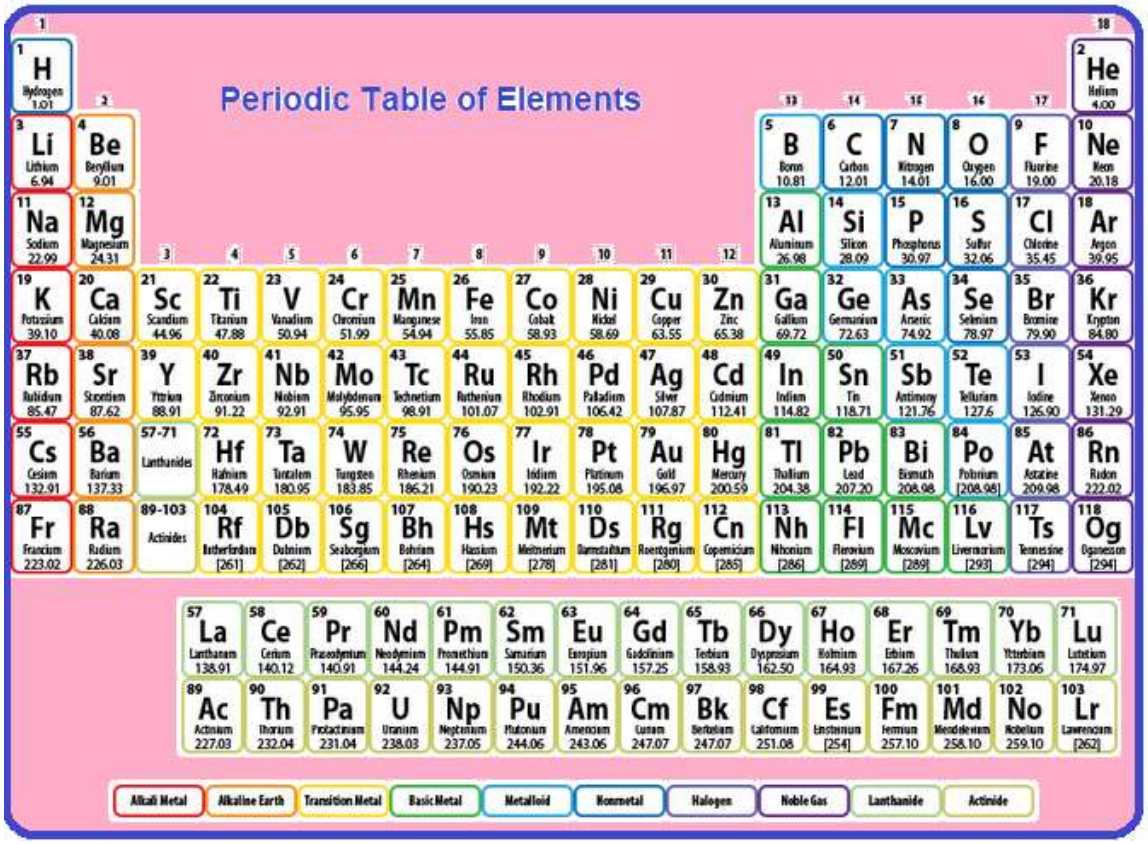

Fig. 1.4. Position of RE ions in periodic table.

The arrangement of electrons in ground state is such that spin angular momentum (S) is maximum. The notification of electronic state is given by $^{2S+1}L_J$, where L and J are

orbital angular momentum and total angular momentum respectively. L specifies the shell as S, P, D, E, F, G, H, I, J, K, L, M,…. With numerical value of L for these being 0, 1, 2, 3, 4, 5, 6, 7, 8, 9,….. accordingly. Relation between S, L and J is [34, 35]:

J= L-S, if the number of 4f electrons is < 7

J=L+S, if the number of 4f electrons is > 7

Energy levels of RE ions are categorized into three types, $4f^n$ configuration, $4f^{n-1}$-5d configuration and levels participating in charge transfer with nearby ions. This categorization helps in the notion of PL characteristics of RE ions.

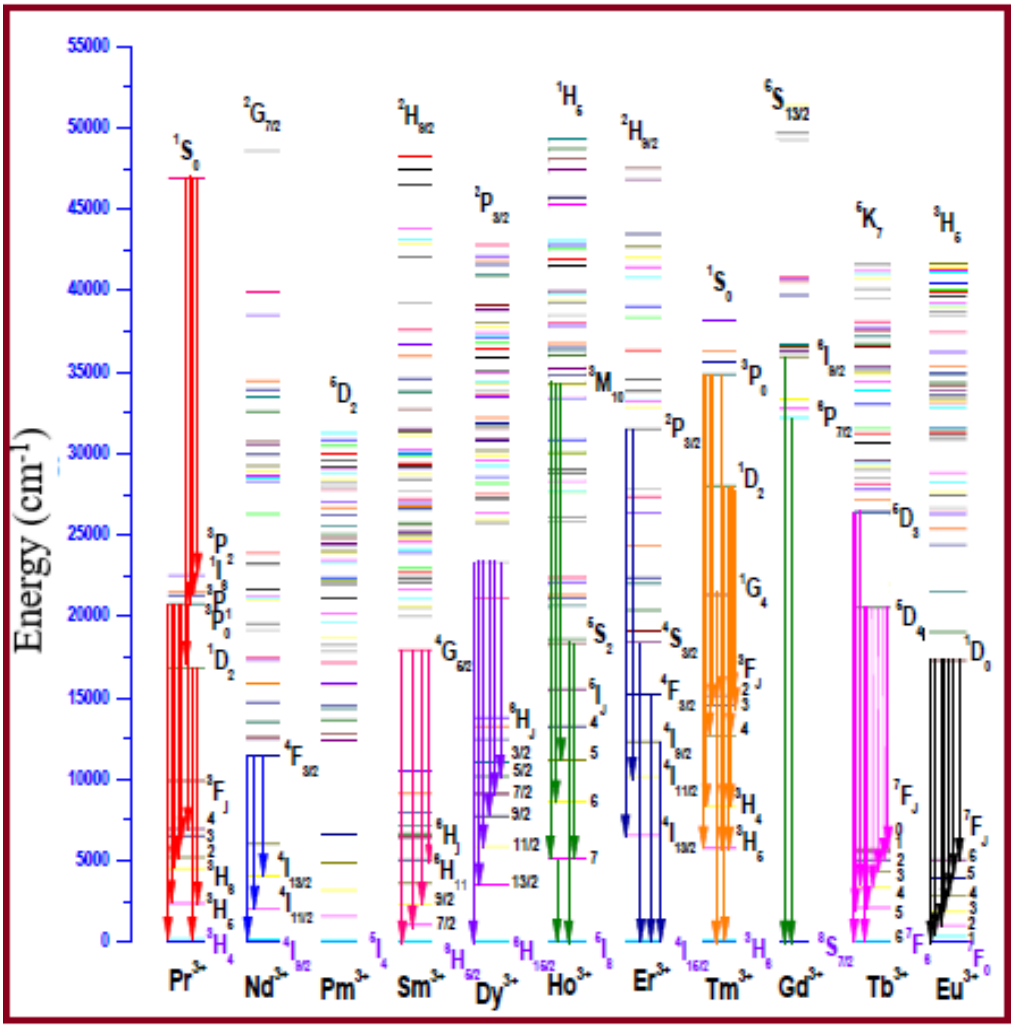

Fig. 1.5. Position and emission transitions of RE ions.

1.4.1. Spectroscopy of RE ions

Due to shielding of 4f electrons by electric fields of $5s^2$ and $5p^6$ electrons, the 4f electronic energy levels of RE ions are not grandly affected by the surroundings. According to Laporte's rule parity remain constant and hence transitions among 4f shells is not allowed. However, these can be permitted if spin orbit interaction takes place. As a result of forbidden nature of photoluminescence transition, the 4f-4f transitions are of millisecond duration [36, 37]. Various position and emission transitions of RE ions are shown in Fig. 1.5. Induced electric dipole (ED), magnetic dipole (MD) and electric quadrupole (EQ) transition are the three mechanisms for getting an idea about 4f-4f transitions.

I. Induced electric dipole (ED) transition

This is the most common transition in RE ions. When interaction via electric dipole takes place between electric field vector and the lanthanide ion which is spectroscopically very active (activator), then the transition which occurs on account of this is termed as electric dipole transition. This transition has odd parity and the resulting electric dipole assumes the charge to follow linear movement. Odd transformation characteristics under inversion for an inversion center are expected for the electric dipole operator. Within the configuration transition corresponding to electric dipole are not allowed as per the Laporte selection rule. Opposite parity electronic states are however allowed to be mixed via non-centrosymmetrical interactions. Judd-Ofelt (J-O) theory specifies them as induced electric dipole transitions.

II. Magnetic dipole (MD) transition

The interaction that occurs between magnetic field component of the EM radiation and spectroscopically active RE ions is via a magnetic dipole, then the transition is termed as magnetic dipole transitions. The path followed by the transitional charge

should be a curved for MD transition. In comparison to induced electric dipole transition, the strength of magnetic dipole transition is very less and is approximately 10^{-8}, as the strength of transition is proportional to square of dipole moment participating in transition. In MD transitions, displacement of charge is observed to be as rotational. In addition to this, the behavior of rotation (spin) is not altered under inversion via a point (center of inversion) and hence the MD transition acquire even parity. The MD transitions possess even parity under inversion and hence allows equal parity states transitions (intra configurational transitions).

III. Electric Quadrupole (EQ) transition

If the nature of charge is quadrupole upon the displacement, then the transition is termed as electric quadrupole transition. The net charge corresponding to four point charges comprising EQ as well as dipole moment for this transition is zero, with arrangement of two dipoles can be pertained to cancellation of dipole moments in between these two dipoles. Parity for electric quadrupole transition is found to be even. EQ transition are weakest among the three transitions. Very rare, electric quadrupole transition is found in lanthanide spectra [38, 39]. Pseudo quadrupole transitions are termed as hypersensitive transitions, as the later follow selection rules of quadrupole transitions.

1.4.2. Hypersensitive transitions

Host lattice does not provide much variance in the strength of ED transitions associated with the RE ions. Variation in the intensity of the specific transition of a RE ion is not much appreciable for other host matrices. Some transitions which are oversensitive to the surroundings finds variance in intensity in complexed RE ion in

comparison to the aqueous solution possessing the RE ion. This variance can be found even 200 times its value, some with decrement in intensity are as well found in literature [40-42]. "Hypersensitive transitions" term is provided for such transitions by Jorgenson and Judd in 1964. The selection rule obeyed these hypersensitive transitions are identical to that of quadrupole transition and are:$|\Delta S| = 0$, $|\Delta L| \leq 2$ and $|\Delta J| \leq 2$. However, intensities for hypersensitive transitions are far too high than the quadrupole transitions. Due to similarity in selection rule and dissimilarity in intensity for hypersensitive and quadrupole transitions, they have earned the title of pseudo-quadrupole transitions also. Hypersensitive transitions for various RE ions are mentioned in the Table 1.1.

Table 1.1. Hypersensitive transitions of certain RE ions.

Ion	Excitation	≈ Energy (eV)
Pr^{3+} ($4f^2$)	$^3H_4 \rightarrow {}^3F_2$	0.64
Nd^{3+} ($4f^3$)	$^4I_{9/2} \rightarrow {}^4G_{5/2}$	2.14
Pm^{3+} ($4f^4$)	$^5I_4 \rightarrow {}^5G_2, {}^5G_3$	2.23
Sm^{3+} ($4f^5$)	$^6H_{5/2} \rightarrow {}^6F_{1/2}$,	0.79
	$^6H_{5/2} \rightarrow {}^6P_{7/2}$	3.29
Eu^{3+} ($4f^6$)	$^7F_1 \rightarrow {}^5D_1$	2.32
	$^7F_0 \rightarrow {}^5D_2$	2.66
	$^7F_2 \rightarrow {}^5D_0$	2.02
Gd^{3+} ($4f^7$)	$^8S_{7/2} \rightarrow {}^6P_{7/2}, {}^6P_{5/2}$	4.03
Dy^{3+} ($4f^9$)	$^6H_{15/2} \rightarrow {}^6F_{11/2}$	0.95
	$^6H_{15/2} \rightarrow {}^4I_{15/2}, {}^4G_{11/2}$	2.90
Ho^{3+} ($4f^{10}$)	$^5I_8 \rightarrow {}^5G_6$	2.74
	$^5I_8 \rightarrow {}^3H_6$	3.43
Er^{3+} ($4f^{11}$)	$^4I_{15/2} \rightarrow {}^2H_{11/2}$	2.38
	$^4I_{15/2} \rightarrow {}^4G_{11/2}$	3.27
Tm^{3+} ($4f^{12}$)	$^3H_6 \rightarrow {}^3F_4$	0.73
	$^3H_6 \rightarrow {}^3H_4$	1.57
	$^3H_6 \rightarrow {}^1G_4$	2.64

Appearance of hypersensitive transitions is predicted by Jorgenson and Judd, according to which if the environment around the RE ion has non-uniform nature, then there is a possibility of increment in the intensity of hypersensitive transitions [43]. Other important parameter associated with these transitions are reduced matrix elements, higher value of $||U^2||$ (Ω_2) and smaller values of $||U^4||$and $||U^6||$. The extent of hypersensitivity is studied by the difference in Ω_2 values for the RE ion in various host matrices [44]. As per the coordination and symmetry of the RE ion, variation in hypersensitive transition will appear. Site symmetry can be perfectly identified on the basis of band structure and hypersensitive transition intensity [43].

1.5. Nephelauxetic effect and bonding parameter

Through the absorption spectral data nephelauxetic effect and bonding parameters can be studied. Due to incomplete f- shell orbitals, the presence of covalency in between RE ion and oxygen bond in glass matrix can be determined by the nephelauxetic effect. This effect causes contortion of 4f electronic orbitals when a RE ion set foot in the host matrix. Shift in wavelength is observed due to overlaying of 4f orbitals and oxygen orbitals, which results in contraction of energy level scheme of the RE ion. From the relation provided in literature, one can find the values of nephelauxetic ratio (β), type of RE ligand bond and bonding parameters (δ) [45, 46]:

$$\beta = \frac{\theta_c}{\theta_a} \quad \text{and} \quad \delta = \frac{1-\bar{\beta}}{\bar{\beta}}$$

where, θ_c represent wave number of specific transition corresponding to RE ion, θ_a is wave number for specific transition corresponding to an aqua ion and $\bar{\beta}$ is mean of β. Covalent or ionic bonding can be observed if the value of "δ" is positive or negative respectively.

1.6. Intensity of absorption bands: oscillator strengths

Area under the curve of absorption bands is used to determine oscillator strength (energy) of the absorption band for the RE doped host matrix. The estimate of intensity of a transition is termed as the oscillator strength, which is the ratio of primary intensity to the intensity radiated by an electron oscillating harmonically in the three dimensions [16, 47]. Value for experimental oscillator strength (f_{exp}) is obtained by the relation:

$$f_{exp} = \frac{2.303mc^2}{N\pi e^2} \int \varepsilon(\theta) d\theta \quad = 4.318 * 10^{-9} \int \varepsilon(\theta) d\theta$$

where, mass and the charge of electron are represented by m and e respectively, while the speed of light is represented by c and Avogadro's number is N. $\varepsilon(\theta)$ represents molar extinction coefficient for average energy θ in cm^{-1}. Area under the curve is represented by the integral part of the relation. Oscillator strength is the quantity which possess no dimension. Molar extinction coefficient is determined by Beer-Lambert's law:

$$\varepsilon(\theta) d\theta = \frac{1}{cl} log \frac{I_0}{I}$$

Where, c represents the concentration of RE ions (mol/l), l represents light path in absorbing medium (in cm) and logarithmic part of the relation stands for optical density.

1.7. Judd-Ofelt (J-O) theory: J-O parameters

Approximating methods for calculation of oscillator strength was used by Judd and Ofelt individually in the year 1962 for the absorption in RE ions possessing forced ED transitions for the f-f configurations [48, 49]. On accordance of identical results and

publication of theory around the same time, it got the term as Judd- Ofelt (J-O) theory. Some of the transitions are not purely ED or MD transition but comprises of ED as well as MD characteristics, hence the measured oscillator strengths are determined by the contributions of these transition and as expressed by the relation:

$f_{exp} = f_{ED} + f_{MD}$

As per the J-O theory, measured oscillator strength corresponding to ED of f-f transitions for RE ions arising from initial state (ψ_j) to the specific state ($\psi'_{j'}$) is:

$$f_{exp}(\psi_j, \psi'_{j'}) = \frac{8\pi^2 mcv}{3h(2J+1)}\left[\frac{(n^2+2)^2}{9n} S_{ED}(\psi_j, \psi'_{j'}) + nS_{MD}(\psi_j, \psi'_{j'})\right]$$

where, the first term in bracket is correction term for the Lorentzian local field corresponding to dipole-dipole correction for the recorded absorption, c and h stands for the speed of light and universal Planck's constant respectively and m represents the mass of the electron. Total angular momentum is stated by J parameter, n is index of refraction for medium, wave number of specific transition is stated by v and ground state degeneracy is predicted by (2J+1) for $^{2S+1}L_J$. While the line strengths of ED and MD transitions are expressed as S_{ED} and S_{MD} respectively. If the two transitions (ED and MD) are compared, then the MD transition hold very less weightage in the determination of oscillator strengths as the intensities of the MD transition (ratio of the intensities of ED/MD transition is approximately 9:1) are very feeble and do not depend upon the RE environment in the host matrix [50, 51]. Hence the contributing factor for the oscillator strength is determined by only ED oscillator strength:

$f_{exp} = f_{ED}$

Therefore, according to J-O theory experimental oscillator strength may be equated to calculated oscillator strength for an ED transition arising from ground state (ψ_j) to excited state ($\psi'_{j'}$):

$$f_{exp}(\psi_j, \psi'_{j'}) = f_{cal}(\psi_j, \psi'_{j'}) = \frac{8\pi^2 mc\nu}{3h(2J+1)}\left[\frac{(n^2+2)^2}{9n} S_{ED}(\psi_j, \psi'_{j'})\right]$$

With the help of least square fitting mode applied to the above equations are deployed to evaluate the J-O parameters, providing the best fit among the experimental and calculated oscillator strengths [16]. The goodness of fit is estimated by root mean square (rms) deviations among the experimental and calculated oscillator strengths through the relation:

$$\delta_{rms} = \left[\frac{\sum(f\text{exp}-f\text{cal})^2}{N}\right]^{1/2}$$

Where, N stands for total count of transitions used in least square fitting mode. Applying the J-O theory, the three intensity parameters ($\Omega_{2,4,6}$) for the RE ions are estimated. Efficiency and the capabilities of the luminescent substances is figured out with the help of these intensity parameters. Chemical behavior of metal ligand bond or structure of host matrix can be correlated to the intensity parameters of RE ions, as the intensity of RE ions corresponding to the f-f transitions depends upon the ligands. From the three, Ω_2 stands for the ligand field asymmetry for the RE ion [52, 53]. Ω_2 hangs on the short range consequences like structural variations in the domain of RE ion and covalency of ligand field. Ω_4 hangs on the long range consequences and so is equated to the bulk characteristics of glass [54, 55]. The trend between the two intensity parameters (Ω_4 and Ω_6) are alike according to the observations of Reisfeld and Jorgensen. Viscosity in glasses doped with RE ions can be studied by Ω_4 and Ω_6

[56]. Lasing potentialities are very well estimated by the spectroscopic quality factor (χ) which talks about the stimulated emission process necessary for any active medium associated with the lasing action. Spectroscopic quality factor is measured as ratio of the two intensity parameters associated with the bulk characteristics:

$$\chi = \frac{\Omega_4}{\Omega_6}$$

1.8. Luminescent and radiative properties of RE ions

The rate of decay of electrons from any excited state ($\psi'_{j'}$) to lower state (ψ_j) is expressed as radiative transition rate. This radiative transition rate is estimated with the help of intensities of the f elements evaluated through the J-O theory analysis of absorption and emission spectral data. Einstein coefficient or probability corresponding to spontaneous emission or spontaneous emission coefficient is estimated by the relation [57]:

$$A_R(\psi_j, \psi'_{j'}) = \frac{64\pi^4 v^3}{3h(2J+1)}\left[\frac{(n^2+2)^2}{9n} S_{ED}(\psi_j, \psi'_{j'}) + nS_{MD}(\psi_j, \psi'_{j'})\right]$$

Where, the term A_R corresponds to rate of spontaneous emission with respect to the time, ψ_j and $\psi'_{j'}$ corresponds to the ground and excited states respectively. Energy gap between these two levels is given by v in centimeter inverse. Refractive index associated with the medium is represented by n. Electric and magnetic line strengths are S_{ED} and S_{MD} respectively.

For various spontaneous transitions occurring before reaching the ground state, the term total radiative transition probability (A_T) is used to specify summation of all emissions occurring in between as:

$$A_T(\psi_j, \psi'_{j'}) = \sum_{\psi'j'} A_R(\psi_j, \psi'_{j'})$$

Radiative lifetime ($\boldsymbol{\tau}_R$) can be evaluated through the A_T as:

$$\boldsymbol{\tau}_R (\psi_j, \psi'_{j'}) = \frac{1}{A_T (\psi_j, \psi'_{j'})}$$

Ratio of the specific spontaneous emission probability to the total radiative transition probability is termed as fluorescence branching ratio for relaxing to the lower lying level is:

$$\beta_R (\psi_j, \psi'_{j'}) = \frac{A_R (\psi_j, \psi'_{j'})}{A_T (\psi_j, \psi'_{j'})}$$

While the experimental branching ratios are determined by area under the curve of emission peaks. β_R is an important parameter in field of laser designing as it speaks about the probability of achieving stimulated emission for a particular transition.

For better lasing action, stimulated emission cross-section should be relatively large. The stimulated emission cross-section between excited and lower lying state is calculated by the equation:

$$\sigma_{se} (\psi_j, \psi'_{j'}) = \frac{\lambda_p^4}{8\pi c\, n^2 \Delta\lambda_{eff}} A_R(\psi_j, \psi'_{j'})$$

where, the transition peak wavelength is represented by λ_p, refractive index by n and effective line width is presented by $\Delta\lambda_{eff}$. $\Delta\lambda_{eff}$ is estimated as the ratio of area of emission band and its average height, by the relation:

$$\Delta\lambda_{eff} = \int \frac{I(\lambda)}{I_{max}} d\lambda$$

Where, intensity corresponding to wavelength λ is represented by I and the highest emission intensity is marked as I_{max}. Effective linewidth is also termed as full width at half maximum (FWHM). Rapid decay and shorter lifetimes are accompanied in a transition if there are numerous transitions and the values of emission probabilities is

very high. Experimental ($\boldsymbol{\tau}_{exp}$) and radiative ($\boldsymbol{\tau}_R$) lifetimes are comparable to each other, however the latter is calculated from the J-O intensity parameters. Variation in between these two lifetimes is embodiment of radiationless transitions (W_{NR}) in the form of multi phonon relaxation rate (W_{MPR}) or energy transfer rate (W_{ET}). The W_{NR} is estimated from the two types of lifetimes ($\boldsymbol{\tau}_{exp}$ and $\boldsymbol{\tau}_R$) by the given equation:

$$W_{NR} = \frac{1}{\tau_R} - \frac{1}{\tau_{exp}}$$

A host material with relatively less phonon energy will act as a good luminescent material relatively. Some of the network former along with their phonon energy in descending order is represented in Table 1.2.

Table 1.2. Network former and phonon energy

S.No	Glass system	Phonon energy (cm^{-1})
1	Borate glass	1300
2	Phosphate glass	1200
3	Silicate glass	1100
4	Germinate glass	900
5	Tellurite glass	700

Further the quantum efficiency can also be estimated by the ratio of two lifetimes ($\boldsymbol{\tau}_{exp}$ and $\boldsymbol{\tau}_R$) as:

$$\eta = \frac{\tau_{exp}}{\tau_R}$$

1.9. Relaxation of energy from excited state of RE ions

Excitation process is better perceived by the analysis of excitation and relaxation of RE ions because of intra 4f transitions in the electron. Intensity spectrum upon time resolution is shown in Fig.1.6. With the help of rate equations defining the excitation

and relaxation process and taking their pertinent integral solutions in the form of the curve is shown in the figure. Relaxation of excited electron to its initial state can be achieved via radiative transition or liberation of energy in terms of phonon or shifting of energy to surrounding RE ions or by a mixture of these processes. PL decay curves can be single exponentially fit if the concentration of dopant ions is very small and a result association between them is very rare. Hence for single exponential decay, energy transfer among the RE ion is very feeble and so the lifetime linked with the excited state is dependent only on first e-folding times. PL intensity with respect to variation in time is expressed by the relation:

$$I(t) = I_0 e^{-\frac{t}{\tau}}$$

Where, the intensity when time t = 0 is represented by I_0. Excited state lifetime is presented by **τ**. Intensity is reduced to 1/e of the initial value after the time is **τ**. If the decay profiles are fitted by bi-exponential function, then the PL intensity is determined by:

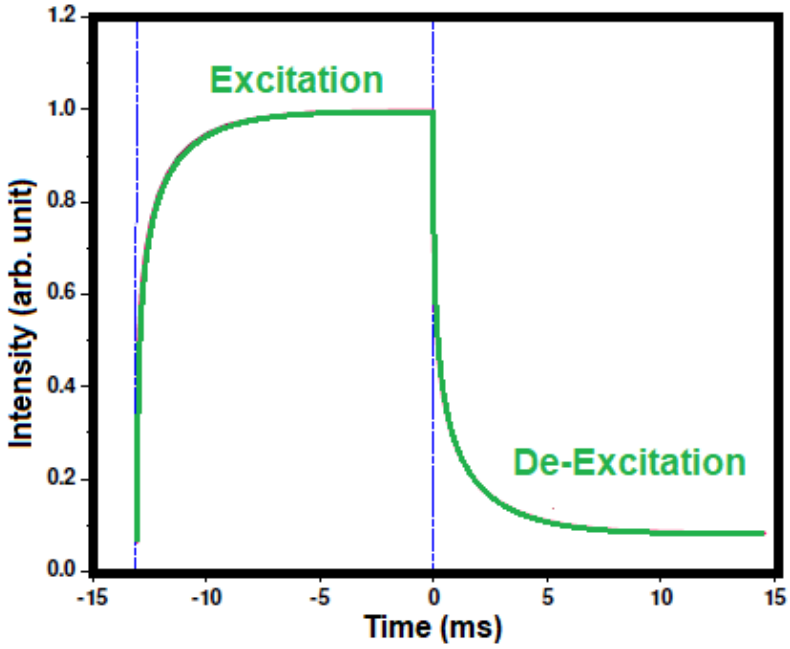

Fig. 1.6. Mechanism of excitation and de-excitation upon time resolution for RE ions.

$I_t = I_0 + A_1 \exp\left(\frac{t}{\tau_1}\right) + A_2 \exp\left(\frac{t}{\tau_2}\right)$ and

$\boldsymbol{\tau}_{exp} = (A_1\tau_1^2 + A_2\tau_2^2)/(A_1\boldsymbol{\tau}_1 + A_2\boldsymbol{\tau}_2)$

Where, A_1 and A_2 are the constants and $\boldsymbol{\tau}_1$ and $\boldsymbol{\tau}_2$ are lifetime components obtained from decay curves.

1.10. Energy transfer mechanism in RE ions

During relaxation of an electron from higher to lower state, the energy loss can be in the form of radiation as well as radiationless transition. When the energy is imparted to neighboring atom through some sort of mechanism resulting in improving the efficiency of lasers and phosphors under the experiment. According to Foster and Dexter, energy transfer process between two neighboring electrons (donor and acceptor or sensitizer and activator) named A and B can be analyzed and are shown in Fig. 1.7. [58, 59]. This energy transfer process takes place between various active ions, which arises due to generation of ion pairs or alteration in intensities of emission pattern. Energy mitigation arises in various methods like:

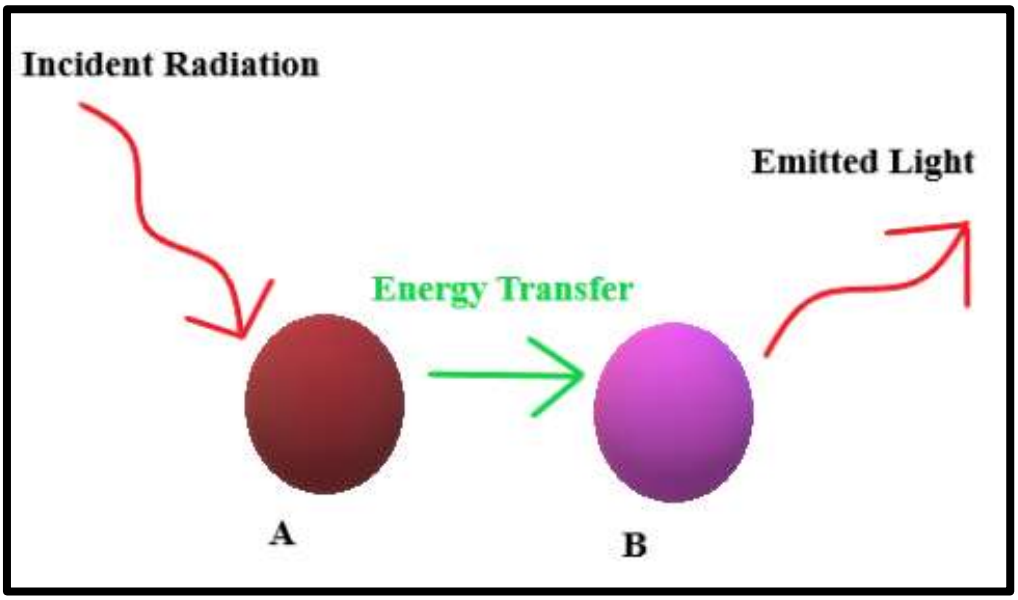

Fig. 1.7. Energy transfer process among donor and acceptor

(I) Resonant energy transfer: Selected sensitizer (S) ion loose energy to decay to its ground state, releasing a photon which excites acceptor (A) ion to higher state from its ground state. Under this method, the two transitions having identical energy are called as resonant energy transitions as shown in Fig. 1.8.

(II) Phonon assisted energy transfer: When there is a variation in excitation energies of activator and sensitizer, then during energy transfer process the variance in energy is absorbed or released via phonons. Such type of mechanism is termed as non-resonant energy transfer or phonon assisted energy transfer and is shown in Fig. 1.8.

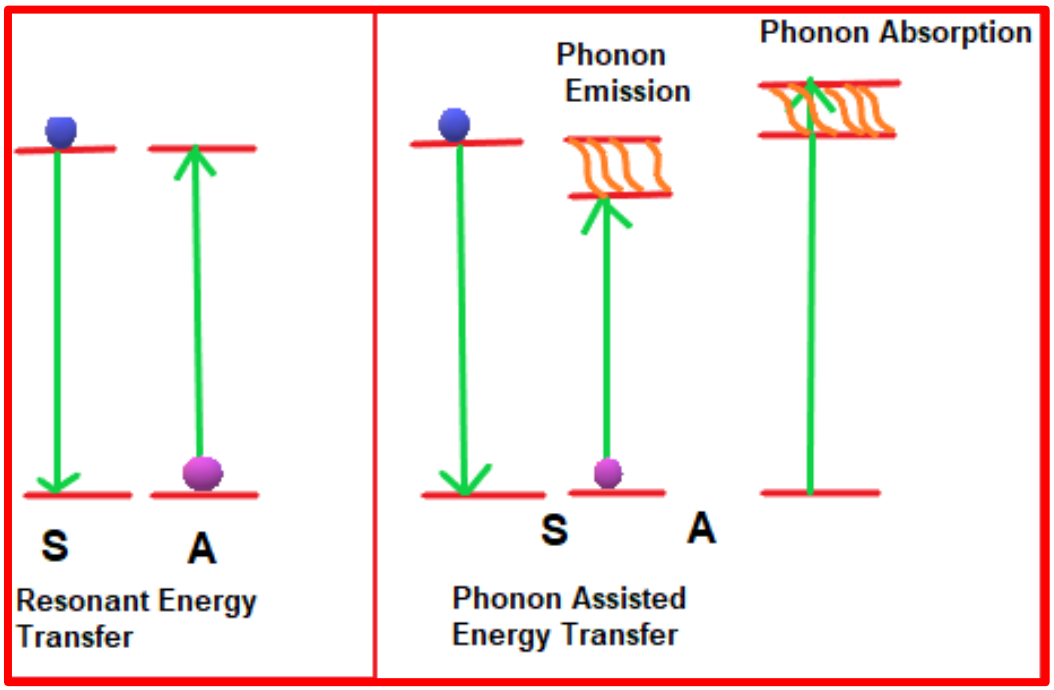

Fig.1.8. Resonant energy transfer and phonon assisted energy transfer process.

(III) Ion pair emission and absorption: Simultaneously acceptor and sensitizer are raised to their excited states. Loss of energy in between excited state of acceptor and excited state of sensitizer takes place in the form of a radiation transition. This mechanism is shown in Fig. 1.9. The interactions taking place in the emission process are multipolar (electric and/or magnetic) and /or a quantum mechanical exchange

interaction. Interaction process which is in more mature state is governed by the parting between donor and acceptor ions as well as their wave functions behavior. The most general interaction mechanism reported in RE ions is electric multipolar interaction mechanism. Under this interaction, we can further find three categories.

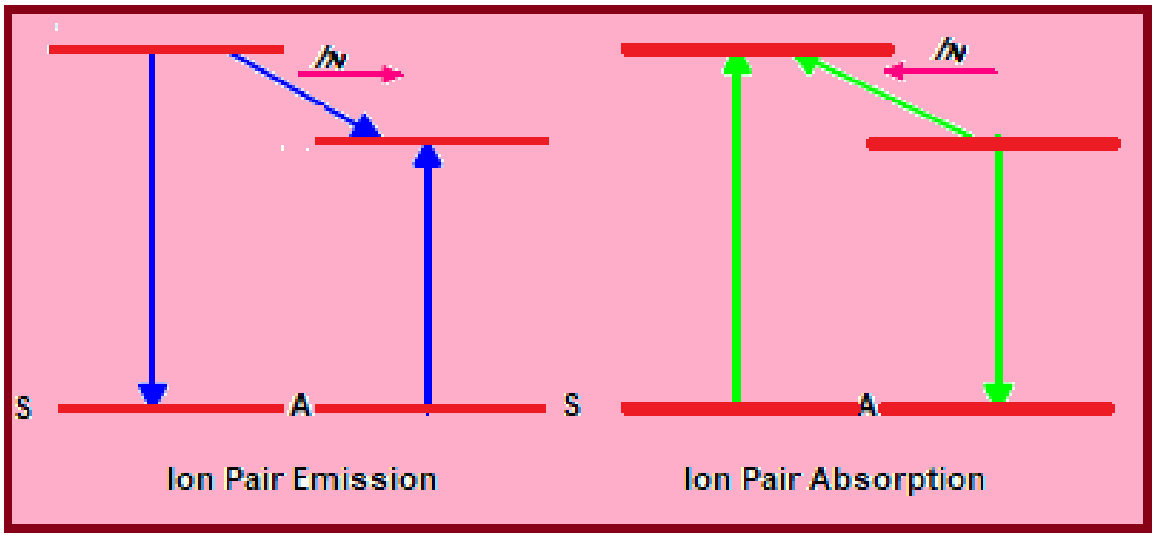

Fig. 1.9. Ion pair absorption and emission

If the behavior of donor and acceptor transition is an electric dipole, then we can observe the electric dipole-dipole (d-d) interaction. The d-d mechanism is observed when the order is of long range and probabilities associated with mitigation process varies by $1/R_6$, here R stands for the difference between acceptor and donor. The remaining two interactions are related to short range order. Variation of dipole-quadrupole (d-q) and quadrupole- quadrupole (q-q) is $1/R_8$, and $1/R_{10}$. Similar is the behavior of magnetic multipolar interactions, however, they are feebly significant in comparison to electric multipolar interactions. For the better accountability of energy mitigation among the 4f shells of RE ions, Foster and Dexter theory is modified by

Inokuti and Hirayama [60]. Relation used to express the decay process by Inokuti and Hirayama is

$$I(t) = I_0 \exp[-\frac{t}{\tau_0} - Q\left(\frac{t}{\tau_0}\right)^{\frac{3}{S}}]$$

Time after excitation is represented by t while the decay time corresponding to donors when devoid of acceptors is $\boldsymbol{\tau}_0$, energy transfer parameter is represented by Q, which can be evaluated as:

$$Q = \frac{4\pi}{3} \Gamma\left(1 - \frac{3}{S}\right) N_0 R_0^3$$

Here, the value of S and Euler's function Γ varies as 6, 8, 10 and 1.77, 1.43, 1.30 for d-d, d-q and q-q interactions respectively. Total concentration of acceptors (≈ concentration of RE ions) is represented by N_0 while the R_0 stands for critical transfer distance. R_0 is length in between donor and acceptor when probability of energy transfer to acceptors is similar to probability of intrinsic decay of donors.

$$C_{DA} = \frac{R_0^S}{\tau_0}$$

Where, the primary energy transfer corresponding to direct acceptor interaction among the RE ions at the separation of R_0 is specified as d-d interaction parameter C_{DA}.

1.11. Colorimetric analysis and CIE color coordinates

Determination of color and the intensity of an emission from a material is termed as colorimetric analysis. When the emission lies only in the visible part of EM spectrum, an impact can be felt on the spectator's eye. Quantitative analysis of the emission from the material is performed through its wavelength [61]. Color characteristics of

any source are performed by correlated color temperature (CCT) and color rendering index (CRI). CCT is temperature of a perfect black body radiator emitting a radiation whose color is corresponding to that of the light source. A warm light source has temperature less than 3000 K, having occurrence in red, orange or yellow range from the visible part of EM spectrum. On the other hand, cool light has temperature more than 4000K, possessing radiation in blue range (bluish white). The basic methodology for the comparison in between light source and the perfect black body radiator is a particular temperature. This temperature is used to allocate point on CIE chromaticity diagram which lies in vicinity to the temperature. The CCT of any light source does not imply it to its physical temperature rather it indicates that the black body is heated up to this temperature and resulting in emission of light having a particular color which is identical to the color of radiation emitting by the source. Blending of various colors, which are visible to human eye are calculated by theoretical functions. These are presented in CIE chromaticity diagram. Equation governing color of any light source is in terms of $\bar{x}$, $\bar{y}$, and $\bar{z}$ which are functions of wavelength (color matching functions) [62] and are given by:

$$X = \int \bar{x}(\lambda)\, P(\lambda) d\lambda$$

$$Y = \int \bar{y}(\lambda)\, P(\lambda) d\lambda$$

$$Z = \int \bar{z}(\lambda)\, P(\lambda) d\lambda$$

The power (stimulus) of the basic colors red, green and blue required for correlating the stimulation extent to the color of P(λ) (spectral power density) is provided by color matching functions (X, Y and Z). From these tri-stimulus values (X, Y and Z)

one can further determine the chromaticity coordinates x and y through the equations [61]:

$$x = \frac{x}{x+y\ z}$$

$$y = \frac{y}{x+y\ z}$$

All monochromatic color coordinates are engulfed in periphery of Commission Internationale de I'Eclairage (CIE) 1931 chromaticity diagram and is represented in Fig. 1.10.

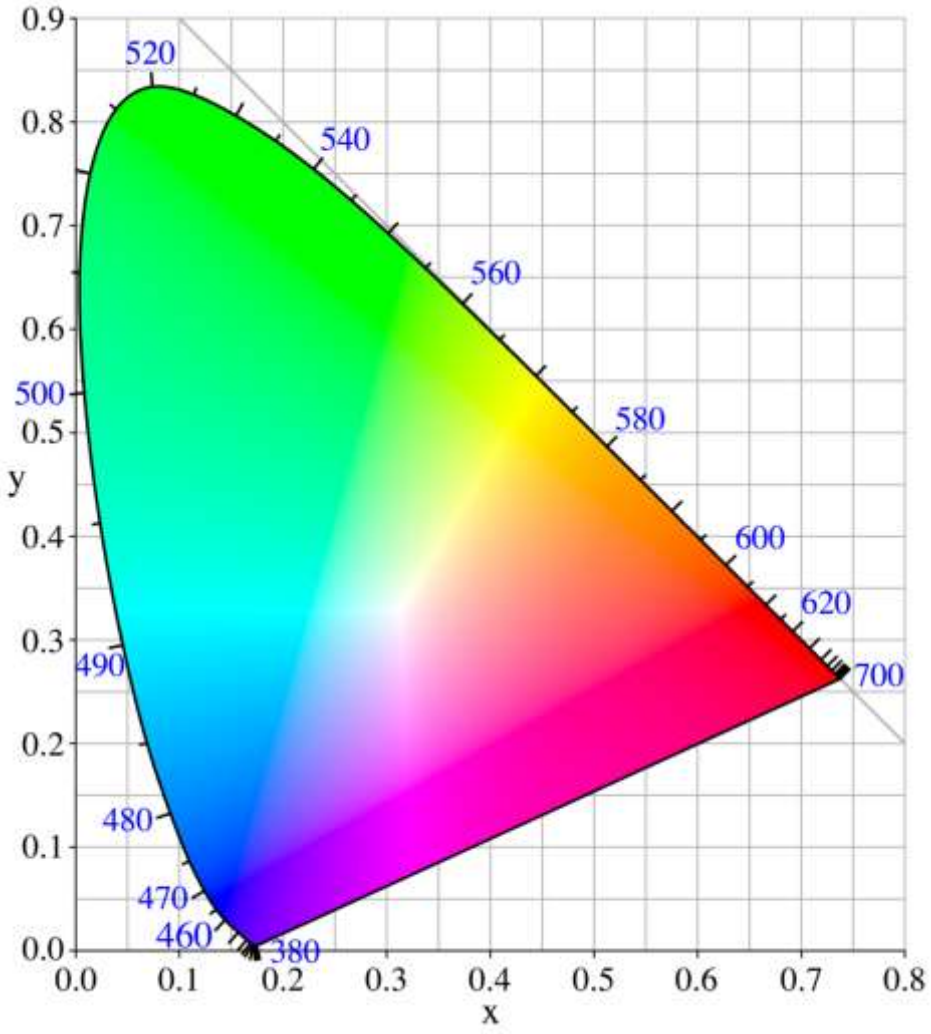

Fig. 1.10. CIE color chromaticity diagram

Wavelengths which are multichromatic reside in the circumference of chromaticity diagram. Saturation of color or color purity corresponding to a dominant color for the source is determined as the ratio of separation between color coordinates of emission and coordinates of equal energy point and separation in equal energy point and point of dominant wavelength. The relation for the color purity is:

$$\text{Color purity} = \frac{\sqrt{(x-x_{ee})^2+(y-y_{ee})^2}}{\sqrt{(x_d-x_{ee})^2+(y_d-y_{ee})^2}}$$

Where, the chromaticity coordinates of emission light, point of equal energy and point of dominant wavelength are represented by (x, y), (x_{ee}, y_{ee}) and (x_d, y_d) respectively [63, 64].

1.12. Present glass system

Novel glasses with RE ions are hugely explored as behavior of luminescence characteristics vary with the environment and the phonon energy of the host matrix. If the phonon energy is relatively less, then the probability of radiationless transition is decreased, yielding in better quantum efficiency. In the current research work, it is aimed to prepare the host matrix having relatively less phonon energy along with better RE ion solubility, transparency and thermal stability so as to fit for many applications discussed above [65-70]. As discussed in earlier section of the work, glass former is the basic building block for glassy system. From the various glass formers, we have selected the combination of two glass formers, borates and silicates. Borates have many advantages like there are very tough, immense transparency towards light, chemical durability and low melting point, along with these it is very economical [71-76]. One major problem with the borates is that, they are hygroscopic

in behavior, which tends to absorb moisture from the surrounding. In addition, borates possess relatively high phonon energy due to the stretching vibrations formed while network building [77]. To fix the problems generated by borates, one can introduce modifiers which further improvise the optical and other characteristics drastically [73]. While, the silicates have excellent chemical and thermal stability. They possess good bondage with standard optical components. However, the silicates suffer with high phonon energy and low RE solubility. Combination of these two formers provide relatively lower melting temperature, huge resistance to corrosion, increases toughness and stability of the matrix and others. When the silicates are introduced in the borate matrix density of the glass network is reduced, which favors the formation of BO_4 at the cost of BO_3 leading to more convenient practical applications.

In the present work heavy metal oxides such as PbO and ZnO are used to enhance the photoluminescence performance of the borosilicate glass. Primary advantage of adding them is that help in reduction of phonon energy which paves the way for utility in photonic applications as radiationless transition probability are reduced. PbO incorporated glasses acquire high refractive index, better transmittance in IR range, fine chemical and thermal durability along with enhanced probability corresponding to spontaneous emission. PbO containing glass matrix holds better lasing action [78-81]. Addition of ZnO has dual purpose as it works both as former and modifier for the glass system. ZnO has covalent behavior, stability towards heat and are sublime. ZnO even provides better window for intrinsic emitting characteristics, hygroscopic behavior and are environment friendly. ZnO enhances mechanical strength and possess wide translucency for UV- IR range of the EM spectrum [82-85]. Inculcating Al_2O_3 in the glass matrix alters the BO_3 units to BO_4 units. Al_2O_3 is a

magnificent compound which can acquire octahedral as well as tetrahedral sites in the glass matrix leading to enhancement of the optical behavior of the matrix [86-90]. Li_2O addition to a glass matrix eliminates the air bubble formation and results in its durability. Apart from it, it improvises the glass transition temperature and diminishes the expansion of thermal coefficient [91, 92]. Cerebrating the above listed scientific facts for the constituents like Li_2O, PbO, ZnO, Al_2O_3, Si_2O_3 and B_2O_3 has prompted us to prepare Lithium Lead Zinc Alumino Borosilicate (LPZABS) glass. Doping or codoping the LPZABS glass by various RE ions has been taken up for better efficiency and lasing characteristics [93-101]. Hence, we aim at studying the optical and photoluminescence characteristics of LPZABS glass when doped/codoped by RE ions like Sm^{3+}, Dy^{3+} and Eu^{3+}, ions.

1.13. Objectives of the research work

Framing of the present research work is to produce a device with improvised luminescence efficiency using a glass host doped with specific RE ions showing emission in numerous ranges of EM spectrum. New emerging trends in technology have led to the development of glasses doped with RE ions for usage in solid state lasers, LED, color paneled phosphors, concentrators for solar energy, optical fibers and many more.

- To optimize the conditions of fabrication of a good optical glass doped with RE ions for wide range of photonic applications.
- Extensive physical and structural characterization of glasses by measuring the properties such as refractive index, density etc. and using techniques such as XRD and FT-IR.

- To study the absorption, excitation and emission spectral features of the RE ions doped LPZABS glasses to understand the glass host as well as concentration of RE ion dependency and evaluation of emission cross-section & quantum efficiency of the as prepared glasses by correlating the absorption spectral data with the emission and decay measurements.
- RE concentration optimization and co-doping with suitable RE ions for better luminescence efficiency.

****

CHAPTER 2

EXPERIMENTAL TOOLS AND TECHNIQUES

Focus of this chapter is on experimental procedures used for the preparation of RE doped glasses along with the characterization techniques essential for understanding its fluorescent characteristics. Among all the synthesizing methods, melt quench method is deployed for preparing the RE doped glasses, which is discussed in detail. Techniques used to study the physical, structural and PL characteristics of as prepared glasses are further discussed via X-ray diffraction (XRD), Fourier-transform Infrared Spectroscopy (FT-IR), UV-VIS spectrophotometer and spectro-fluorophotometer.

2.1. Glass preparation methods

The following are some of the techniques used by the glass workers to prepare glasses [102, 103]:

- Melt quench
- Gel-desiccation
- Sputtering
- Chemical reaction
- Thermal evaporation
- Irradiation
- Glow-discharge decomposition
- Sol-gel process
- Chemical vapour decomposition

From the above listed methods, we have used the most commercially viable technique, i.e., melt quench method. This method is very useful in attaining any desirable shape and size from the melt which is forced to cool suddenly [104]. Non-crystalline solid is formed by hardening of the molten mix which is subjected to sudden cooling as shown in Fig. 2.1. Conducting substance like brass or copper plates are used for quickly cooling the hot molten mix, which is further subjected to annealing in a separate furnace at adequate temperature. Finally, glass pellets are formed which are investigated with the help of various characterizations. The selected precursors were procured from manufactures having high purity (99.9 % mandate for the RE ions to be doped) and are listed in Table 2.1.

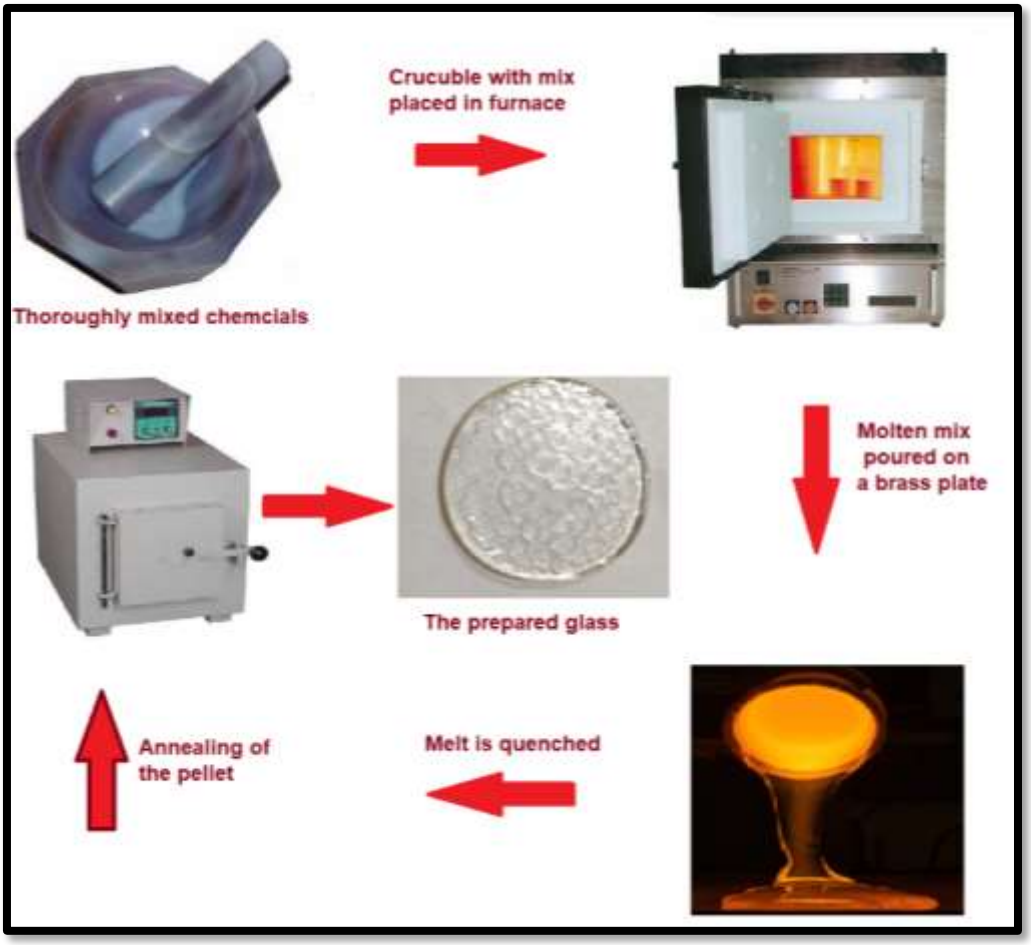

Fig.2.1. Glass samples preparation by melt quench method.

Table 2.1. The list of chemicals used in the present work along with their purity and manufacturer details.

S. No.	Name of Chemical	Purity (%)	Manufacturer
1.	B_2O_3	99.90	Fisher Scientific
2.	SiO_2	99.90	CDH
3.	Al_2O_3	99.90	Fisher Scientific
4.	PbO	99.90	Fisher Scientific
5.	ZnO	99.90	Qualigens
6.	Li_2O	99.90	Fisher Scientific
5.	Sm_2O_3	99.99	Sigma Aldrich
6.	Dy_2O_3	99.99	Sigma Aldrich
7.	Eu_2O_3	99.99	Sigma Aldrich

LPZABS glasses doped/co-doped with RE ions like Sm^{3+}, Dy^{3+} and Eu^{3+} were synthesized having the molar composition:

$10Li_2O$–5PbO-(5-x)ZnO-$10Al_2O_3$-$10SiO_2$-$60B_2O_3$-xRE,

Where, x = 0.1, 0.5, 1.0, 1.5, 2.0 and 2.5 mol%

Digital balance (Shimadzu modal: ATX244) possessing an accuracy of 0.0001g was used for the measurements of chemical composition required as per the molar equation for the selected glass host. Measured samples (approximately 7 g) were crushed in an agate mortar and pestle to turn it into homogeneous mix as shown in Fig. 2.1. Alumina crucible is used to keep the mix in a heating furnace at 1100°C for 2-3 hrs. Further the molten mix so obtained is suddenly quenched via two identical and preheated brass plates. Lastly the pellets so obtained are annealed at 350°C for 4 hrs to remove any air bubbles or thermal strains that are formed inside the as prepared glass. Such RE doped LPZABS glass pellets are now used for physical and optical characterizations after polishing them.

2.2. Physical and structural properties of the titled glasses

Firstly, the un-doped and RE ion doped LPZABS glass samples are tested for various physical and structural properties. Thorough study of the physical properties of the titled glasses and the procedures used are discussed under this section.

2.2.1. Physical properties

Spectroscopic examination is dependent on some physical parameters like thickness, density, refractive index and concentration of the RE ion. In the calculation of experimental oscillator strengths (f_{exp}), the above mentioned physical parameters are

required, through which intensity parameters and radiative parameters can be determined providing insight towards the as prepared glass utility.

(I) Thickness: Screw gauge is the instrument used for the determination of the thickness (l) of LPZABS glass samples. Least count of the screw gauge is ± 0.001 cm. All sets of LPZABS glasses have even thickness of 2.9 ± 0.01 mm.

(II) Density: Estimation of density (d) is successfully done by Archimedes' principle holding ± 0.0001 g of accuracy with immersion liquid being water. Equation used for the determination of density is:

$$d = \frac{W_1}{W_1 - W_2}$$

Where, W_1 is the weight of glass in presence of air while W_2 is the weight of glass in water.

(III) Refractive index: Brewster's angle technique with He-Ne laser (6328 $X10^{-10}$m) is used to estimate the refractive indices (n_d) of LPZABS glasses.

(IV) Concentration (C) of RE ion: Calculation of concentration (C) (mole/liter) of RE ion is done by the relation [105]:

$$C = \frac{M_{RE}}{M_T} \times \frac{d}{MW} \times 100$$

Where, mass of RE salt, total weight of chemical composition, density of glass and molecular weight of RE salt is given by M_{RE}, M_T, d and M_W respectively. Units of the concentration can be altered from mole/liter to cm^{-3} if it is multiplied by Avogadro's number (N).

These four physical parameters are further used to estimate other physical parameters like Avogadro molecular weight ($\bar{M}$) (g), mean atomic volume (g/cm^3/atom), molar

volume (V_m) (cm^3/mol), dielectric constant (ϵ), optical dielectric constant, molar refractivity, reflection losses, polaron radius, interionic distance, molecular electronic polarizability, optical basicity and field strength of RE ions doped LPZABS glasses through the following the expressions presented in the literature [105]:

Dielectric constant, $\epsilon = {n_d}^2$

Optical dielectric constant, $\epsilon - 1 = {n_d}^2 - 1 = P\frac{\delta t}{\delta P}$

Molar refractivity, $R_M = \left[\frac{({n_d}^2-1)}{({n_d}^2+1)}\right]^2 \frac{\bar{M}}{d}$

Reflection loss, $R = \frac{(n_d-1)^2}{(n_d+1)^2}$

Polaron radius, $r_P = \frac{1}{2(\pi/6n)^{\frac{1}{3}}}$

Interionic distance, $r_i = \left(\frac{1}{N}\right)^{1/3}$

Molecular dielectric polarizability factor (α), $\alpha = \frac{1}{\frac{4\pi N}{3}}\left[\frac{({n_d}^2-1)}{({n_d}^2+1)}\right]$

Optical basicity, $\Lambda_{th} = \sum_i \frac{Z_i r_i}{2\gamma_i}$, where $\gamma_i = 1.36\,(x_i - 0.26)$

Field strength, $F = \frac{Z}{r_p^2}$

Where, the oxidation number of cations i, the ionic ratio with respect to total number of oxides, basicity moderating parameter and the Pauli electronegativity are represented by Z_i, r_i, γ_i and x_i respectively. Values of above listed parameters are represented in respective chapters.

2.2.2. X- Ray diffraction spectral analysis

A substance is possessing crystalline or non-crystalline state is confirmed by X-ray diffraction (XRD). In addition to this it provides clear insight to the crystallographic

structure of the unknown sample. One can determine lattice parameters and their orientations. XRD works on the basis of Bragg's law for diffraction. When an EM radiation (comparable to atomic spacing of the unknown sample) is incident on the given sample, it gets scattered. If the waves that are scattered by the sample are in phase results in constructive interference. Hence according to Bragg, the equation for constructive interference in between these waves is [106]:

$2d\ sin\theta\ = n\lambda$

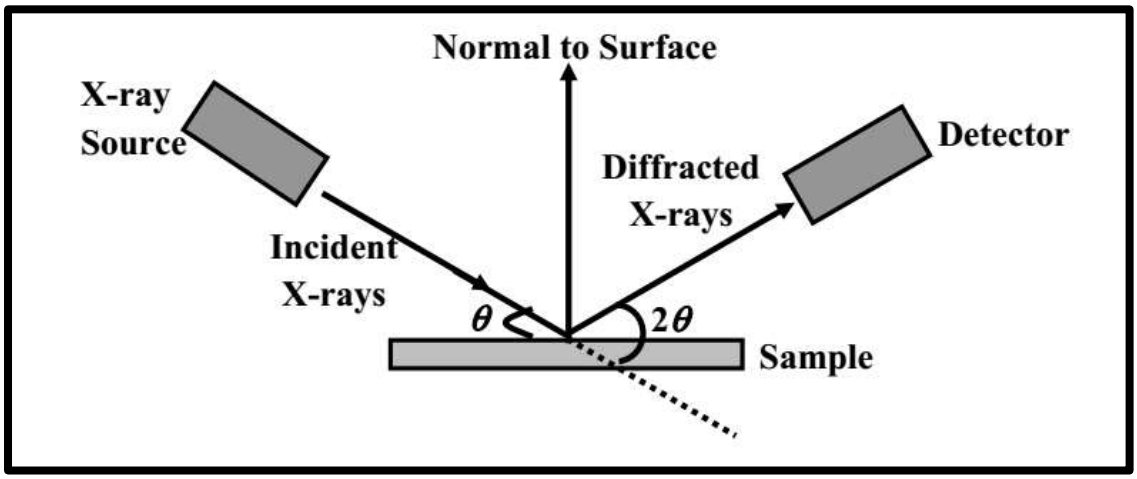

Fig. 2.2. Schematic representation of X-ray diffraction method.

Where, θ, d, n and λ are angle in between scattering plane and incident beam, interplanar spacing, an integer and wavelength of incident X-ray beam respectively. An X-ray diffractometer sketch is shown in Fig. 2.2, comprising of an x-ray source, sample plate and the detector. As per the Bragg's law, the angle at which it is satisfied for constructive interference, strong peaks are recorded in the detector. The angle and intensity of the peak is used for further calculation of structural data of the crystalline sample. Bruker built D8 advance X-ray diffractometer is shown in Fig. 2.3.

Fig. 2.3. Bruker D8 Advance X-ray diffraction machine.

2.2.3. FT-IR spectral analysis

Summation of rotational, electronic and vibrational energy levels of a molecule constitutes its total internal energy. When the IR range of EM radiation interacts with the spectroscopically effective ions, then this examination is known as IR spectroscopy. A molecule is shifted to higher vibrational states, when the IR radiation from the EM radiation is absorbed by the molecule. Here in the IR range, interaction among the radiation and molecule is in vibrational mode. Aforementioned facts led to the development of IR spectroscopy for structural analysis of the unknown sample. FT-IR spectroscopy works on principle of Michelson's interferometer. Fig. 2.4 represents the schematic diagram and FT-IR instrument used for the analysis.

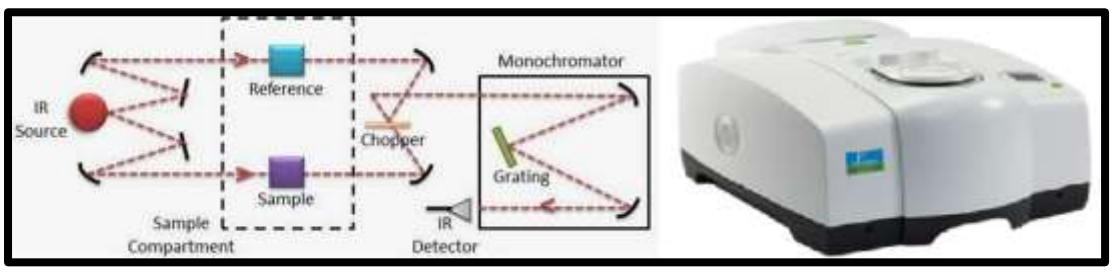

Fig. 2.4. Schematic diagram and Perkin Elmer's Frontier FT-IR Spectrometer.

We can find two mirrors placed at right angles to each other through a beam splitter. Among these two mirrors, one is moveable and other is fixed. Resultant beam from these two mirrors interferes and we can obtain the pattern through the implementation of Fourier transformation. For the present study we have used the undoped sample for the structural analysis. The undoped sample is crushed to its powdered form and mixed with KBr to form a pellet, which is subjected to 1.5 ton of mechanical pressure through hydraulic press.

2.3. Absorption spectra

Absorption spectroscopy is the examination of UV-vis-NIR range of EM radiation and the interacting molecule. Under this spectroscopic analysis, we can observe various transitions referring to structural groups of the molecule under absorption analysis. JASCO V-670 model and LAMBDA-950, Perkin Elmer, USA are used for the absorption spectral recordings. Absorption spectrophotometer simply quantify the percentage of radiation absorbed or transmitted in UV-vis-NIR range. The schematic diagram of absorption spectrophotometer comprises of various mirrors, filters, lenses and detector for the purpose and are shown in Fig. 2.5. Beer -Lambert's law is the principle behind the working of UV-vis-NIR spectrophotometer. According to the law, as per the passage of EM radiation in an absorbing medium, decrement in the intensity of radiation along with thickness of the absorbing medium is proportionate to the incoming beam along with the concentration of the solution [107]:

A= $log_{10}(\frac{I_t}{I_0})$

Here, I_0 and I_t represents the incident and the transmitted beam intensity. T= I/ I_0 is termed as transmittance. For the calculation of absorption coefficient (ν) following

equation is used [108] where d represents the thickness of the sample:

$$\alpha(\nu) = \frac{1}{d} \ln\left(\frac{I_t}{I_0}\right)$$

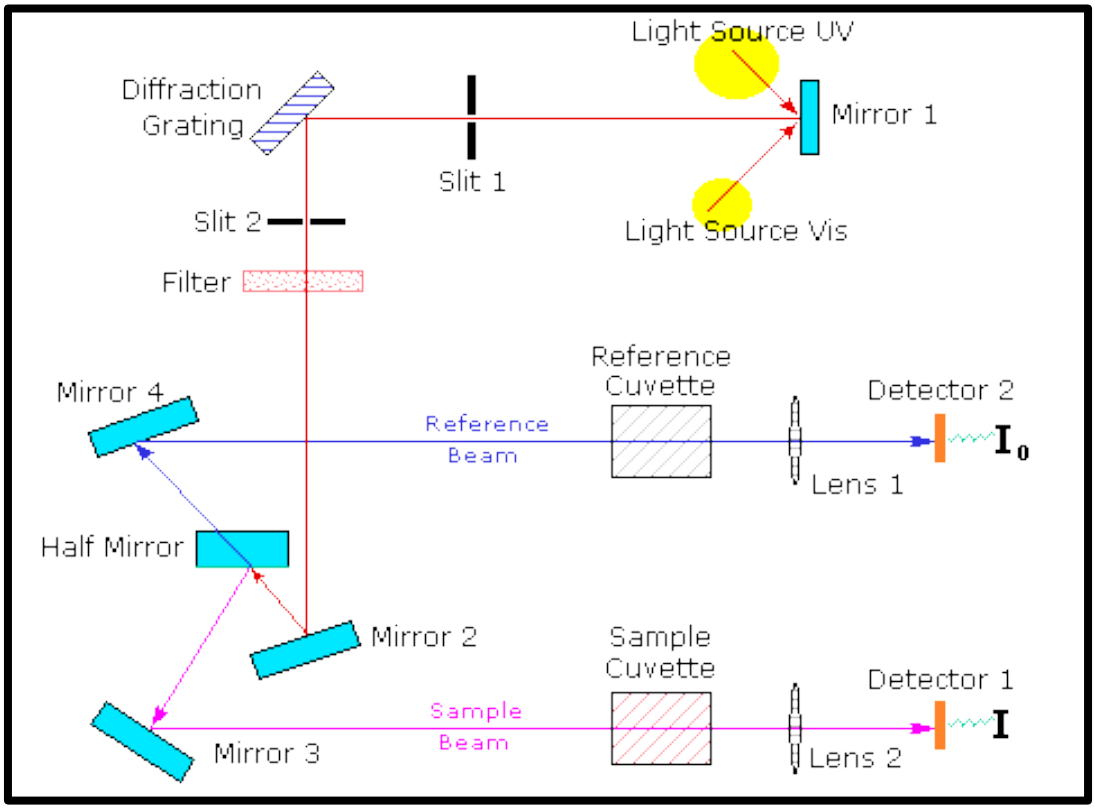

Fig. 2.5. Schematic working diagram of UV-vis-NIR spectrophotometer.

LAMBDA-950, Perkin Elmer UV-vis-NIR spectrophotometer is used for absorption recording and is shown in Fig. 2.6. In this technique the broad signals are converted into discrete wavelengths. The filters used in this technique prevent the overlapping of the diffracted lines. As per the double beam technique, we have here two beams, one is assigned for the sample and other as the reference beam which reaches to the detector. The detector used in this technique for IR range is lead sulphide (PbS) cell whereas for the UV and visible range is photomultiplier tube (PMT). Absorption analysis is conducted for RE ions doped LPZABS glasses.

Fig. 2.6. LAMBDA-950, Perkin Elmer, USA UV-vis-NIR spectrophotometer.

2.4. PL and lifetime measurements

Emission, excitation and decay measurements for a RE doped sample are signified as PL spectra. Pumping by a particular excitation, excites atom to higher state from which it decays back to original position via spontaneous emission of light, which is termed as PL. Under this mechanism the absorbed radiation is not identical to the one emitted by the material under PL examination. This process provides clear insight into the electronic structure of the material. Hence, it finds application in probing the forensics, pesticide examination, biochemistry and medicine, environmental analysis, food and pharmaceuticals studies, semiconductors and many more.

The PL spectra for the RE ions doped LPZABS glasses are recorded via Hitachi-F7000 (Sm^{3+} doped LPZABS glasses), JASCO FP-8300 (Sm^{3+}/Eu^{3+} doped LPZABS glasses) and SHIMADZU RF-5301 PC (Dy^{3+} doped LPZABS glasses) - Spectro fluorophotometer. The PL spectro fluorophotometer consists of a flash lamp and numerous filters to produce independent excitation and emission spectra. Fig. 2.7 represents the JASCO FP-8300 spectro-fluorophotometer used for the PL investigation for Sm^{3+}/ Eu^{3+} co-doped LPZABS glasses. Lifetime measurements for

Sm^{3+} doped and Sm^{3+}/Eu^{3+} doped LPZABS glasses were recorded via Hitachi-F7000 spectrofluorophotometer. When the decay in intensity is measured with respect to variation in time is termed as PL decay (lifetime measurements). For this recording, the prepared sample is intended to radiation in the form of a pulse acquiring constant excitation wavelength with the emission intensity marked on the time scale. In the entire process high speed detection unit is used for the recording of emission intensity.

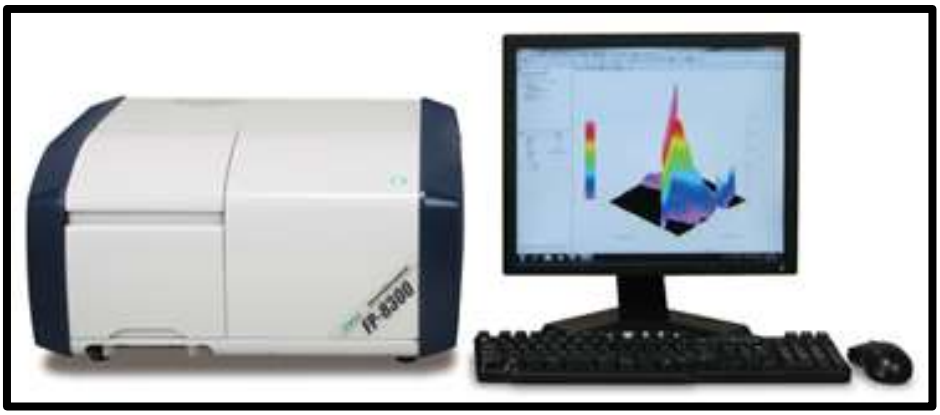

Fig. 2.7. JASCO FP-8300 spectro-fluorophotometer

****

CHAPTER 3

ORANGE COLOR EMITTING SM^{3+} IONS DOPED BOROSILICATE GLASSES FOR OPTOELECTRONIC DEVICE APPLICATIONS

This chapter deals with the synthesis of an undoped and Sm^{3+} ions doped LPZABS glasses. To understand the potentiality of the titled glasses in photonics, various spectroscopic techniques such as XRD, FT-IR, PL and PL decay were performed. Structural details are estimated by the XRD and FT-IR. While the luminescent properties are analysed by absorption, PL and PL decay measurements. By correlating the absorption and emission spectral features, radiative parameters are evaluated to understand the quantum efficiency of the titled glasses. Quantum efficiency and CIE coordinates evaluated reveals the suitability of the titled glasses for visible photonic device applications. All the results obtained allows to contemplate that, 1.0 mol% of Sm^{3+} ions concentration is optimum in LPZABS glass.

Aforementioned facts founded space in renowned International Journal,

Optical Materials 107(2020)110070.

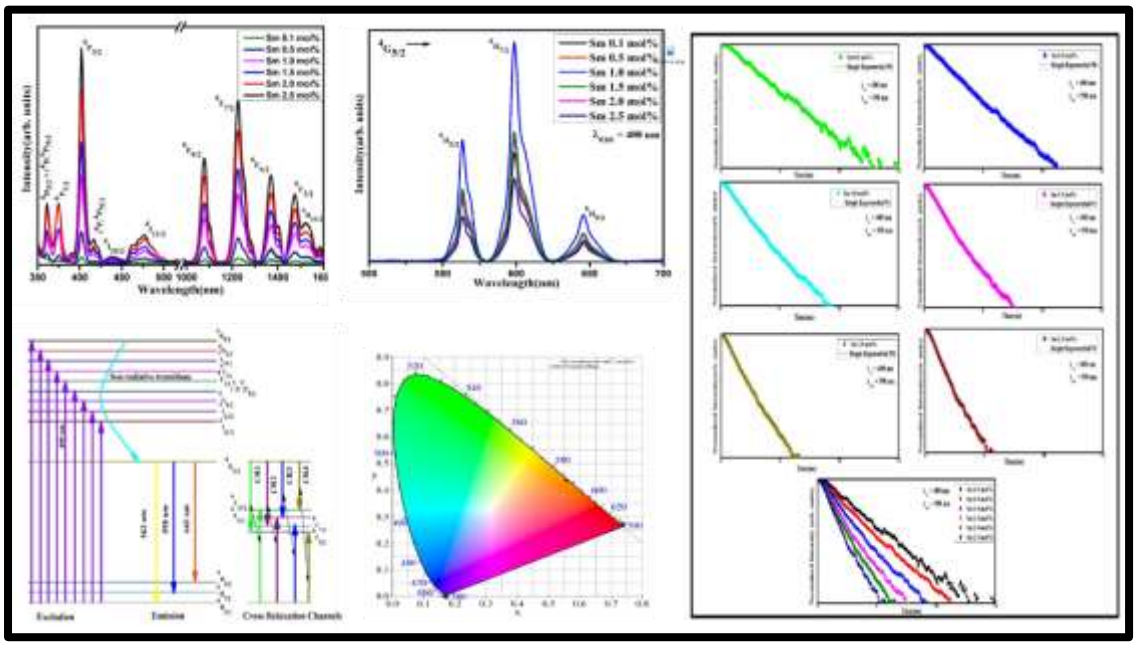

3.1. Introduction

The main aim of the present chapter is to understand the suitability of Sm^{3+} ions doped borosilicate host glass comprising the network modifiers and intermediates like Li_2O, PbO, ZnO and Al_2O_3 for visible photonic devices. Purpose of adding these constituents to a borosilicate glass is to reduce the redundant phonon energy of host glass system and to enhance the radiative emission. B_2O_3 and SiO_2 are used as the network formers, which possess brilliant characteristics like immense stability and immune to corrosion [109-117]. However, they suffer from high phonon energies, which we intend to reduce by addition of heavy metal oxides (HMO) like lead and zinc [118-120]. Fine radiative characteristics is built in the host glass, as these addends let some of the BO_3 units to transform into BO_4 units, leading to lesser radiationless transitions to take place. ZnO not only figures out how to improvise the optical but also the magnetic properties of the glassy system. It is the constituent which is highly hygroscopic as well as non-toxic in behavior. ZnO also provides huge intactness in the glass system, finding better emission properties [121]. Al_2O_3 as a very key usage in adding it to the RE ions containing host matrix. It prevents formation of RE-O-RE bonds as the distance between the RE ions is increased due to formation of Al-O-RE bonds. Hence it hinders the energy transfer among RE ions and elevates the emission efficiency of the glassy system [122-124]. Furthermore, adding Li_2O to the system with various constituents, helps in suppressing the formation of air bubbles leading to better stability. Glass transition temperature and thermal coefficient of expansion is also positively tailored by the addition of lithium oxide. Above mentioned constituents (Li_2O, PbO, ZnO, Al_2O_3, SiO_2 and B_2O_3) have been

hence incorporated in the glass matrix, which is termed as Lithium Lead Zinc Alumino Borosilicate (LPZABS) glass.

In the present research work, the LPZABS host glass is prepared via melt quench technique along with incorporation of Sm^{3+} ions in host matrix. Aiming towards study of spectral characteristic of RE ion doped LPZABS glasses and its optimization, several characterizations are performed on the prepared undoped and doped glass host like, XRD, FT-IR, UV-vis-IR spectroscopy, PL and PL decay measurements.

3.2. Synthesis and characterization

Selected materials are taken in stoichiometric ratio as per the molar equations:

$10Li_2O–5PbO\text{-}5ZnO\text{-}10Al_2O_3\text{-}10SiO_2\text{-}60B_2O_3$ and

$10Li_2O–5PbO\text{-}(5\text{-}x)ZnO\text{-}10Al_2O_3\text{-}10SiO_2\text{-}60B_2O_3\text{-}xSm_2O_3$, for the preparation of undoped and doped glass samples via melt quench technique. The preparation steps are shown in the flowchart below:

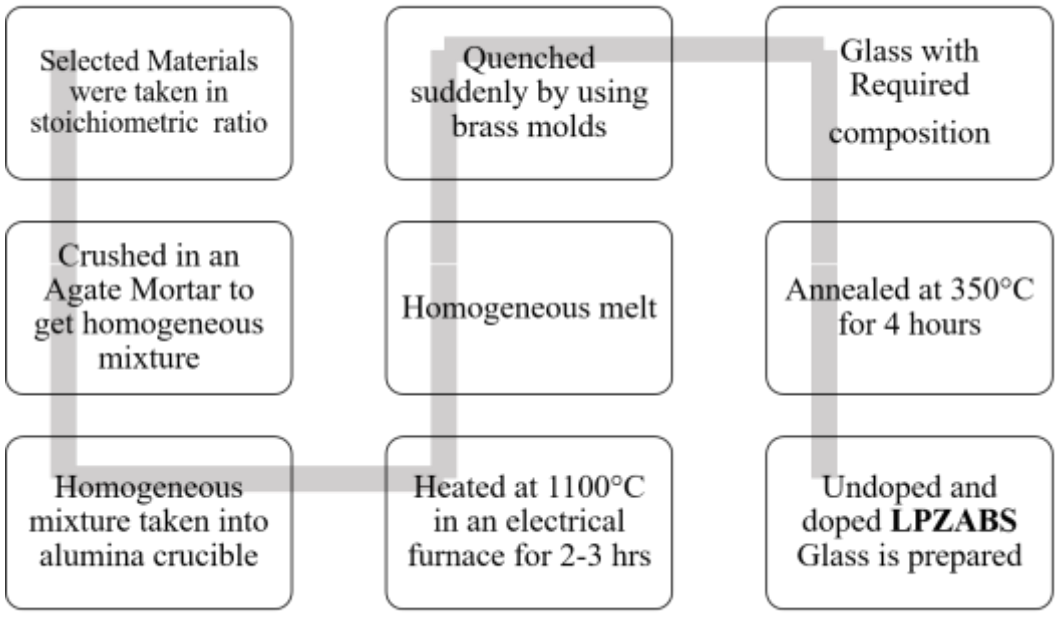

The final pellet so obtained are free from thermal and mechanical stresses, which are further processed for the various characterizations. Table 3.1 shows the value of different molar concentration kept for RE ion doped in selected host glass matrix and abbreviation used for the prepared glass samples.

Table 3.1 Abbreviations of LPZABS glasses undoped and doped with Sm^{3+} ions.

S.No.	Molar composition	Dopant mol%	Abbreviation Used
1	$10Li_2O–5PbO\text{-}5ZnO\text{-}10Al_2O_3\text{-}10SiO_2\text{-}60B_2O_3$	NIL	LPZABS
2	$10Li_2O–5PbO\text{-}(5\text{-}x)\ ZnO\text{-}10Al_2O_3\text{-}10SiO_2\text{-}60B_2O_3\text{-}xSm_2O_3$	0.1	Glass A
		0.5	Glass B
		1.0	Glass C
		1.5	Glass D
		2.0	Glass E
		2.5	Glass F

XRD, FT-IR, absorption, PL and PL decay spectral data was recorded for the prepared LPZABS glass samples. Densities and refractive indices were determined by Archimedes principle and Brewster's angle technique respectively.

3.3 Result and discussion

3.3.1. Structural analysis and physical properties

XRD pattern obtained for an un-doped LPZABS glass was represented in Fig. 3.1. Broad hump obtained at lower angle of diffraction (20°-30°) confirms the absence of any crystalline entity in the prepared compositions. The broad hump observed due to characteristics long-range disorder network of glass.

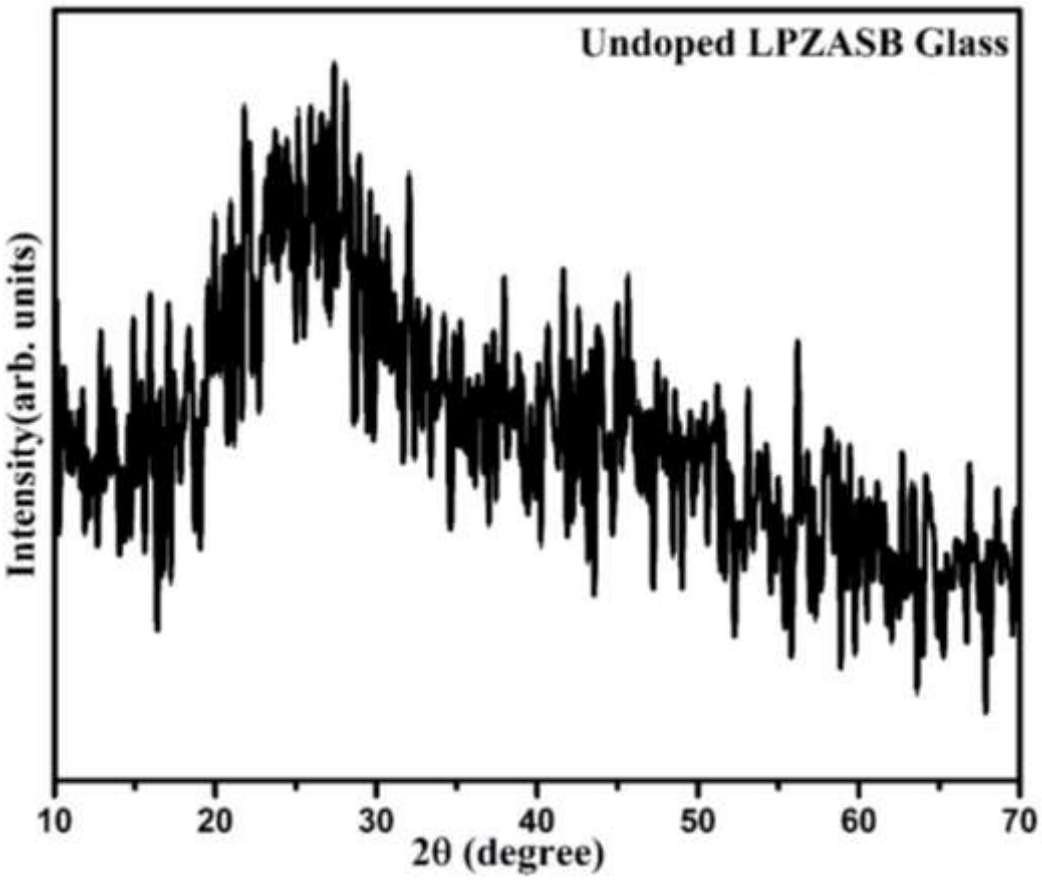

Fig. 3.1. XRD pattern for an un-doped LPZABS glass.

Taking inputs like density and refractive different physical parameters were evaluated and are depicted in Table 3.2. Necessary formulae needed to evaluate all the physical were collected from literature [105]. Density of a material can be used to understand degree of structural compactness and modifications occurring due to variations on doping percentage of constituents. From Table 3.2, it conspicuous that, the density and refractive index measured for LPZABS glasses are showing opposite trends (density increasing and refractive index decreasing) with increase in Sm^{3+} ion concentration. Increase in density with Sm^{3+} ion concentration indicates replacement of B_2O_3 with Sm_2O_3. On the other hand, decrease in refractive indices with increase in Sm^{3+} ion concentration is attributed to duel nature of ZnO. ZnO can acts as network

modified (at low Sm^{3+} ions concentration) as well as network former (at higher Sm^{3+} ion concentration). Molar volume shows the opposite trends with the Sm^{3+} ion concentration which indicates increase in non-bridging oxygen atoms and expansion of glass network with doping. Here, Sm^{3+} ions have high tendency to occupy interstitial sites in glass network created by added network modifiers. The glass network bonding can be analyzed by molar refractions which indicates the contribution of both oxygen ionic and cationic refractions. Relatively smaller values of field strengths obtained for titled glasses indicates high solubility of the Sm^{3+} ion in host glass. The non-linearity in molecular electronic polarization values gives most advantageous result to gather significant information about glass stability, chemical durability, optical absorption and dielectric properties of prepared glasses.

Table 3.2. Physical properties of Sm^{3+} ions in LPZABS glasses.

S.No	Physical Property	Glass A	Glass B	Glass C	Glass D	Glass E	Glass F
1	**Refractive index (n_d)**	1.5941	1.5939	1.5936	1.5934	1.5931	1.5929
2	**Density (gm/cm^3)**	2.5223	2.5303	2.5403	2.5503	2.5603	2.5703
3	**Average molecular weight**	80.86	81.93	83.26	84.6	85.94	87.27
4	**Sm^{3+} ion concentration, N(10^{22} ions/cm^3)**	0.187	0.930	1.837	2.723	3.588	4.434
5	**Mean atomic volume (g/cm^3/atom)**	0.117	0.118	0.119	0.121	0.122	0.124
6	**Dielectric constant (ϵ)**	2.5411	2.540	2.539	2.538	2.537	2.533
7	**Optical susceptibility ($\epsilon - 1$)**	1.541	1.540	1.539	1.538	1.537	1.535
9	**Reflection losses (R %)**	5.245	5.2422	5.2381	5.2354	5.2313	5.2286
10	**Molar refraction (R_m)(cm^{-3})**	10.87	10.98	11.11	11.24	11.37	11.50
11	**Polaron radius (r_p) (Å)**	3.26	1.91	1.52	1.33	1.22	1.13
12	**Inter-atomic distance (r_i) (Å)**	8.10	4.75	3.78	3.32	3.03	2.82
13	**Molecular electronic polarizability (10^{-23} cm^3)**	4.31	0.871	0.440	0.297	0.225	0.182
14	**Optical basicity (Λ_{th})**	0.331	0.342	0.356	0.367	0.371	0.378
15	**Field Strength F (X10^{15} cm^{-2})**	2.812	8.169	12.86	16.72	20.09	23.14

3.3.2. FT-IR analysis

Fig. 3.2 has FT-IR spectrum recorded for an un-doped LPZABS glass. This is mainly used to understand the local structure and functional groups present in LPZABS glass. Absorption band at 702 cm^{-1} confirms presence of Si-O-B linkages in the glass structure. The absorption bands in the region from 1200-1500 cm^{-1} arises due to BO_3 structural units. The band at 1384 cm^{-1} is due to stretching vibrations of trigonal BO_3 units. Edges at 1528 cm^{-1} and 1603 cm^{-1} occurs due to Si-OH stretching. Above 2300 cm^{-1}, bands represent the existence of hydroxyl groups. Here, wide bands at 2350 cm^{-1}, 3455 cm^{-1} and 3849cm^{-1} signifies symmetric O-H stretching. Quantifying the amount of OH content in a glass has importance it reduces radiative emission, thereby decreases quantum efficiency. More OH content less will be the quantum efficiency and vice versa [125-127].

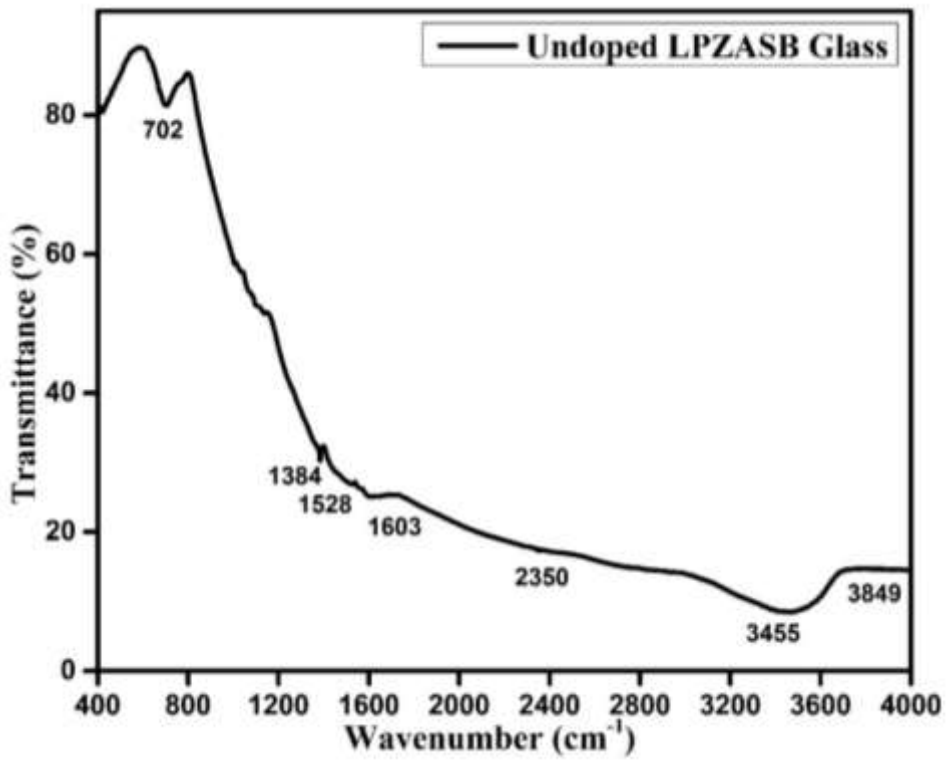

Fig. 3.2. FT-IR spectrum for pure LPZABS glass.

The OH content present in a material is measured by following equation:

$$\alpha_{OH} = ln\ (T_0/T_D)/l$$

where, l is glass sample thickness and T_0/T_D is the ratio of maximum transmittance to transmittance at 3000 cm^{-1}. The OH content estimated using the above formula for the as prepared glass is 181.8 ppm. Relatively less OH content present in the as prepared glass shows potentiality of LPZABS glass to act like a good luminescent material.

3.3.3. Analysis of optical absorption spectra and bonding parameters

Optical absorption spectra of LPZABS glasses doped with varying concentrations of Sm^{3+} ions are shown in Fig. 3.3. Spectra shown in Fig. 3.3 is quite similar and comparable to the results observed in previous studies [128]. Obtained spectra enclose several bands corresponding to different f-f transitions between different energy levels of Sm^{3+} ion and its ground state $^6H_{5/2}$ when placed in LPZABS host matrix. Fig. 3 clearly show eleven absorptions peaks originated from $^6H_{5/2}$ ground state to various higher energy states at 360, 374, 402, 416, 438, 477, 1078, 1222, 1371, 1472 and 1523 nm Absorption bands identification and assignment was done as per the procedure outlined by Carnal [129]. These absorption bands were occurred mostly due to induced electric dipole and magnetic dipole contributions and follow $|\Delta J| \leq 6$ and $|\Delta J| = 0, \pm 1$ selection rules respectively [130]. From Fig. 3.3, the most intense transition in visible region is at 402 nm ($^6H_{5/2} \rightarrow {}^6P_{3/2}$) and in NIR region at 1078, 1222 & 1371 nm ($^6H_{5/2} \rightarrow {}^6F_{9/2}$, $^6F_{7/2}$, $^6F_{5/2}$). Transitions from $^6H_{5/2}$ ground state to excited ^6H and ^6F_J states are spin allowed in nature ($|\Delta S| = 0$) and usually observed when material is exposed in NIR region. These transitions are intense and distinct, as

they arise due to effective shielding of 4f shells by inner 5s and 5p electrons in Sm^{3+}-ion system.

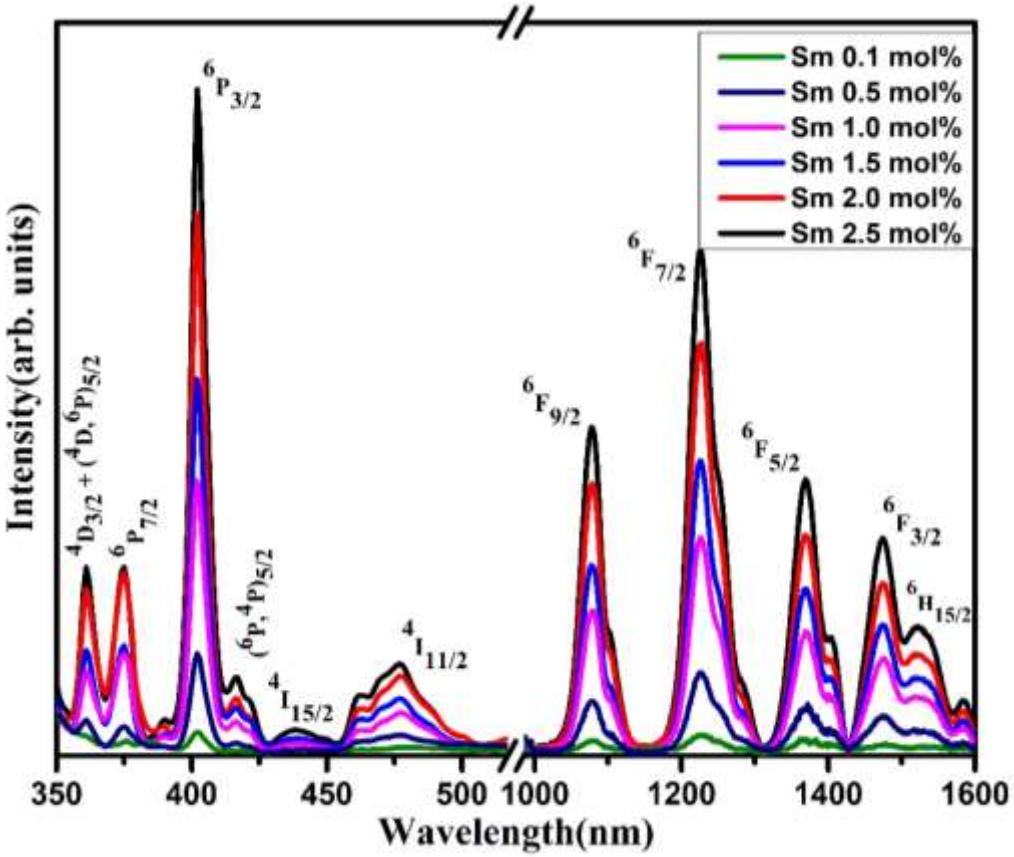

Fig. 3.3. Absorption spectra of Sm^{3+} ions in LPZABS glasses.

Generally, nephelauxetic effect usually arise from the partially filled f-orbitals of RE ion. In present study, nephelauxetic effect results in deformation of 4f-electronic orbitals of Sm^{3+} ion located in ligand field of LPZABS glass matrix. Nephelauxetic ratio (denoted by β) while bonding parameters (denoted by δ) determine the covalency of bond between RE ions (i.e., Sm^{3+}-ions in present case) and neighboring oxygen in host glass matrix. [131, 132]. β and δ are evaluated as per equations mentioned in chapter 1 and are shown in Table 3.3. Average of β is $\bar{\beta}$ and its values are decreasing from 1.0077 to 1.0064 with Sm^{3+} ion concentration from x =0.1 to x =2.5 mol% in LPZABS glasses. δ values for glass A to F are -0.7633, -0.7376,

-0.6918, -0.6766 -0.6668 and -0.6401 respectively. Negative values of δ indicates nature of bonding between Sm^{3+} ions and nearby ligands as ionic in LPZABS glasses. Overall increase in value of δ (towards positive side on scale) with Sm^{3+} ion content marks decrease in ionic character existing between Sm^{3+} ions and oxygen ligands in the titled glasses.

3.3.3.1. Oscillator strength and Judd-Ofelt (J-O) analysis

To understand radiative properties possessed by Sm^{3+} ions in the titled glasses, J-O theory was employed to energies of absorption bands called experimental oscillator strength (f_{exp}). The J-O intensity parameters (Ω_2, Ω_4 and Ω_6) are essential to calculate various radiative properties of doped RE ions in a host material. Apart from this, they are also useful in understanding the structural disorder in the vicinity of RE ions (i.e., Ω_2) and bulk properties (i.e., Ω_4 and Ω_6) like rigidity and viscosity [133-135]. Experimental and calculated oscillator strengths (f_{exp}) & (f_{cal}) and δ_{rms} is measured as per relations given in chapter 1 and are reported in Table 3.3. Hypersensitive transitions which are actually the electric dipole in nature will follow the selection rule $|\Delta S| = 0$, $|\Delta L| \leq 2$, $|\Delta J| \leq 2$ [136]. Quadrupole transitions discussed on the basis of $||U^{\lambda}||$ matrix element, which is a reduced matrix element of 2, 4 and 6 rank tensor operators. These transitions mostly depend on $||U^2||$ and independent of $|U^4||$ and $||U^6||$ matrix elements. From Fig. 3.3, the variation in relative area under the curve for highly intense/hypersensitive transitions i.e., $^6H_{5/2} \rightarrow {}^6P_{3/2}$ (in visible region) and $^6H_{5/2} \rightarrow {}^6F_{7/2}$ (in NIR region) gives the enough information to explain the degree of hypersensitivity acquired by Sm^{3+} ion in LPZABS glasses. J-O theory has been widely used for gathering information about intensities of 4f electrons of RE ions in solids and liquid solutions.

Table 3.3. Experimental (f_{exp}) ($x10^{-6}$), calculated (f_{cal}) ($x10^{-6}$) oscillator strengths, r.m.s deviation (δ_{rms}), refractive index (n_d), nephelauxetic ratio ($\bar{\beta}$) and bonding parameters of Sm^{3+} ions in LPZABS glasses.

Transitions $^6H_{5/2}\rightarrow$	Glass A		Glass B		Glass C		Glass D		Glass E		Glass F	
	f_{exp}	f_{cal}	f_{exp}	f_{cal}	f_{exp}	f_{cal}	f_{exp}	f_{cal}	f_{exp}	f_{cal}	f_{exp}	f_{cal}
$^6H_{15/2}$	0.07	0.01	.072	.0111	0.117	0.012	0.23	0.014	0.25	0.016	0.47	0.16
$^6F_{3/2}$	0.16	0.11	.256	.2033	0.297	0.264	0.30	0.26	0.44	0.39	0.68	0.64
$^6F_{5/2}$	0.90	1.14	.957	1.209	1.27	1.42	1.28	1.45	1.31	1.53	1.49	1.69
$^6F_{7/2}$	2.038	1.915	2.19	2.09	2.36	2.34	2.57	2.56	2.87	2.83	2.99	2.94
$^6F_{9/2}$	1.07	1.22	1.22	1.35	1.494	1.497	1.67	1.68	1.85	1.91	1.87	1.95
$^4I_{11/2}$	0.28	0.08	0.40	.09	0.56	0.099	0.58	0.11	0.73	0.13	0.92	0.13
$^4I_{15/2}$	0.22	0.215	0.30	0.24	0.36	0.263	0.49	0.29	0.58	0.33	0.69	0.33
$(^6P,^4P)_{5/2}$	0.20	0.39	0.25	0.41	0.28	0.478	0.33	0.49	0.48	0.50	0.59	0.54
$^6P_{3/2}$	3.67	2.60	3.82	2.71	3.98	3.178	4.15	3.25	4.39	3.34	4.5	3.59
$^6P_{7/2}$	0.34	0.73	0.40	0.82	0.45	0.902	0.68	1.02	0.96	1.16	1.13	1.19
$^4D_{3/2}+(^4D,^6P)_{5/2}$	0.32	0.358	0.38	0.37	0.42	0.438	0.56	0.45	0.79	0.46	0.88	0.49
$\delta_{rms}(x\ 10^{-6})$	±0.366		±0.386		±0.323		±0.342		±0.402		±0.424	
n_d	1.5941		1.5939		1.5936		1.5934		1.5931		1.5929	
$\bar{\beta}$	1.0077		1.0074		1.0070		1.0068		1.0067		1.0064	
δ	-0.7633		-0.7376		-0.6918		-0.6766		-0.6668		-0.6401	

The three J-O parameters are reported in Table 3.4. The hypersensitive transitions influence the magnitude of J-O parameters. Ω_2 is directly connected to covalency, hypersensitivity and symmetry of metal-ligand bond. The Ω_4 and Ω_6 intensity parameters revealing rigidity of host LPZABS glass medium where the Sm^{3+} -ions are located [137-140]. As given in Table 3.4, the trend of J-O intensity parameters is: $\Omega_4 > \Omega_2 > \Omega_6$, for LPZABS glasses. The observed trend in parameters suggests fine probability of cubic symmetry around Sm^{3+} ions. Magnitude of Ω_4 which is relatively greater than Ω_6 and Ω_2 indicates variation of crystal field of Sm^{3+}-ions from the cubic

symmetry [141-147]. For comparison purpose, the J-O parameters measured for various other Sm^{3+} ions doped solids are compared with values attained and are presented in Table 3.4 which are in analogy to the values reported in literature [148-152].

Table 3.4. Judd-Ofelt Parameters ($\Omega_\lambda \times 10^{-20} cm^2$) of Sm^{3+} ions in LPZABS glasses along with other reported values.

Glass System	Ω_2	Ω_4	Ω_6	Trend	References
Glass A	1.497	2.380	1.365	$\Omega_4 > \Omega_2 > \Omega_6$	Present work
Glass B	1.522	2.475	1.511	$\Omega_4 > \Omega_2 > \Omega_6$	Present work
Glass C	1.684	2.904	1.672	$\Omega_4 > \Omega_2 > \Omega_6$	Present work
Glass D	1.893	2.976	1.743	$\Omega_4 > \Omega_2 > \Omega_6$	Present work
Glass E	2.168	3.055	1.307	$\Omega_4 > \Omega_2 > \Omega_6$	Present work
Glass F	2.217	3.283	0.514	$\Omega_4 > \Omega_2 > \Omega_6$	Present work
Tellurite	3.17	3.65	1.61	$\Omega_4 > \Omega_2 > \Omega_6$	[148]
PKANbSm10	6.89	10	2.96	$\Omega_4 > \Omega_2 > \Omega_6$	[149]
SKBL-0.5Sm^{3+}	2.81	3.05	1.52	$\Omega_4 > \Omega_2 > \Omega_6$	[150]
TeO_2-WO_3-ZrO_2-Sm_2O_3	2.01	4.38	1.56	$\Omega_4 > \Omega_2 > \Omega_6$	[151]
$Li_2B_4O_7$ or 33.33Li_2O-66.66B_2O_3	3.19	5.68	2	$\Omega_4 > \Omega_2 > \Omega_6$	[152]

3.3.4. PL spectral analysis

Intense emission spectra can be obtained at an excitation wavelength corresponding to most intense excitation band. In order to determine this preferential excitation wavelength (λ_{exc}) firstly, the excitation spectra are recorded by fixing emission at 598 nm and represented in Fig. 3.4. As show in Fig. 3.4, a transition observed at 400 nm ($H_{5/2} \rightarrow {}^4F_{7/2}$) is most intense and is employed to get PL spectra of Sm^{3+} doped LPZABS glasses. A series of excitation bands observed from 341 to 471nm in the as prepared glasses indicates that, Sm^{3+} ion in LPZABS glasses can be pumped by commercially available UV-blue & bluish green LEDs. Fig. 3.5, has PL spectra obtained for LPZABS

glasses under λ_{exc}= 400 nm. The PL spectra depicted in Fig. 5 has three bands in visible region at wavelengths 562nm (yellow), 598nm (orange) and 645nm (red) for $^4G_{5/2} \rightarrow {}^6H_{5/2}$, $^4G_{5/2} \rightarrow {}^6H_{7/2}$ and $^4G_{5/2} \rightarrow {}^6H_{9/2}$ transitions, respectively [153].

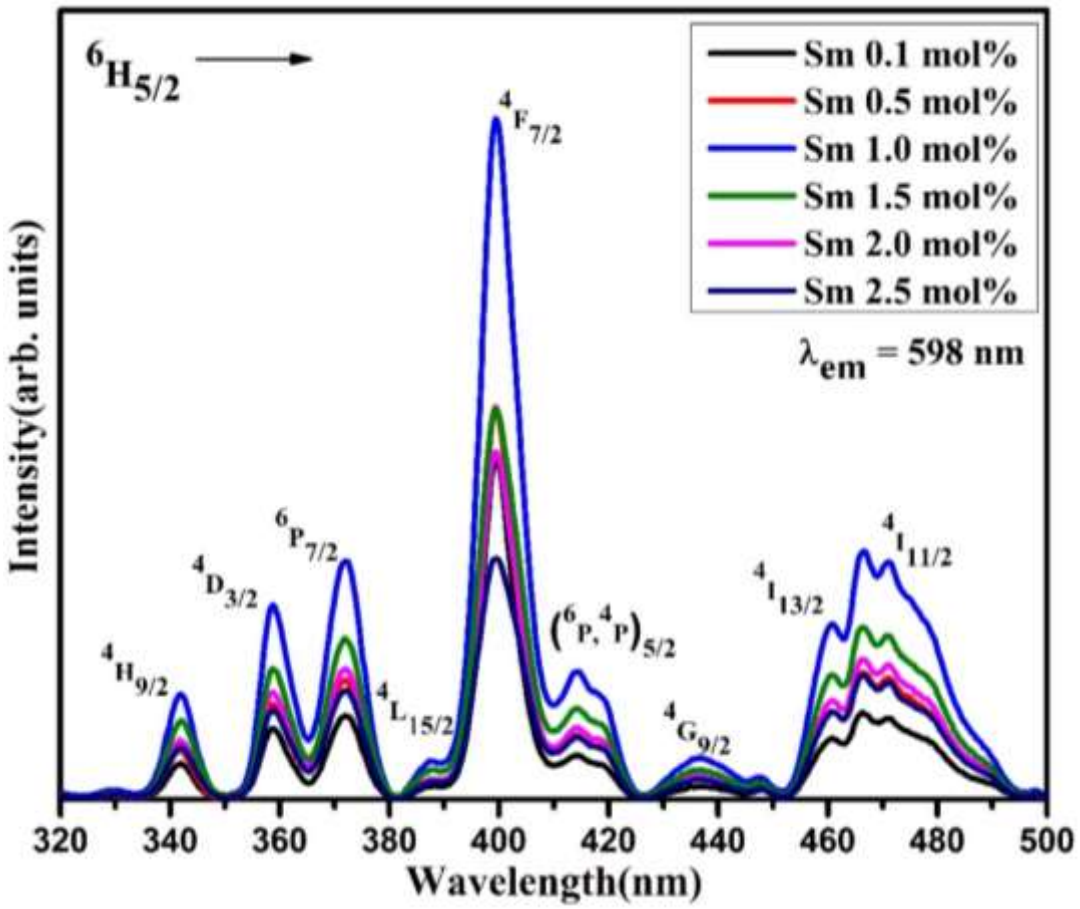

Fig. 3.4. Excitation spectra of Sm^{3+} ions in LPZABS glasses under 598 nm emission.

As show in Fig.3.5, the intensity of all the emission bands increases with Sm^{3+} ion content up to 1.0 mol% and beyond decreases due to concentration quenching because of cross relaxation energy transfer. The magnetic dipole allowed transition $^4G_{5/2} \rightarrow {}^6H_{7/2}$ obeys selection rule $\Delta J \leq 1$, while transition $^4G_{5/2} \rightarrow {}^6H_{9/2}$ is an electric dipole allowed transition. Ratio of intensity of ED transition to MD transition signifies the asymmetry of Sm^{3+} ions in LPZABS host network [154]. Asymmetry ratios are calculated to be 0.2058, 0.2252, 0.21851, 0.2253, 0.2248 and 0.2280 for

glasses with x = 0.1, 0.5, 1.0, 1.5, 2.0, 2.5 mol% respectively. Highest value of asymmetric ratio is for glass with x =2.5 mol% show high local disorder while the value is least for glass with x = 0.1 mol% indicate comparatively high symmetry for Sm^{3+} ions in the LPZABS glass matrix. Overall conclusion from obtained results is that, Sm^{3+} ions are in presence on an inverse symmetry site in selected host matrix as the values of asymmetric ratios are < 1 for all as prepared glasses.

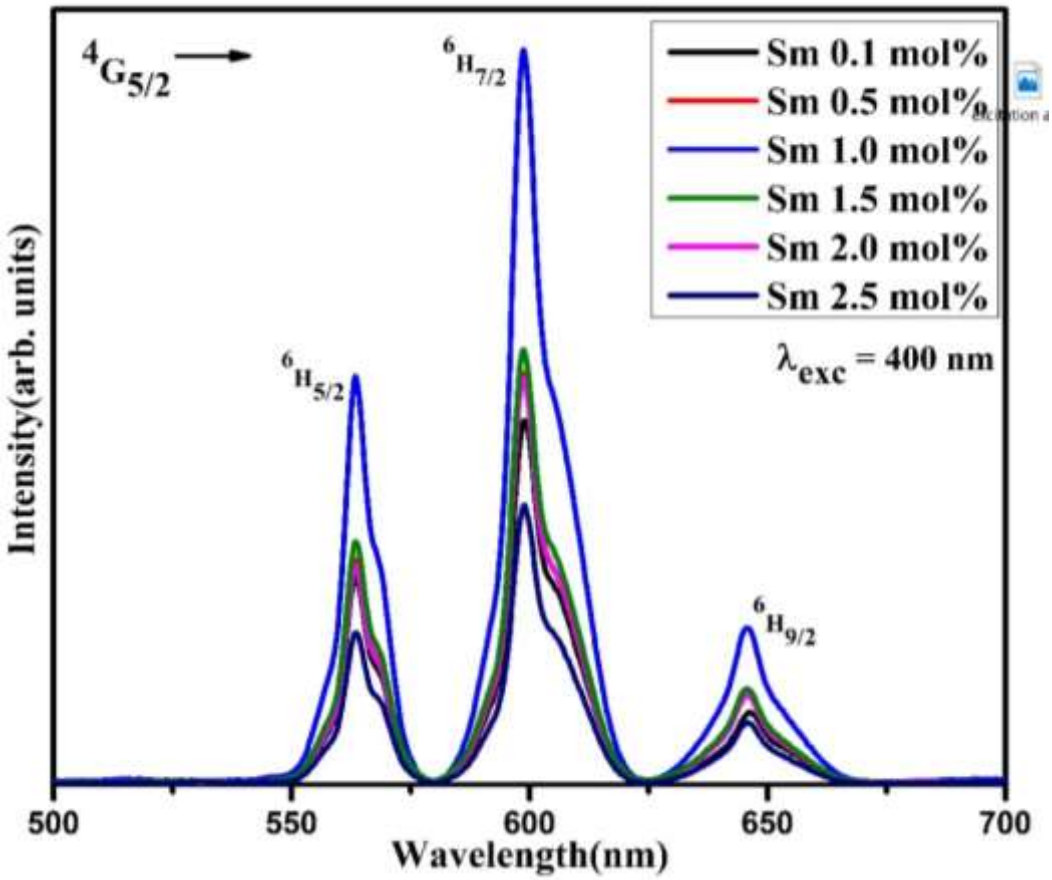

Fig. 3.5. Emission spectra of Sm^{3+} ions in LPZABS glasses under 400 nm excitation.

The excitation, radiative & non-radiative emissions and energy transfer cross-relaxation channels observed for LPZABS glasses are shown in Fig. 3.6. As shown in Fig. 3.6, under 400 nm intense excitation, the atoms will reach to energy states existing above $^4G_{5/2}$ level. The closely placed higher energy levels above $^4G_{5/2}$ energy

state suffer non-radiative transitions towards $^4G_{5/2}$ level causing high population in $^4G_{5/2}$ level. Radiative emissions occur by transition between $^4G_{5/2}$ and $^6F_{11/2}$ all due to wide energy gap of about 7250 cm^{-1}. Hence depopulation of $^4G_{5/2}$ level takes place by radiative transitions and relaxation through non radiative transitions. The radiative transitions take place from $^4G_{5/2}$ to lower levels with emission in yellow (562nm), blue (598nm) and orange (645nm) region of visible spectrum (as shown in Fig. 3.6). For Sm^{3+} ions doped LPZABS glasses possible cross-relaxation channels are as follows [155, 156]:

CR1: $^4G_{5/2}$, $^6H_{5/2} \rightarrow {}^6F_{7/2}$, $^6F_{9/2}$

CR2: $^4G_{5/2}$, $^6H_{5/2} \rightarrow {}^6F_{9/2}$, $^6F_{7/2}$

CR3: $^4G_{5/2}$, $^6H_{5/2} \rightarrow {}^6F_{5/2}$, $^6F_{11/2}$

CR4: $^4G_{5/2}$, $^6H_{5/2} \rightarrow {}^6F_{11/2}$, $^6F_{5/2}$

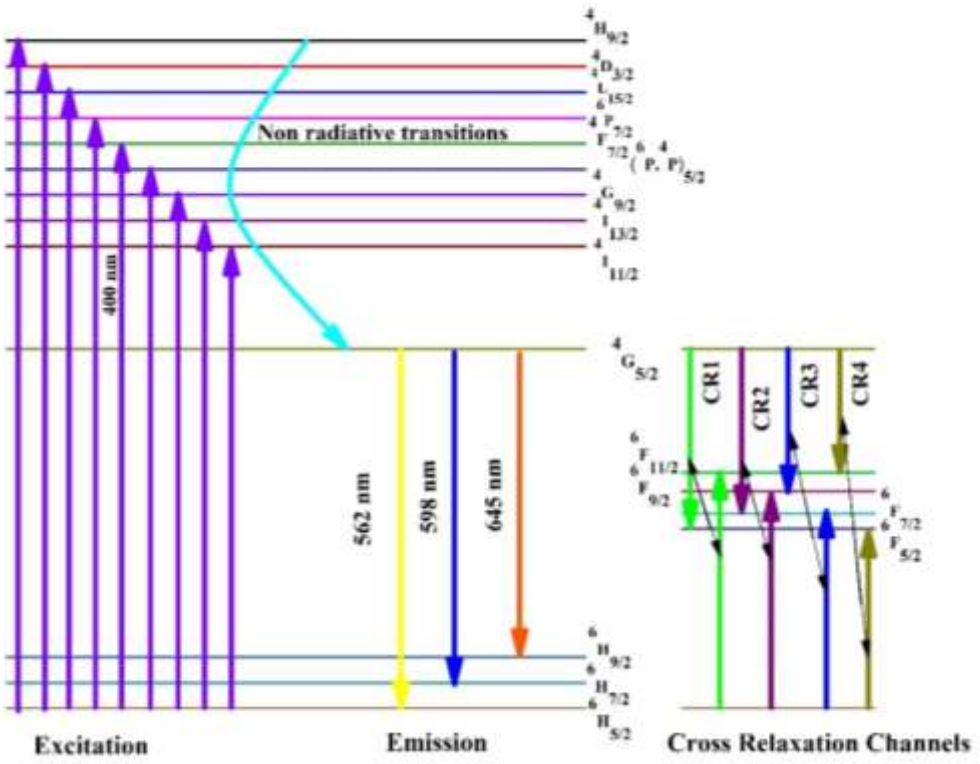

Fig. 3.6. Partial energy level diagram showing excitation, emission and cross-relaxation mechanism for Sm^{3+} ions in LPZABS glasses.

According to the Dexter theory, dipole-dipole interaction, quadrupole-quadrupole interaction and dipole-quadrupole interionic interaction are the three interactions within the activator ions effected by nearest neighbor ions for s = 6, 10 and 8 respectively [157]. Dexter Morgan has given a mathematical relation between concentration of activator ions and intensity as:

$$\log\frac{I}{c} = \log f - \frac{s\,log(c)}{d}$$

where, the symbols with standard explanation as in reference [157]. show graph plotted between log (I/c) versus log(c) is presented in Fig. 3.7. Slope of linear fit is -1.96 for higher concentrations of Sm^{3+} ions.

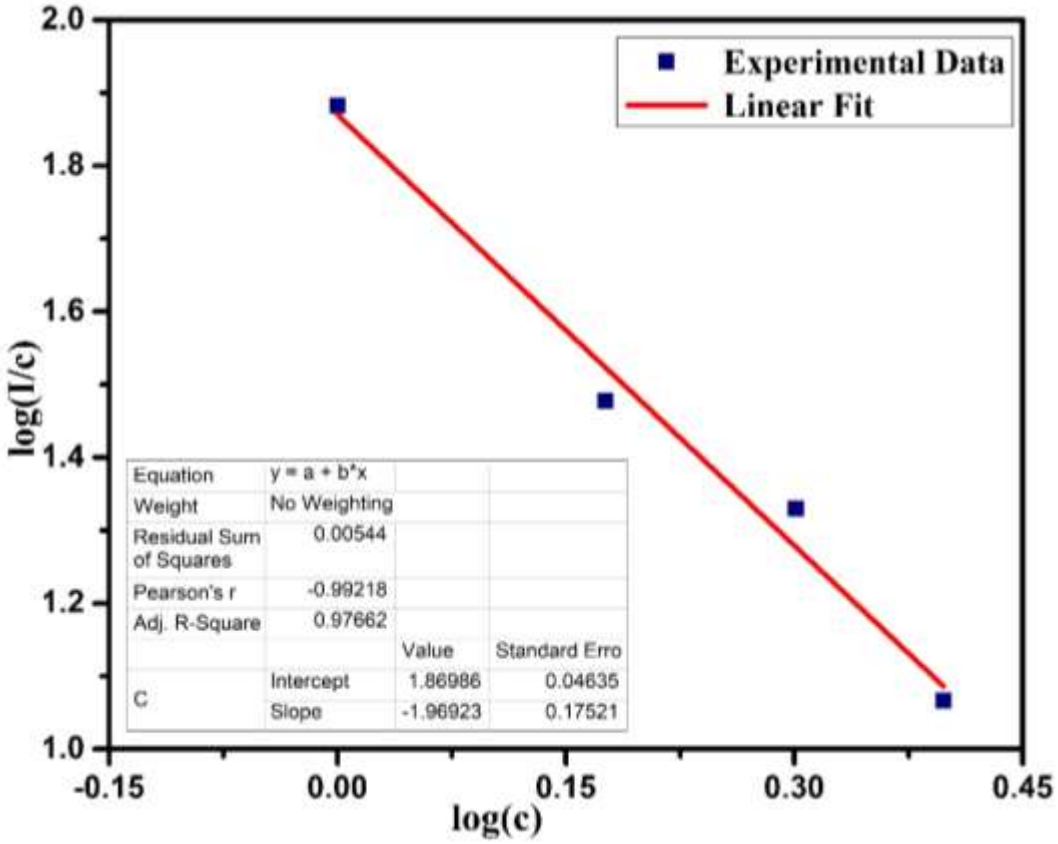

Fig. 3.7. Plot of log (I/c) v/s log (c) of Sm^{3+} ions in LPZABS glasses.

Hence the value of "s" so obtained is 5.88, which is approximate to 6. This allows us to contemplate that, dipole-dipole interaction is responsible mechanism observed due to concentration quenching in LPZABS glasses.

3.3.4.1 Radiative properties

Lasing potentiality of Sm^{3+} ions in titled glasses are explained by evaluation of radiative parameters like transition probabilities (A_R), total transition probability (A_T), branching ratios (β_R) and radiative lifetimes (τ_R) utilizing equations available in literature is discussed in chapter 1. The A_R, A_T, τ_R and β_R values evaluated for LPZABS glasses are given in Table 3.5. Probability of occurrence of emission cross section will be higher, if β_R value is ≥ 0.5. The glass sample with 1.0 mol% of Sm^{3+} ions show branching ratio (β_R) around 0.5 and can be used in laser action.

Table 3.5. Transition probability (A_R) (s^{-1}), total transition probability (A_T) (s^{-1}), measured and experimental branching ratio (β_{exp} and β_R) and radiative lifetimes (τ_R) (μs) for observed emission transitions of Sm^{3+}ions in LPZABS glasses.

Sample name	Transition	A_R	A_T	β_R	β_{exp}	τ_R
	$^4G_{5/2} \rightarrow {}^6H_{9/2}$	46.38		0.2839	0.2428	
Glass A	$^4G_{5/2} \rightarrow {}^6H_{7/2}$	64.57	163.34	0.3953	0.4856	6122
	$^4G_{5/2} \rightarrow {}^6H_{5/2}$	16.53		0.1012	0.1398	
	$^4G_{5/2} \rightarrow {}^6H_{9/2}$	62.96		0.2891	0.2451	
Glass B	$^4G_{5/2} \rightarrow {}^6H_{7/2}$	88.04	217.77	0.4042	0.4940	4592
	$^4G_{5/2} \rightarrow {}^6H_{5/2}$	25.66		0.1178	0.1427	
	$^4G_{5/2} \rightarrow {}^6H_{9/2}$	106.95	333.11	0.3210	0.2524	
Glass C	$^4G_{5/2} \rightarrow {}^6H_{7/2}$	164.71		0.4944	0.5950	3002
	$^4G_{5/2} \rightarrow {}^6H_{5/2}$	28.43		0.0853	0.1520	
	$^4G_{5/2} \rightarrow {}^6H_{9/2}$	119.77		0.3276	0.2430	
Glass D	$^4G_{5/2} \rightarrow {}^6H_{7/2}$	155.29	365.49	0.4248	0.5482	2736
	$^4G_{5/2} \rightarrow {}^6H_{5/2}$	30.17		0.0825	0.1534	
	$^4G_{5/2} \rightarrow {}^6H_{9/2}$	129.69		0.3352	0.2512	
Glass E	$^4G_{5/2} \rightarrow {}^6H_{7/2}$	158.9	386.9	0.4107	0.5049	2584
	$^4G_{5/2} \rightarrow {}^6H_{5/2}$	28.19		0.0728	0.1499	
	$^4G_{5/2} \rightarrow {}^6H_{9/2}$	140.34		0.3261	0.2474	
Glass F	$^4G_{5/2} \rightarrow {}^6H_{7/2}$	189.18	430.29	0.4396	0.4831	2324
	$^4G_{5/2} \rightarrow {}^6H_{5/2}$	30.9		0.0718	0.1485	

Apart from branching ratio, the larger values of stimulated emission cross section (σ_{se}) is another important property for lasers to have high gain. Higher value of σ_{se} gives larger optical gain with lower low threshold value. Value of "σ_{se}" is estimated using equations provided in literature and is detailed in chapter 1. Table 3.6. gives the values of λ_P, $\Delta\lambda_P$, σ_{se} for the titled glasses. σ_{se} values are relatively larger for 1.0

mol% of Sm^{3+} ions in LPZABS glasses for all the reported emission transitions. For advanced photonic devices and optical fibers the laser parameters λ_P,$\Delta\lambda_P$, β_R& β_{exp}, σ_{se}, $\sigma_{se} \times \Delta\lambda_P$ and $\sigma_{se} \times \tau_R$ must have higher values. The data given in Table 3.6 finally reveals that, 1.0 mol% of Sm^{3+} ions in the titled glasses is optimum for luminescent applications in visible orange region.

Table 3.6. Emission peak wavelength (λ_P) (nm), effective band widths ($\Delta\lambda_P$)(nm), stimulated emission cross-sections (σ_{se}) (cm^2), gain band width ($\sigma_{se} \times \Delta\lambda_P$) ($cm^3$) and optical gain parameters ($\sigma_{se} \times \tau_R$) ($cm^2$ s) for emission transitions for Sm^{3+} ions in LPZABS glasses.

Spectral parameters	Glass A	Glass B	Glass C	Glass D	Glass E	Glass F
$\lambda_P = 562\ nm$ ($^4G_{5/2} \rightarrow {}^6H_{5/2}$)						
Δλp	8.64	8.64	8.73	8.77	8.33	8.98
σ_{se} **(x 10^{-22})**	0.99	1.54	1.79	1.78	1.75	1.79
$\sigma_{se} \times \Delta\lambda_P$ **(x 10^{-28})**	0.86	1.33	1.57	1.56	1.46	1.61
$\sigma_{se} \times \tau_R$ **(x 10^{-25})**	6.10	7.10	5.39	4.87	4.52	4.16
$\lambda_P = 598\ nm$ ($^4G_{5/} \rightarrow {}^6H_{7/2}$)						
Δλp	11.30	10.51	10.4	10.97	11.15	11.99
σ_{se} **(x 10^{-22})**	3.83	5.63	10.67	9.51	9.59	10.61
$\sigma_{se} \times \Delta\lambda_P$ **(x 10^{-28})**	4.34	5.92	11.10	10.44	10.69	12.73
$\sigma_{se} \times \tau_R$ **(x 10^{-25})**	23.50	25.85	32.03	26.04	24.78	24.67
$\lambda_P = 645\ nm$ ($^4G_{5/2} \rightarrow {}^6H_{9/2}$)						
Δλp	12.30	11.67	11.56	12.88	12.35	12.85
σ_{se} **(x 10^{-22})**	3.41	4.87	8.37	8.40	9.49	9.87
$\sigma_{se} \times \Delta\lambda_P$ **(x 10^{-28})**	4.19	5.69	9.67	10.83	11.73	12.70
$\sigma_{se} \times \tau_R$ **(x 10^{-25})**	20.85	22.38	25.12	22.99	24.53	22.95

3.3.5. PL decay analysis

Fig. 3.8. show PL decay curves obtained for LPZABS glasses under 400nm excitation along with their single exponential fit. The whole series of glasses under investigation (Glass A-F) are exhibiting nearly single exponential decay. Through the equations

mentioned in chapter 1 based upon literature survey experimental lifetimes (τ_{exp}) and quantum efficiencies (η) are calculated for all LPZABS glasses, which are shown in Table 3.7 with other data [116, 117, 128, 130]. From the Table 3.7 we can find the 1.0 mol% (Glass C) as having the highest value of quantum efficiency. This confirms the application of the as prepared glass for efficient lasing action in visible orange region [158, 159].

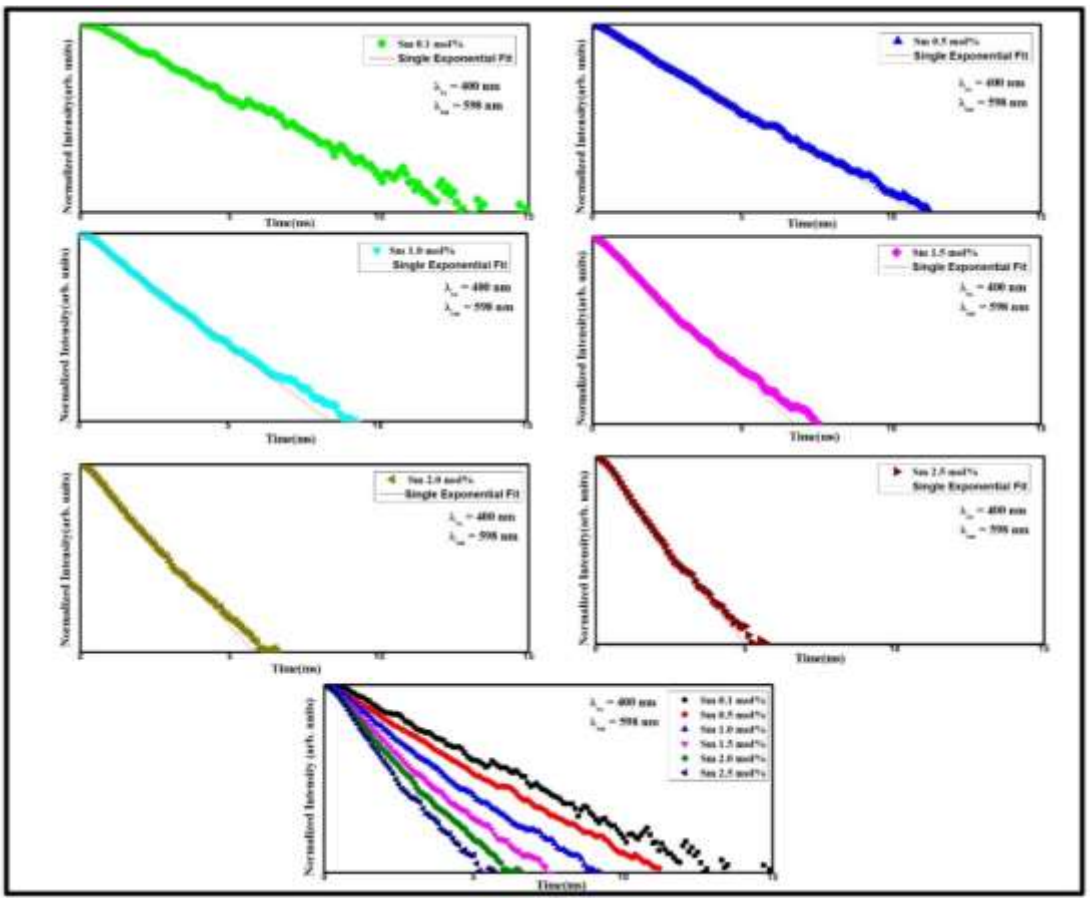

Fig. 3.8. Decay profiles of Sm^{3+} ions in LPZABS glasses for $^4G_{5/2} \rightarrow {}^6H_{7/2}$ transition under 400 nm excitation.

Table 3.7. Experimental lifetime (τ_{exp}) (μs), radiative lifetime (τ_R) (μs), quantum efficiency (η), and non-radiative decay rates (W_{NR}) for Sm^{3+} ions in LPZABS glasses along with other reported values.

Name of sample	τ_{exp}	τ_R	η (%)	W_{NR}	Reference
Glass A	2850	6122	46.55	187.53	Present Work
Glass B	2360	4592	51.39	205.95	Present Work
Glass C	2198	3002	73.21	121.84	Present Work
Glass D	1460	2736	53.36	319.43	Present Work
Glass E	1250	2584	48.37	413	Present Work
Glass F	1009	2324	43.41	560.78	Present Work
OFBSm01	2802	4994	56.1	156.6	[116]
AEBTSm0.1	1339	1996	67	246	[117]
LiPbAlBSm1.0	966.4	1600	60.41	433.08	[128]
0.5SmPbFB	1403	2613	58	283	[130]

3.3.6. CIE color co-ordinates and correlated color temperature (CCT)

From emission spectral, it is possible to analyze color emitted by LPZABS glasses by adopting commission International de I'Eclaiage France methodology [160]. The CIE coordinated evaluated for 1.0 mol% Sm^{3+} ions in LPZABS glasses are shown in Fig. 3.9. PL spectra of the Sm^{3+} ion consists of three main components; yellow region as the first part, orange as the second one and the red region as the third part under 400 nm excitation. From these three regions, orange shows the maximum intensity. The CIE coordinates evaluated for the optimized LPZABS glass are (0.561, 0.435) in line with the values (0.570, 0.420) given by Nichia Corporation developed Amber LED NSPAR 70BS for intense visible orange color. The CCT values for the titled glasses are also estimated using standard equations and are shown in Table 3.8 along with CIE co-ordinates.

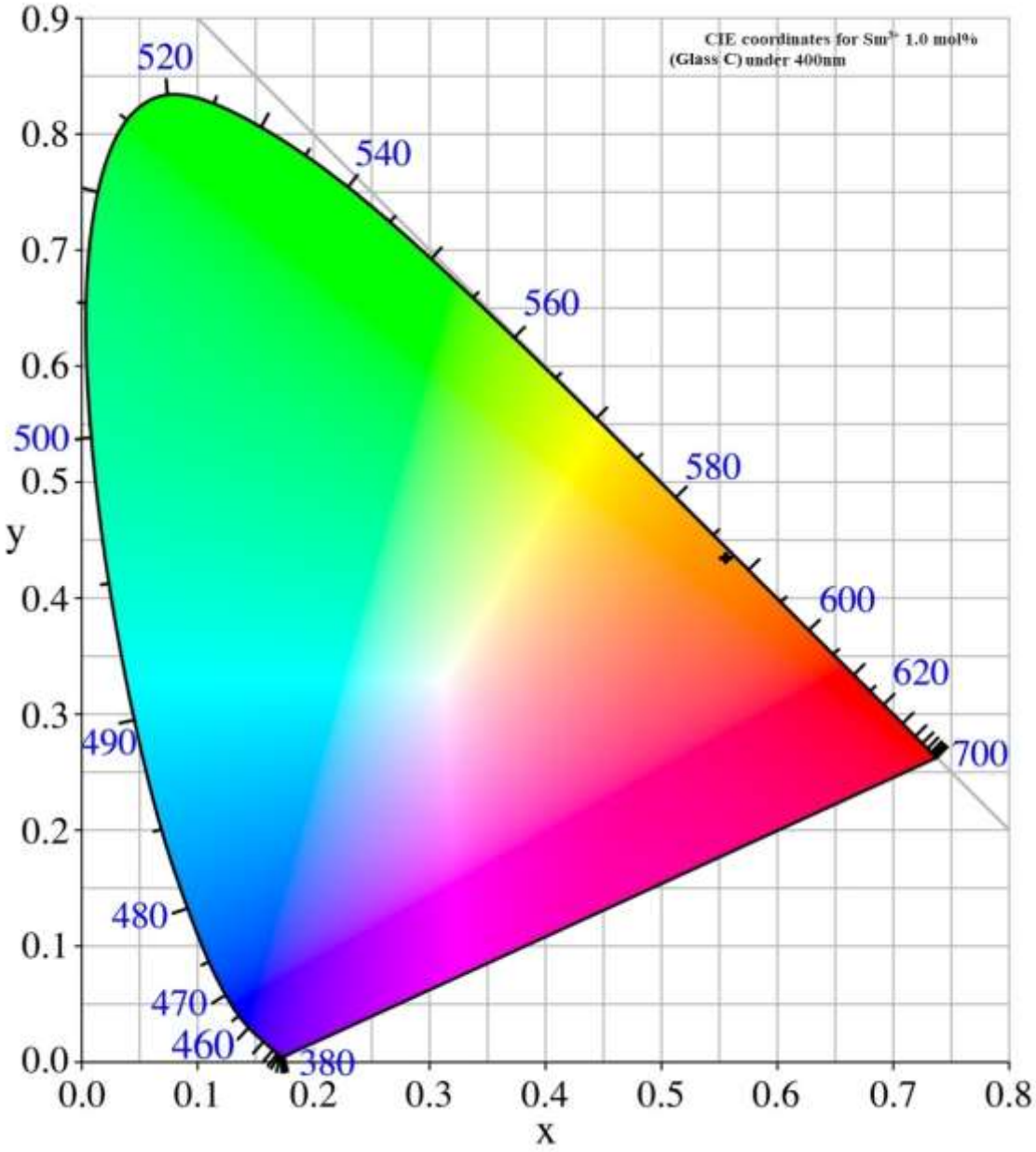

Fig. 3.9. CIE chromaticity coordinates of 1.0 mol% of Sm^{3+} ions in LPZABS glass.

Table 3.8. CIE-chromaticity co-ordinates and CCT values of Sm^{3+} ions in LPZABS glasses.

Name of the sample	CIE co-ordinates		CCT(K)
	x-co-ordinate	y-co-ordinate	
Glass A	0.542	0.449	2124
Glass B	0.544	0.449	2104
Glass C	0.561	0.435	1918
Glass D	0.521	0.465	2395
Glass E	0.578	0.421	1790
Glass F	0.522	0.464	2377

3.4. Conclusions

Samarium ions doped LPZABS glasses were fabricated by using melt quench method and subjected to XRD, FT-IR, absorption, excitation, PL and PL decay studies to understand their utility visible luminescent devices. The XRD and FT-IR recorded for an un-doped LPZABS glass confirms the glassy nature and various functional groups existing in it respectively. The PL spectra recorded under 400nm excitation wavelength show three peaks at 562 nm ($^4G_{5/2} \rightarrow {}^6H_{5/2}$), 598 nm ($^4G_{5/2} \rightarrow {}^6H_{7/2}$) and 645 nm ($^4G_{5/2} \rightarrow {}^6H_{9/2}$). Among the three, a transition corresponding to 598 nm is relatively more intense. The J-O intensity parameters derived from the absorption spectral features are used to estimate various radiative properties for the observed emission transitions of Sm^{3+} ions in the titled glasses. The experimental lifetimes are found to be decreasing gradually with Sm^{3+} ion concentration because of non-radiative energy due between the Sm^{3+} ions in the titled glasses. Dexter theory reveals dipole–dipole interaction as responsible phenomenon for energy transfer. The CIE coordinates obtained for the optimized LPZABS glass (0.561, 0.435) are in line with the valued

reported by Nichia Corporation (0.570, 0.420) for intense orange color. Relatively high values of branching ratios, stimulated emission cross sections, quantum efficiency, optical gain, gain band width and CIE chromaticity coordinates manifest that the 1.0 mol% Sm^{3+} ions doped LPZABS glass is quite suitable for the visible orange luminescent device applications and lasers.

****

CHAPTER 4

SPECTROSCOPIC ANALYSIS OF Dy^{3+} IONS ACTIVATED BOROSILICATE GLASSES FOR PHOTONIC DEVICE APPLICATIONS

This chapter deals with the synthesis of Dy^{3+} ions doped LPZABS glasses. A thorough study of luminescent properties of LPZABS glass is done by absorption and PL studies to understand the utility of the titled glasses in photonic device applications. Absorption and PL has helped in further evaluation of J-O intensity parameters, radiative parameters, and CIE coordinates. 1.5 mol% of Dy^{3+} ion is the optimized content of the dopant for the LPZABS glass. Application of Dexter theory signifies the type of interaction mechanism present in the Dy^{3+} ions doped LPZABS glasses. The CIE coordinates evaluated from the PL spectra of Dy^{3+} ions doped LPZABS glasses reveal white light emission.

The aaforementioned facts founded space in a renowned International Journal,

Optical Materials 117(2021) 111112.

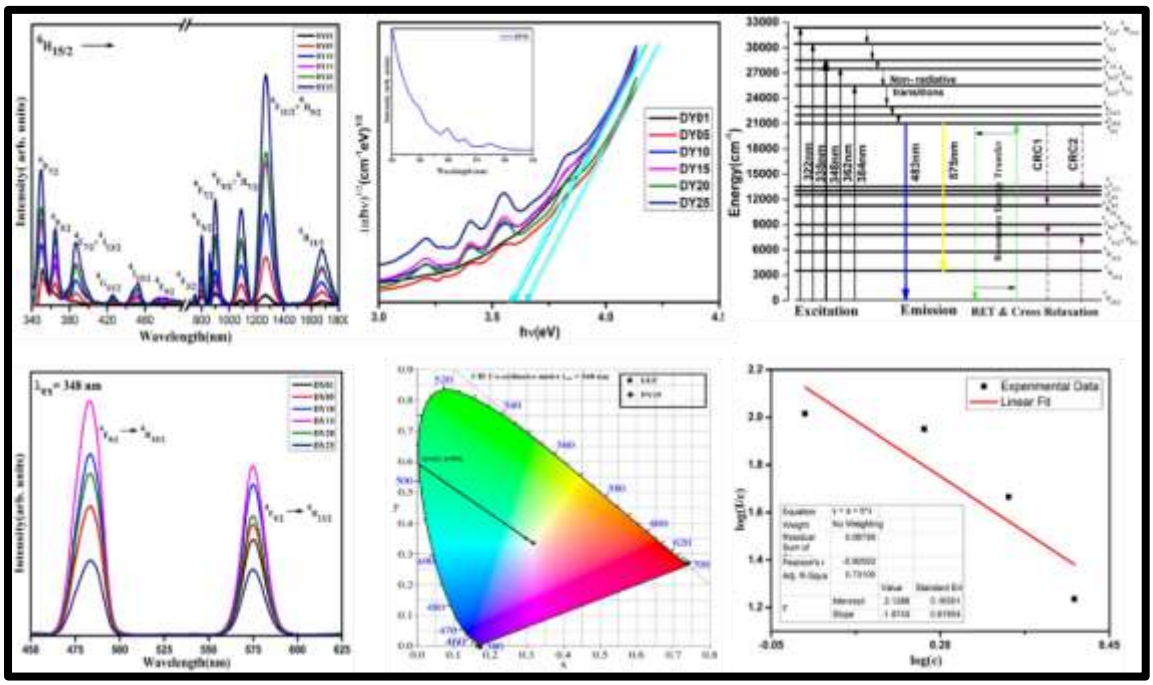

4.1. Introduction

From the history of various lighting tools, solid state lighting (SSL) devices are most notable and SSL devices are not only known for environmentally friendly by producing lesser carbon emissions, but also save electrical energy by taking relatively very less amount of power for their operation. There are number of SSL devices used nowadays like white light emitting diodes (w-LEDs), cellular phone illumination, automotive displays, traffic signals, full color displays, etc. Usage of SSL devices for all the aforementioned applications show cost effectiveness, durability and performance over previously used conventional lighting devices. Apart from being more durable, the SSL devices are compact in size, better transparencies, longer lifespan, more reliable, shock resistance and can be designed to greater extent [72, 161, 162]. The w-LEDs are prepared by two techniques commercially; first one phosphor based white light emitting diodes (pc w-LEDs) consists of a consolidation of blue LED (InGaN) and a yellow phosphor (YAG: Ce^{3+}). Next method consists of phosphors comprising of three prominent colors red, green and blue, excited with ultraviolet (UV) chip. First method shows high brightness with less production cost. However, it suffers from mediocre color rendering index (CRI) equal to 70~80 and larger color correlated temperature (CCT) equal to 7750K in addition to halo effect. Second method has better CRI but still it bears low luminescent efficiency as blue light gets absorbed in the process. In addition to the above-mentioned individual draw backs, both the methods are suffering with a common problem of using epoxy resin to encapsulate the phosphors. The epoxy resin has some serious draw backs like cracking and delamination. In addition to this, with time, its surface turns into pale yellow color and starts hampering the quality of the output LEDs. RE doped glasses

can be thought of a best alternative for the preparation of LEDs in place of phosphor-based LEDs for the prime reason of not using any epoxy resin in their fabrication. Nevertheless, RE doped glasses are superior than phosphors for the fabrication of LEDs from many perspectives such as intense emission in visible & infrared regions, simple to manufacture, low production cost and more durable [163-167].

For the present investigation, we have doped LPZABS host glass with Dy^{3+} ions to recognize its aptness for visible lasers and white LEDs. Dy^{3+} doped glass scintillators can be used for the measurements of radiations, dose monitoring for X-rays and protons. For the utility in the fields of astronomy and biomedicine, blue and yellow laser emission are beneficial. Dysprosium (III) with $4f^9$ electronic configuration is capable of giving emission in yellow ($^4F_{9/2} \rightarrow {}^6H_{13/2}$) and blue ($^4F_{9/2} \rightarrow {}^6H_{15/2}$) regions; a combination of these two provides an excellent white light emission. These emissions can be utilized for UV detectors and fluorescent display systems [168-170]. Dy^{3+} ions can be used as an electron trappable and light conversion material if it is combined with other RE ions in a host matrix. In addition to this, Dy^{3+} ion is best suited for understanding the local environment in a host matrix and this could be attained by altering Dy^{3+} ions concentration or by altering glass composition [170, 171]. In the present work, LPZABS glasses are activated with Dy^{3+} ions at varying concentrations and studied their PL as well as radiative characteristics features to understand their practical usage in various photonic devices by engaging different spectroscopic techniques like absorption and PL studies including excitation & emission [172-174].

4.2. Experimental procedure

Dysprosium doped LPZABS glasses used in present investigation were developed by using melt quench technique. Chemical composition used for the preparation of Dy^{3+} doped LPZABS glass along with its labelling is represented in Table 4.1.

Table 4.1 Abbreviations of LPZABS glasses doped with Dy^{3+} ions.

S. No.	Molar composition	Dopant mol%	Abbreviation Used
1	$10Li_2O–5PbO-(5-x)$ $ZnO-10Al_2O_3-10SiO_2-60B_2O_3-xDy_2O_3$	0.1	DY01
		0.5	DY05
		1.0	DY10
		1.5	DY15
		2.0	DY20
		2.5	DY25

High purity AR grade chemicals (H_3BO_3, SiO_2, PbO, ZnO, Al_2O_3, Li_2O and Dy_2O_3) were taken in an appropriate requirement and crushed in to a homogeneous mixture through an agate mortar. Homogeneous mix kept into alumina crucible is slowly melted in an electric furnace for 2.5 hours at 1100°C. The melt was rapidly transferred from alumina crucible to a brass plate (pre heated one) and pressed quickly with another brass plate to prepare glasses of same width. Soon after that, titled glasses are made free from cracks and air bubbles by annealing them at 350°C for 4 hours. Fig. 4.1 show the photograph of Dy^{3+} ions doped LPZABS glasses. Densities of LPZABS glasses are measured using Archimedes' principle (with xylene as an immersion liquid) and are found to be 2.65, 2.68, 2.7, 2.75, 2.77 and 2.79 for DY01 to DY25 glasses respectively. The optical absorption spectral measurements were done by spectrophotometer (LAMBDA-950, Perkin Elmer, USA). Emission and excitation

spectra for Dy^{3+} doped LPZABS glasses were obtained through SHIMADZU RF-5301 PC-spectro fluorophotometer, with Xenon arc lamp as an excitation source.

Fig. 4.1. Dy^{3+} ions doped LPZABS glass samples.

4.3. Results & discussion

4.3.1. Absorption spectrum, band gap & nephelauxetic effect analysis.

Absorption spectra for Dy^{3+} ions activated LPZABS glasses for all concentrations is presented in Fig. 4.2 (a) in range 340-1800 nm. Spectra consist of 12 peaks arising from $^6H_{15/2}$ initial state to numerous excited levels for $4f^9$ transitions designated to Dy^{3+} ions, arranged increasingly with respect to energy as $^6H_{11/2}$ (1675 nm), $^6F_{11/2}$ + $^6H_{9/2}$ (1269 nm), $^6F_{9/2}$ + $^6H_{7/2}$ (1089 nm), $^6F_{7/2}$ (903 nm), $^6F_{5/2}$ (803 nm),

$^6F_{3/2}$ (750 nm), $^4F_{9/2}$ (474 nm), $^4I_{15/2}$ (453 nm), $^4G_{11/2}$ (426 nm), $^4F_{7/2}$ + $^4I_{13/2}$ (386 nm), $^6P_{5/2}$ (365 nm) and $^6P_{7/2}$ (350 nm). Identification of bands has been done in accordance with the reports published by Carnall et al. in literature [174].

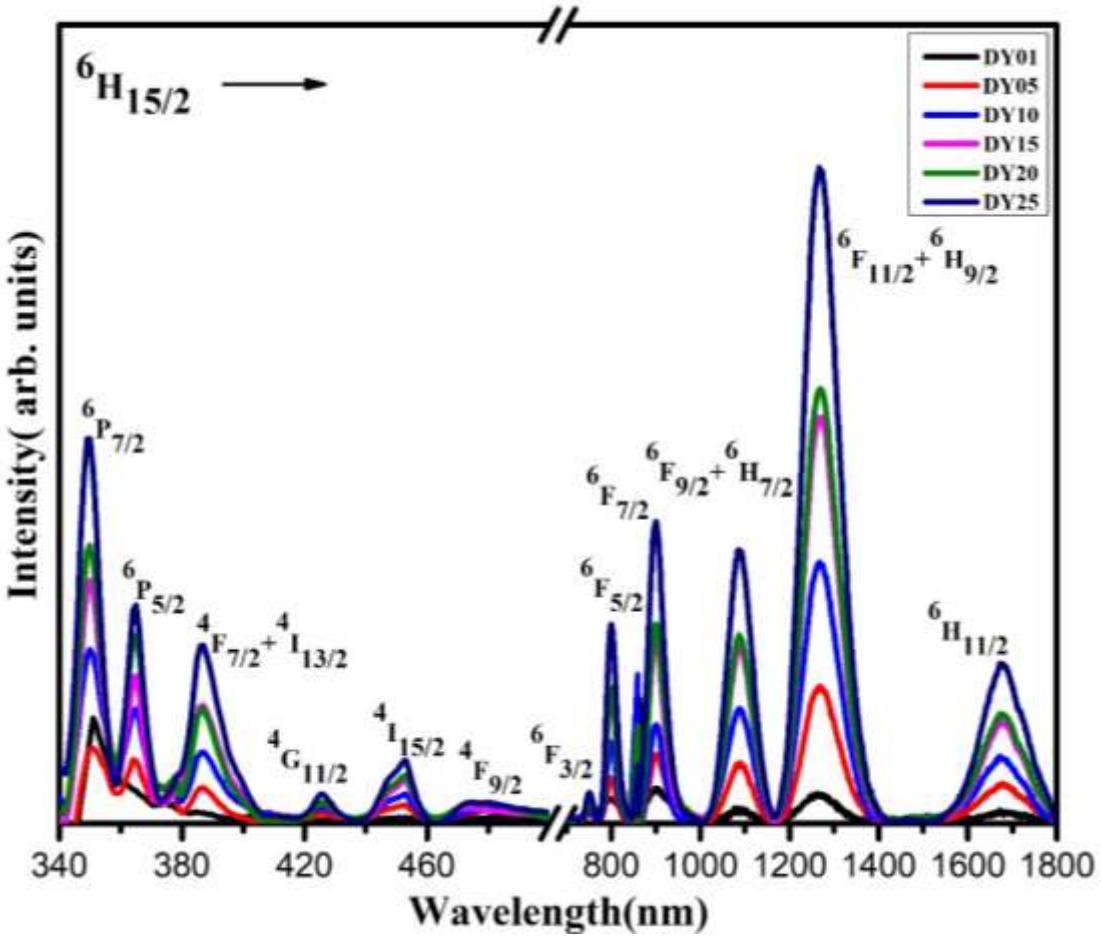

Fig. 4.2 (a). Absorption spectra of Dy^{3+} ions doped LPZABS glasses.

These transitions are alike to other reported transitions for Dy^{3+} ion [175-177]. From the absorption spectra, intensities of all the bands are escalating with increase in Dy^{3+} ion concentration in the host glass. Some specific transitions of RE ions are most intense and extremely responsive to the environment of the host. These transitions are designated to be hypersensitive in nature and follows selection rule $|\Delta S| = 0$, $|\Delta L| \leq 2$ and $|\Delta J| \leq 2$ [115].

From all the transitions shown in Fig. 4.2(a), one can infer that, $^6H_{15/2} \rightarrow {}^6F_{11/2} + {}^6H_{9/2}$ transition observed in NIR region is hypersensitive in nature. This hypersensitive band observed are in consonance with the data reported for different Dy^{3+} doped glasses [73, 162].

For crystalline and amorphous substances, cutoff wavelength of absorption spectral recordings highlights about band structure and optical transitions. Using such spectral information, it is possible to ascertain the band gap data for direct allowed transitions and indirect allowed transitions. Expression connecting band gap and coefficient of absorption (α) is provided by Davis and Mott relation [178]:

$$(\alpha h\upsilon)^n = B(h\upsilon - E_g)$$

Here, α represents absorption coefficient, hυ represents the energy due to applied photon, υ represents the frequency of striking photon, h represents Planck's constant, n can be 2 or ½ for direct or indirect allowed transitions; B represents band tailing parameter and E_g represents band gap [107]. Fig. 4.2(b) represents indirect band gap for all Dy^{3+} doped LPZABS glasses along with absorption spectrum for DY15 LPZABS glass. Optical band gap value can be deduced from this graph through extrapolation of linear region to null absorption band. The intersection of the extrapolated linear line on x-axis gives the optical band gap energy (E_g). E_g data obtained for the as prepared glasses are 3.59eV, 3.65eV, 3.60 eV, 3.59 eV, 3.64 eV and 3.57 eV for DY01, DY05, DY10, DY15, DY20 and DY25 glasses respectively. The optical band gap energy obtained for LPZABS glasses are comparable to the values reported for other glasses in literature [170, 173]. Relatively higher band gap values obtained for the titled glasses indicate a greater number of non-bridging

oxygens existing in it and intensification of degree of localization. This may lead for oxygen bonding in network and leads to modification of absorption characteristics and enhancement in optical quality [170, 173].

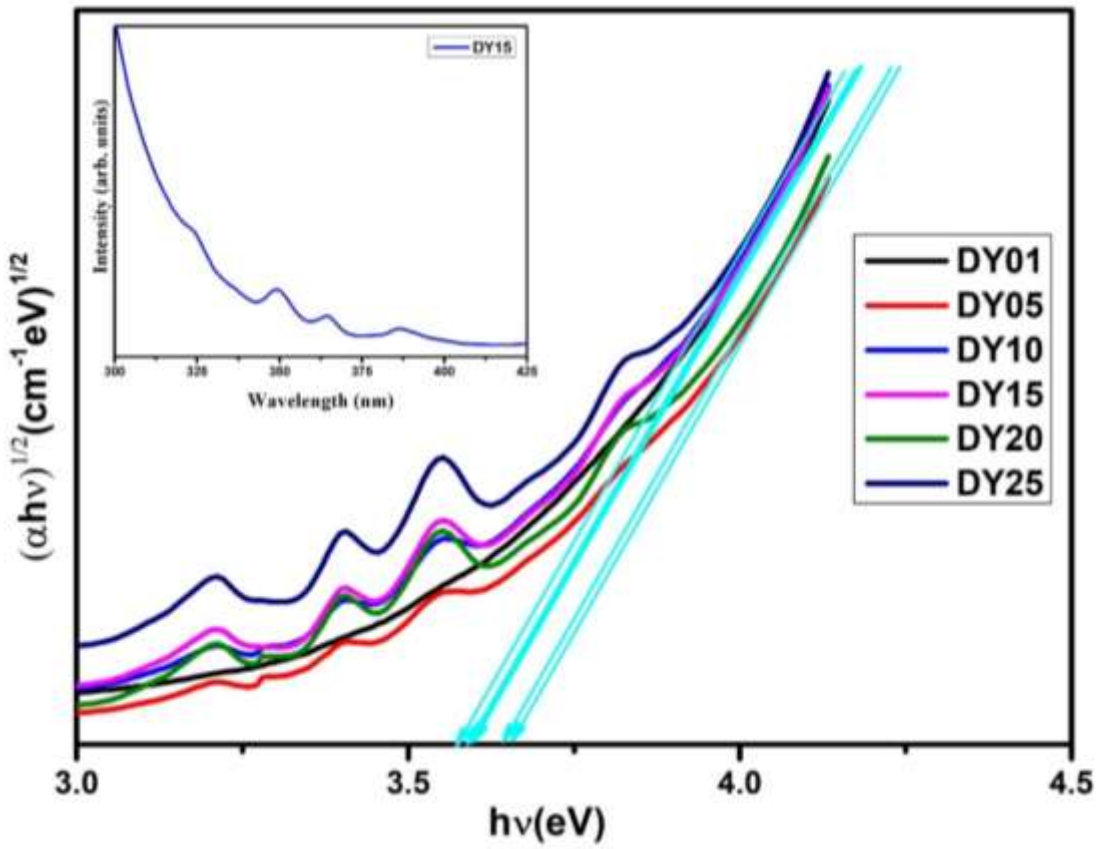

Fig. 4.2(b). Indirect band gap plot for Dy^{3+} ions in LPZABS glasses (Inset: Absorption spectrum of 1.5 mol% of Dy^{3+} ions doped LPZABS glass).

The ratio estimated between observed energy to relative transition of aqua ion for a specific transition of the RE ions is termed as nephelauxetic ratio (β). In present investigation, average nephelauxetic ratio ($\bar{\beta}$) values are decreasing gradually (1.0070, 1.0068, 1.0067, 1.0064, 1.0059 and 1.0045) from DY01 to DY25 glasses. Bonding parameter (δ) is evaluated as discussed in chapter 1. The bonding parameter estimated for the Dy^{3+} doped LPZABS glasses using the aforementioned equation are negative (-0.6965, -0.6830, -0.6730, -0.6319, -0.5895 and -0.4462) and increasing with

increase in Dy^{3+} ions content from 0.1 to 2.5 mol%. This allows us to contemplate that, bonding nature between Dy^{3+} ions and the surrounding ligands is predominantly ionic in nature. It can also be observed that, the nature of ionic bonding gradually increases with increase in Dy^{3+} ion concentration in LPZABS glasses.

4.3.2. *Oscillator strengths & Judd-Ofelt (J-O) analysis*

Experimental oscillator strengths (f_{exp}) and J-O intensity parameters (Ω_λ) can be measured from intensities of the observed absorption transition bands (by calculating the integrated areas), experimentally measured oscillator strengths and applying least square fit method, as explained in chapter 1. For the present work, the details pertaining to the experimental, calculated oscillator strengths and root mean square deviation (f_{exp} & f_{cal} and δ_{rms}) along with the transitions observed are presented in Table 4.2 and are in accordance with other reported data [72, 162, 166]. Relatively smaller δ_{rms} values obtained indicates validity of least square fit employed and reliability in J-O parameters estimated thereof. The J-O parameters estimated for Dy^{3+} ions doped LPZABS glasses are shown in Table 4.3 and values for reported glasses in literature. Covalency for metal ligand bond-skewness for ion sites around environment of RE ions is estimated by J-O intensity parameters, which help us to understand the local arrangement and bonding nature for RE ions. High Ω_2 intensity parameters represent structural disorder in environment of RE ions and their symmetry in host matrix. Relatively higher Ω_2 value obtained for entire series of Dy^{3+} ions doped LPZABS glasses signifies that RE ion sites are pertaining to lower asymmetry in host matrix. It has been found that Ω_2 depends on the hypersensitive transitions, hence greater the oscillator strengths corresponding to hypersensitive

transition, greater will be the value of Ω_2 (Table 4.2 and Table 4.3). Highest value of Ω_2 is attained for 1.5 mol% Dy^{3+} ions among the entire set of prepared LPZABS glasses. The bulk properties such as viscosity, rigidity and impact of vibrational bond to ligand atoms can be analyzed by Ω_4 and Ω_6 parameters.

Table 4.2. Experimental (f_{exp} $x10^{-6}$), calculated (f_{cal} $x10^{-6}$) oscillator strengths and r.m.s deviation (δ_{rms}) for Dy^{3+} ions in LPZABS glasses.

Transitions from $^6H_{15/2}\rightarrow$	DY01		DY05		DY10		DY15		DY20		DY25	
	f_{exp}	f_{cal}	f_{exp}	f_{cal}	f_{exp}	f_{exp}	f_{cal}	f_{cal}	f_{exp}	f_{cal}	f_{exp}	f_{cal}
$^6H_{11/2}$	0.673	0.796	0.971	1.09	0.990	1.187	1.004	1.301	0.865	1.069	0.81	1.01
$^6F_{11/2} + {}^6H_{9/2}$	4.927	4.911	5.344	5.328	5.437	5.474	5.673	5.635	4.868	4.842	4.44	4.42
$^6F_{9/2} + {}^6H_{7/2}$	0.639	0.738	1.858	1.192	1.876	1.341	2.079	1.500	1.547	1.228	1.49	1.16
$^6F_{7/2}$	1.384	1.130	1.658	1.822	2.142	2.048	2.574	2.307	2.110	1.869	2.07	1.78
$^6F_{5/2}$	0.550	0.514	0.703	0.828	0.711	0.931	0.740	1.053	0.614	0.847	0.60	0.81
$^6F_{3/2}$	-		0.128	0.155	0.129	0.175	0.143	0.197	0.129	0.159	0.09	0.15
$^4F_{9/2}$	-		0.151	0.140	0.159	0.158	0.173	0.177	0.152	0.144	0.13	0.13
$^4I_{15/2}$	0.221	0.273	0.241	0.381	0.278	0.416	0.445	0.459	0.318	0.376	0.28	0.35
$^4G_{11/2}$	-		0.129	0.075	0.172	0.084	0.169	0.092	0.126	0.076	0.11	0.07
$^4F_{7/2} + {}^4I_{13/2}$	0.435	0.267	0.637	0.393	0.653	0.434	0.767	0.478	0.744	0.396	0.68	0.37
$^6P_{5/2}$	0.252	0.229	0.268	0.370	0.293	0.416	0.338	0.470	0.306	0.378	0.29	0.36
$^6P_{7/2}$	1.87	1.886	1.993	3.057	2.43	3.44	2.59	3.804	2.43	3.180	2.24	2.982
$\delta_{rms}(x\ 10^{-6})$	±0.115		±0.380		±0.354		±0.426		±0.281		±0.276	

Bulk characteristics is specific to Ω_4 while converse of rigidity correspond to Ω_6. Moreover, Ω_4 and Ω_6 J-O parameters are not affected by medium where the RE ions are placed. Spectroscopic quality factor denoted by **χ,** which is ratio of J-O intensity parameters (Ω_4/Ω_6) signifies the stimulated emission. Again, for DY01-DY25 glasses, the value of spectroscopic quality factor is quite high indicating good

stimulated emission. From Table 4.3, J-O intensity parameters for investigated glasses are showing $\Omega_2 > \Omega_4 > \Omega_6$ similar to that of other reported glasses [167, 169, 179].

Table 4.3. Judd-Ofelt Parameters ($\Omega_\lambda \times 10^{-20}$cm^2), spectroscopic quality factor χ (Ω_4/Ω_6) and their trend for Dy^{3+} ions in LPZABS glasses along with various reported hosts

Glass System	Ω_2	Ω_4	Ω_6	χ (Ω_4/Ω_6)	Trend	References
DY01	6.1242	1.2689	1.2299	1.031	$\Omega_2 > \Omega_4 > \Omega_6$	Present work
DY05	6.2002	2.0566	1.9819	1.037	$\Omega_2 > \Omega_4 > \Omega_6$	Present work
DY10	6.238	2.3178	2.2275	1.040	$\Omega_2 > \Omega_4 > \Omega_6$	Present work
DY15	6.2957	2.5589	2.5186	1.016	$\Omega_2 > \Omega_4 > \Omega_6$	Present work
DY20	5.4661	2.1415	2.0287	1.055	$\Omega_2 > \Omega_4 > \Omega_6$	Present work
DY25	4.9475	2.0072	1.9447	1.032	$\Omega_2 > \Omega_4 > \Omega_6$	Present work
Dy:LiLTB	8.75	2.62	2.07	1.26	$\Omega_2 > \Omega_4 > \Omega_6$	[167]
PbF_2-WO_3-TeO_2	5.19	1.93	1.07	1.803	$\Omega_2 > \Omega_4 > \Omega_6$	[169]
$(NaPO_3)_6$-TeO_2-AlF_3-LiF	7.06	2.20	0.97	2.268	$\Omega_2 > \Omega_4 > \Omega_6$	[179]
$(NaPO_3)_6$-TeO_2-AlF_3-KF	6.05	2.30	1.09	2.110	$\Omega_2 > \Omega_4 > \Omega_6$	[179]

4.3.3. Photoluminescence spectral analysis

From literature it is well known that Dy^{3+} ions doped host matrix will show two intense emission bands; one in blue region (at around 483 nm) and the other one in yellow region (at around 575nm) [74, 173]. The excitation spectra recorded at 483 nm emission wavelength has excitation bands with slight variation in intensity without any change in band positions for Dy^{3+} ions doped LPZABS glasses. Hence, we have shown the excitation spectrum recorded for DY01 glass only in Fig. 4.3.

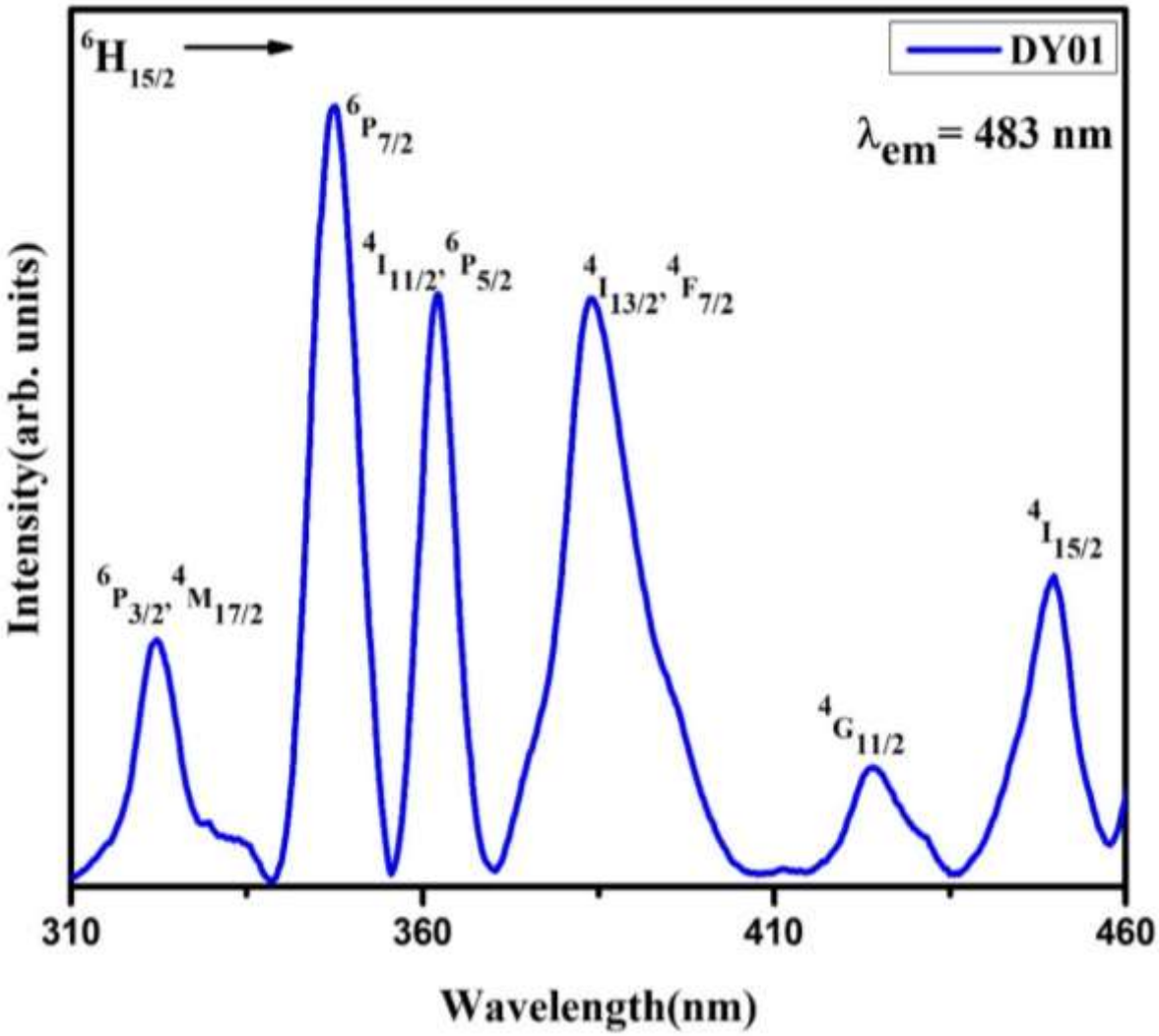

Fig. 4.3. Excitation spectrum of 0.1 mol% of Dy^{3+} ions doped LPZABS glass at 483 nm.

The excitation spectrum displays six transitions under 483 nm emission wavelength arising from the transitions $^6H_{15/2}\rightarrow$ ($^6P_{3/2}$, $^4M_{17/2}$), $^6P_{7/2}$, ($^4I_{11/2}$, $^6P_{5/2}$), ($^4I_{13/2}$, $^4F_{7/2}$), $^4G_{11/2}$ and $^4I_{15/2}$ in the spectral range 310 to 460 nm. Various excitation peaks observed in Fig. 4.3 allows us to contemplate that, Dy^{3+} ions doped LPZABS glasses could be excited with excitation sources from UV to n-UV and blue regions. Therefore, light sources such as n-UV, blue LED and commercially available GaN are quite suitable as an excitation sources for Dy^{3+} ions doped LPZABS glasses. From Fig. 4.3 it is

conspicuous that, an intense excitation band observed at 348 nm is quite suitable for recording the emission spectra of the as synthesized glasses.

Fig. 4.4 show emission spectra of Dy^{3+} ions activated LPZABS glasses under 348 nm excitation. Emission spectra shown in Fig. 4.4 depicts two prime bands pertaining to $^4F_{9/2} \rightarrow {}^6H_{15/2}$ (483 nm) and $^4F_{9/2} \rightarrow {}^6H_{13/2}$ (575 nm) transitions. Among two, the one observed in blue region at 483 nm is due to magnetic dipole ($\Delta J = 0, \pm 1$ but $0 \rightarrow 0$ forbidden) and other one observed in yellow region at 575 nm is due to electric dipole transition ($\Delta L = 2$ and $\Delta J = 2$). The $^4F_{9/2} \rightarrow {}^6H_{15/2}$ transition does not rely upon coordination environment while $^4F_{9/2} \rightarrow {}^6H_{13/2}$ transition relies upon host lattice.

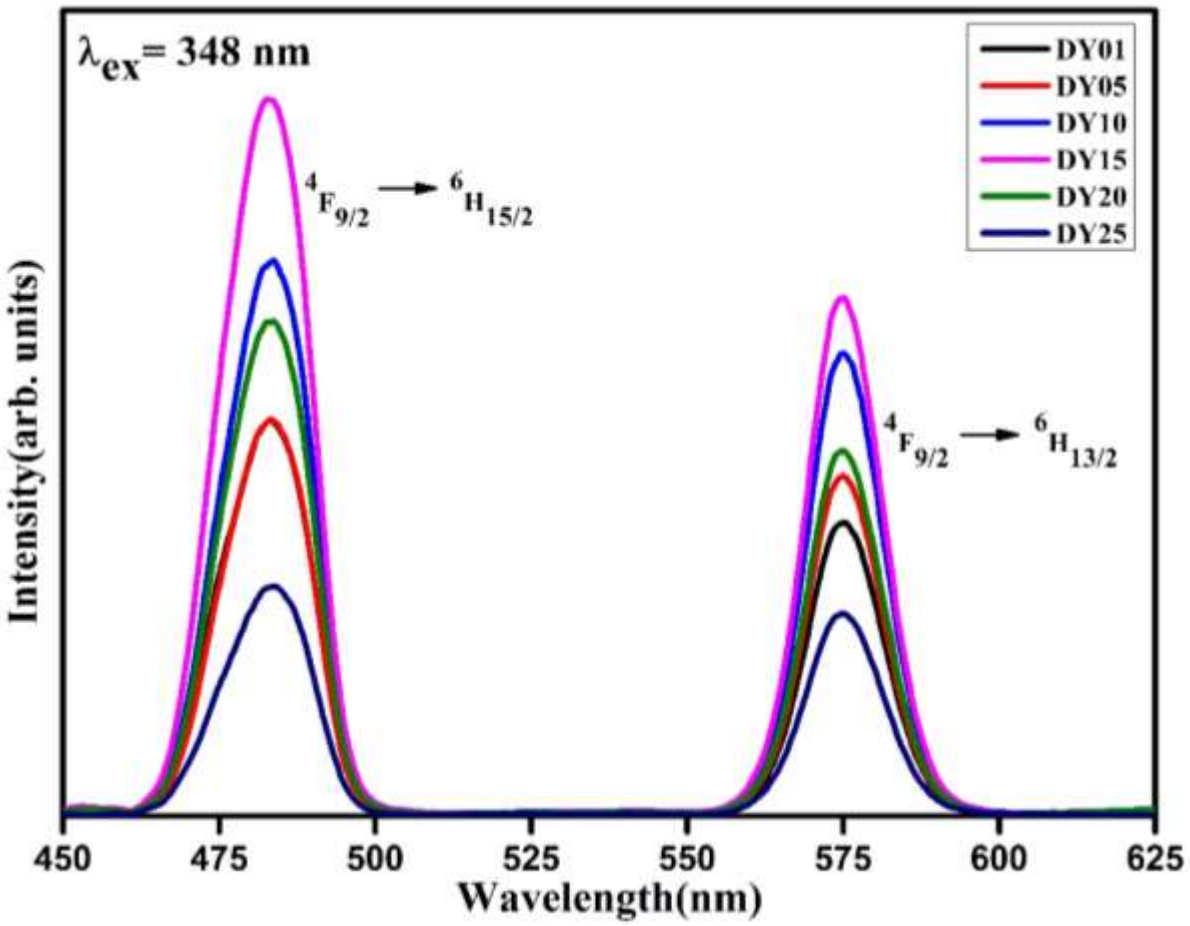

Fig. 4.4. Emission spectra of Dy^{3+} ions doped LPZABS glasses under 348 nm excitation.

From literature it is evident that, $^4F_{9/2} \rightarrow {}^6H_{15/2}$ transition is most intense if Dy^{3+} ions are placed with an inversion center at high symmetry sites. While the $^4F_{9/2} \rightarrow {}^6H_{13/2}$ transition is finest if Dy^{3+} ions are placed without inversion centers at low symmetry sites [74, 173, 180]. From Fig. 4.4 it can also be perceived that the photoluminescent intensity for the two prime bands, blue and yellow increases with Dy^{3+} ions content up to 1.5 mol% (DY15) and decreases beyond due to concentration quenching. Energy relocation among the Dy^{3+} ions may be the reason for quenching observed in LPZABS glasses. The Y/B values attained by LPZABS glasses are placed in Table 4.4 along with the data reported in literature. Y/B ratio values are approximately equal to unity for all the glasses indicates that, the variance in local environment due to increase in Dy^{3+} ion concentration need not affects intensity ratio [181]. Hence LPZABS glasses have an exclusive application in the field of white light emission.

Fig.4.5, shows partial energy level diagram of Dy^{3+} ions in LPZABS glasses indicating the excitation, emission and cross-relaxation channels. Under 348 nm excitation, the Dy^{3+} ions are raised to the energy level of $^6P_{7/2}$ as shown in Fig. 4.5. Due to non-radiative decay process, all the atoms reaching to $^6P_{7/2}$ level are ultimately reaching to $^4F_{9/2}$ metastable state and subsequently giving emission in visible region (blue and yellow) as shown in Fig. 4.4 and 4.5.

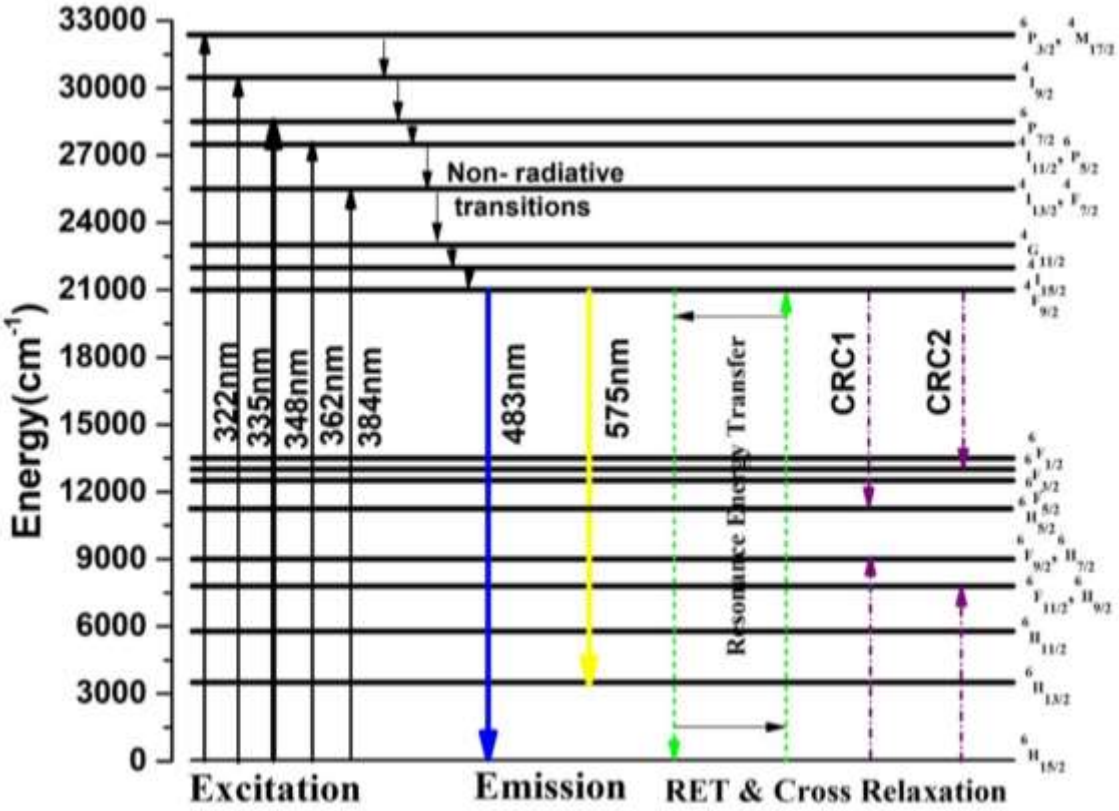

Fig. 4.5. Partial energy level diagram showing excitation, emission and cross-relaxation mechanism for Dy^{3+} ions doped LPZABS glasses

The concentration quenching observed beyond DY15 glasses may be due to resonance energy transfer ($^4F_{9/2} \rightarrow {}^6H_{15/2}$) and cross-relaxation channels (CRC1: $^4F_{9/2} + {}^6H_{15/2} \rightarrow {}^6H_{5/2} + ({}^6H_{7/2}, {}^6F_{9/2})$, CRC2: $^4F_{9/2} + {}^6H_{15/2} \rightarrow {}^6F_{3/2} + ({}^6H_{9/2}, {}^6F_{11/2})$) as depicted in Fig. 4.5 [172]. The information pertaining to kind of energy transfer in Dy^{3+} ions can be understood by applying the Dexter theory [74, 182] to the observed emission spectral features. Fig. 4.6 represent plot between log(I/c) and log (c), along with linear pattern possessing a slope of "s/d". Data for s obtained from graphical result is approximately equal to 6 (1.87*3= 5.62). This allows us to contemplate that, the concentration quenching phenomenon observed in the present work is due to dipole-dipole interaction produced between the Dy^{3+} ions.

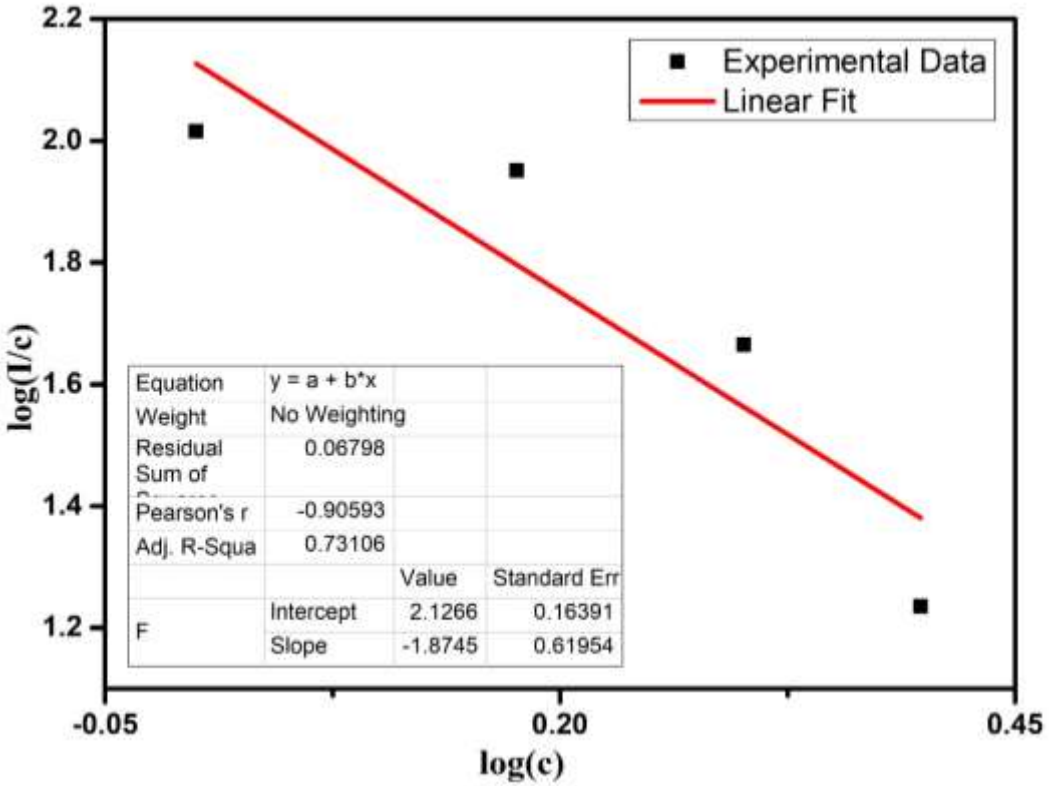

Fig. 4.6. Plot of log(I/c) v/s log (c) of Dy^{3+} ions doped LPZABS glasses.

4.3.4. CIE chromaticity coordinates and CCT values evaluation

Colorimetric calculations were done based on CIE system to study and assess the color emitted by synthesized glasses under 348 nm excitation. The CIE analysis is done as per detailed presented in chapter 1. Table 4.4 show the chromaticity coordinates of LPZABS glasses activated with Dy^{3+} ions under 348 nm excitation wavelength. Fig. 4.7 (a) shows the CIE chromaticity diagram and Fig. 4.7 (b) shows the variation of x, y chromaticity coordinates & CCT, for LPZABS glasses activated by Dy^{3+} ions. Color coordinates (x, y) of LPZABS glasses doped with Dy^{3+} ions are in close proximity of points of white light (x = 0.33 and y = 0.33) & values reported by National Television Standard Committee (NTSC) [180]. The color correlated temperature (CCT) predicts quality of emitted light, the relevant equations for the same are discussed in chapter 1. Table 4.4 also depicts CCT data evaluated for Dy^{3+} ions activated by LPZABS glasses under 348 nm excitation wavelength.

Table 4.4 CIE-chromaticity co-ordinates and Y/B of Dy^{3+} ions in LPZABS glasses

Name of the sample	CIE co-ordinates		CCT(K)	Y/B	References
	X-co-ordinate	Y-co-ordinate			
DY01	0.300	0.349	6991	0.74	Present work
DY05	0.319	0.364	6088	0.85	Present work
DY10	0.313	0.363	6274	0.83	Present work
DY15	0.297	0.348	7156	0.72	Present work
DY20	0.302	0.352	6880	0.74	Present work
DY25	0.321	0.369	5920	0.88	Present work
ZABS: Dy^{3+}	0.376	0.399	4407	1.70	[72]
LiPBAlB: Dy^{3+}	0.304	0.365	6667	0.73	[162]
LMgBDy05	0.37	0.40	4418	1.38	[169]
YCaSBDy0.5	0.353	0.394	4867	1.27	[170]
P_2O_5-PbO-ZnO:Dy^{3+}	0.307	0.345	6642	0.86	[173]

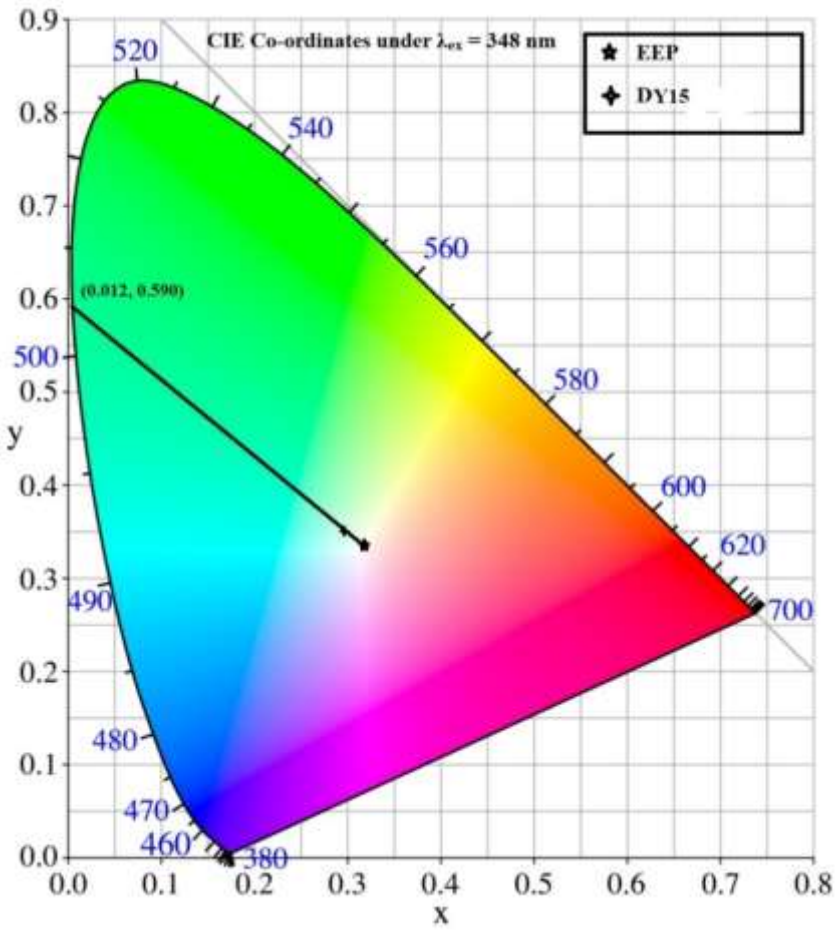

Fig. 4.7(a). CIE chromaticity coordinates of 1.5 mol% of Dy^{3+} ions doped LPZABS glass & its color purity.

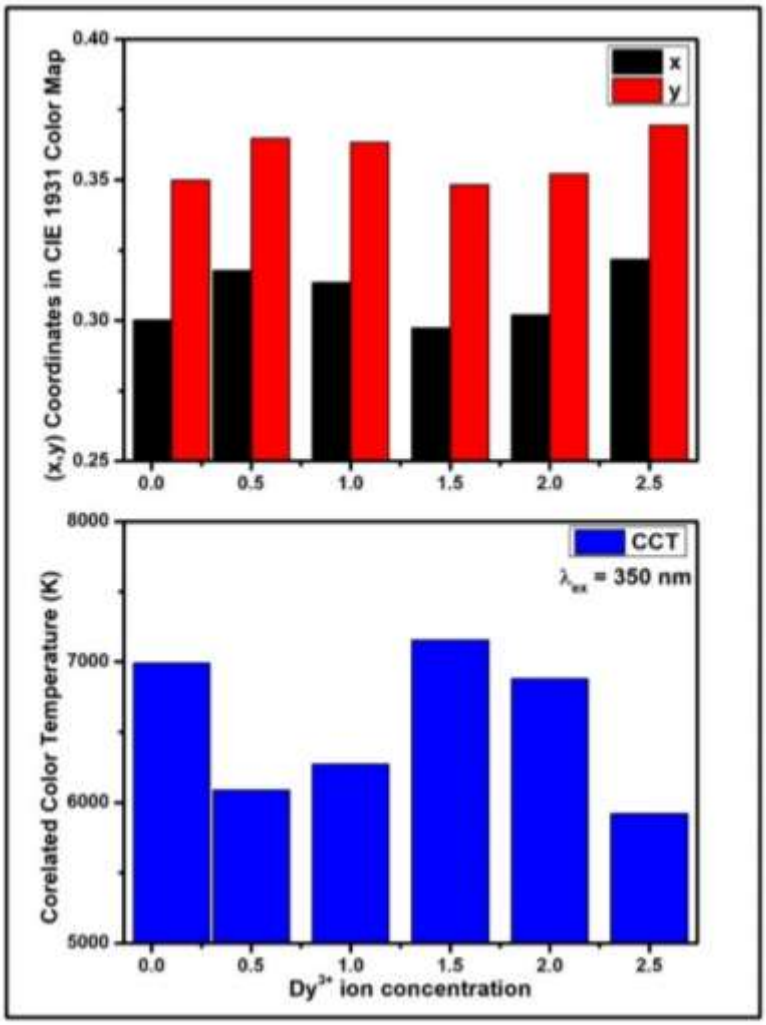

Fig. 4.7(b). x, y v/s Dy^{3+} ion concentration and variation of CCT with Dy^{3+} ion concentration in LPZABS glass.

As the values are in the range 5000- 8500 K, they act as magnificent cool white light source. Higher the CCT value, higher will be perspicuity, which finds application in the field of w-LEDs for public luminescence devices. From various Dy^{3+} ions doped LPZABS glasses, the one with 1.5 mol% of Dy^{3+} ions have chromaticity coordinates comparable to white light source and ambient CCT values.

The color purity values are evaluated through [63]:

$$\text{Color purity} = \frac{\sqrt{(x-x_{ee})^2+(y-y_{ee})^2}}{\sqrt{(x_d-x_{ee})^2+(y_d-y_{ee})^2}}$$

Here, (x, y) represent chromaticity coordinates for test light source, (x_{ee}, y_{ee}) is illuminant point (EEP) with respect to standard source 1930 CIE (0.3101, 0.3162), and (x_d , y_d) is coordinates for dominant wavelength coordinates. (x_d , y_d) evaluated through plotting linear pattern between (x, y) and the (x_{ee}, y_{ee}) [64]. If the obtained value of color purity is low, then it is said to be useful in white light generation. In the current study for optimized LPZABS glass (DY15) color purity is 9.48 x 10^{-2} and is plotted in Fig. 4.7(a) along with the dominant wavelength point.

4.3.5. Radiative properties

With the help of J-O intensity parameters (Ω_λ), where λ is 2, 4 and 6, various radiative parameters such as radiative transition probability (A_R), total radiative transition probability (A_T), luminescence branching ratio (β_R), radiative lifetimes ($\boldsymbol{\tau_R}$) and stimulated emission cross-section (σ_{se}) are evaluated using the expressions discussed in chapter 1 and are shown in Table 4.5. For all the as prepared LPZABS glasses, the β_R value is greater than 0.6. This allows us to contemplate that, all the Dy^{3+} ions activated LPZABS glasses are possessing good lasing potentialities.

Table 4.5. Transition probability (A_R) (s^{-1}), measured branching ratio (β_R), total transition probability (A_T) (s^{-1}) and radiative lifetime ($\boldsymbol{\tau_R}$) (μs) for the observed emission transitions of Dy^{3+}ions in LPZABS glasses.

Sample name	Transition	A_R	A_T	β_R	τ_R
DY01	$^4F_{9/2} \rightarrow {}^6H_{15/2}$	108.12	898.35	0.1203	1113
	$^4F_{9/2} \rightarrow {}^6H_{13/2}$	582.83		0.6487	
DY05	$^4F_{9/2} \rightarrow {}^6H_{15/2}$	175.14	1074.53	0.1629	930
	$^4F_{9/2} \rightarrow {}^6H_{13/2}$	670.38		0.6238	
DY10	$^4F_{9/2} \rightarrow {}^6H_{15/2}$	197.01	1132.28	0.1739	883
	$^4F_{9/2} \rightarrow {}^6H_{13/2}$	699.12		0.6174	
DY15	$^4F_{9/2} \rightarrow {}^6H_{15/2}$	221.8	1198.57	0.1850	834
	$^4F_{9/2} \rightarrow {}^6H_{13/2}$	732.95		0.6115	
DY20	$^4F_{9/2} \rightarrow {}^6H_{15/2}$	28.46	680.73	0.0418	1469
	$^4F_{9/2} \rightarrow {}^6H_{13/2}$	456.64		0.6708	
DY25	$^4F_{9/2} \rightarrow {}^6H_{15/2}$	171.59	953.02	0.1800	1049
	$^4F_{9/2} \rightarrow {}^6H_{13/2}$	572.46		0.6006	

Table 4.6 show emission wavelength (λ_P), corresponding effective band widths ($\Delta\lambda_P$), experimental branching ratio (β_{exp}), stimulated emission cross-sections (σ_{se}), gain band width ($\sigma_{se} \times \Delta\lambda_P$) and optical gain parameter ($\sigma_{se} \times \tau_R$) of Dy^{3+} ions doped LPZABS glasses. From the data given in Table 4.6, it is conspicuous that, σ_{se}, $\sigma_{se} \times \Delta\lambda_P$ and $\sigma_{se} \times \tau_R$ values are quite high. Table 4.7 comprises the obtained values of effective band width, measured branching ratio and stimulated emission cross sections along with other host matrices. This allows us to contemplate that, DY15 glass can be used as an excellent host matrix for lasing applications.

Table 4.6. Emission peak wavelength (λ_P)(nm), effective band widths ($\Delta\lambda_P$)(nm), experimental branching ratio (β_{exp}) , stimulated emission cross-sections (σ_{se}) (cm^2), gain band width ($\sigma_{se} \times \Delta\lambda_P$) ($cm^3$) and optical gain parameter ($\sigma_{se} \times \tau_R$) ($cm^2$ s) parameters for emission transitions for Dy^{3+} ions in LPZABS glasses.

Spectral parameters	DY01	DY05	DY10	DY15	DY20	DY25
$\lambda_P = 483\ nm$			$^4F_{9/2} \rightarrow {}^6H_{15/2}$ (Blue)			
$\Delta\lambda p$	17.49	17.08	17.19	17.19	17.1	17.09
β_{exp}	0.6082	0.5633	0.5692	0.6080	0.5982	0.5745
σ_{se} (x 10^{-22})	1.75	2.91	3.25	3.66	0.47	2.85
$\sigma_{se} \times \Delta\lambda_P$ (x 10^{-28})	3.07	4.97	5.60	6.31	0.81	4.88
$\sigma_{se} \times \tau_R$ (x 10^{-25})	1.95	2.71	2.87	3.05	0.69	2.99
$\lambda_P = 575\ nm$			$^4F_{9/2} \rightarrow {}^6H_{13/2}$ (Yellow)			
$\Delta\lambda p$	14.50	14.22	14.37	14.35	14.35	14.47
β_{exp}	0.3911	0.4317	0.4232	0.3906	0.3969	0.4480
σ_{se} (x 10^{-22})	22.93	26.91	27.77	29.16	18.17	22.61
$\sigma_{se} \times \Delta\lambda_P$ (x 10^{-28})	33.26	38.27	39.93	41.87	26.09	32.72
$\sigma_{se} \times \tau_R$ (x 10^{-25})	25.53	25.02	24.52	24.32	26.70	23.71

Table 4.7 Comparison of emission characteristics parameters like effective band widths ($\Delta\lambda_P$)(nm), measured branching ratio (β_R) and stimulated emission cross-sections (σ_{se} x 10^{-22}) (cm^2) of $^4F_{9/2} \rightarrow {}^6H_{13/2}$ transition in different Dy^{3+} doped LPZABS glasses.

Name of the sample	$\Delta\lambda_P$	β_R	σ_{se}	References
DY01	14.50	0.648	22.93	Present work
DY05	14.22	0.623	26.91	Present work
DY10	14.37	0.617	27.77	Present work
DY15	14.35	0.611	29.16	Present work
DY20	14.35	0.670	18.17	Present work
DY25	14.47	0.600	22.61	Present work
ZABS: Dy^{3+}	15.65	0.616	60.9	[72]
LiPBAlB: Dy^{3+}	14.84	0.629	27.6	[162]
ZnAlBiB: Dy^{3+}	16.50	0.64	24.60	[166]
LMgBDy05	17.76	0.56	33.98	[169]
YCaSBDy0.5	17.93	0.56	9.53	[170]
NPABSDy5	17.19	0.731	27.7	[73]

4.4. Conclusions

Dy^{3+} ions doped LPZABS glasses have been analyzed through various spectroscopic studies to understand their utility in photonic device applications. The absorption spectral information was subjected to J-O theory to understand the radiative properties possessed by the as prepared glasses. The nature of bonding existing between Dy^{3+} ions with its surrounding ligands doped LPZABS glasses is ionic in nature. From the PL analysis, it can be concluded that due to combination of blue and yellow emission, an intense white light is obtained from the as prepared glasses at an excitation of 348 nm. The Y/B ratio is also approximate to unity. CIE chromaticity coordinates obtained for DY15 glass (0.297, 0.348) are in proximity with the values reported by National Television Standard Committee (NTSC) (0.31, 0.31) and commercially available phosphor converted w-LEDs coordinates (0.32, 0.32). The CCT values obtained in current study for Dy^{3+} ions activated LPZABS glasses are in cool white light region and suggests the suitability of the as prepared glasses for w-LEDs applications. Stimulated emission cross- section is maximum for DY15 LPZABS glass. The emission cross-sections obtained along with colorimetric calculations allows us to contemplate that, 1.5mol% of Dy^{3+} ions activated LPZABS glasses are quite suitable for photonic device applications such as lasers and w-LEDs.

****

CHAPTER 5

PHOTOLUMINESCENCE CHARACTERISTICS OF SM^{3+}/ EU^{3+} LPZABS GLASSES FOR SOLAR CELL APPLICATIONS

This chapter deals with the synthesis of Sm^{3+}, Eu^{3+} and Sm^{3+}/Eu^{3+} co-doped LPZABS glasses for solar cell applications. Structural analysis of the as prepared glasses is done by XRD. While the luminescent properties are studied by the absorption, PL and PL lifetime measurements. Sensitizing effects of Sm^{3+} on Eu^{3+} are analyzed thoroughly by PL excitation. The PL emission spectra for Sm^{3+}/Eu^{3+} co-doped LPZABS glasses are examined for the presence of bands due to both ions. The Dexter & Reisfeld's approximation is applied to PL emission spectra while the Inokuti-Hirayama (I-H) model is applied to PL decay profiles, to study type of interaction among activator and sensitizer. Shifting of chromaticity coordinates (CIE) are observed for Sm^{3+}/Eu^{3+} co-doped LPZABS glasses with respect to increase in the activator ion concentration. Aforementioned facts founded space in renowned International Journal,

Solid State Sciences 125(2022) 106834.

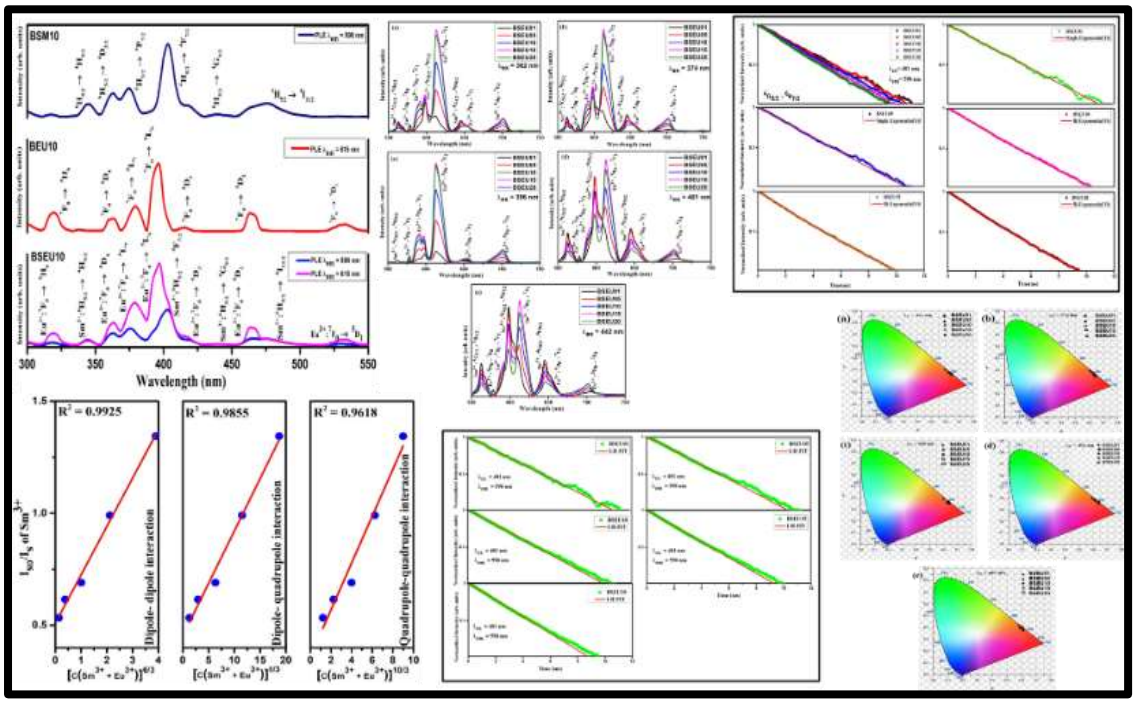

5.1. Introduction

In neoteric years, a substantial number of investigations have been done on RE doped glasses, owing to their incredible optical and spectroscopic properties and applications. They act as excellent luminescent centers on account of their electronic configuration of 4f and 5d-4f shells which are further concealed by $5s^2 5p^6$ electrons, enabling them for light-emitting diodes (LEDs), sensors, solar control devices, lasers, and many more applications [183, 184]. It is well known that, Y_2O_2S: Eu^{3+} and CaS: Eu^{2+} phosphors are widely used as red light-emitting devices. However, the above mentioned sulfide-based phosphors suffer from some drawbacks like generation of poisonous gas, poor chemical and thermal stability, scanty lifetime under ultraviolet (UV) light excitation, etc. These setbacks have prompted a number of researchers in search of alternatives leading to exploration of different luminescent materials doped with RE ions, like Sm^{3+} and Eu^{3+} on account of their application in white LEDs and CuPc based solar cells [185, 186]. Both Sm^{3+} and Eu^{3+} ions are having certain similarities like having ionic radii in proximity and being capable of showing visible luminescence in orange & red regions. This has prompted the use of Sm^{3+} (sensitizer) and Eu^{3+} (activator) in glass matrices for enhancing the excitation wavelength range and enhancing visible red emission. The $^5D_0 \rightarrow {}^7F_2$ transition from the Eu^{3+} ion (activator) is highly sensitive to the crystal field environment which leads to high efficiencies when co-doped with Sm^{3+} ions (sensitizer) by increasing absorption around 400 nm [187, 188]. These two RE ions have energy levels in proximity, which adds to energy transfer activity among Sm^{3+} to Eu^{3+} ions by enhancing emission for Eu^{3+} ions. A strategic energy transfer from electromagnetic radiation to red photons using non-utilized photons is found in absorption range of natural absorber substance

CuPc. Hence, Sm^{3+}/Eu^{3+} co-doped glasses find key role in development of display devices, UV-sensors, optoelectronic devices, lighting devices, and solar cells [187, 189-191].

From various glass systems produced, alumino borosilicate glasses emerge as an excellent choice owing to their excellent transparency from visible to near infra-red (NIR), good chemical and thermal stability [73, 91]. The addition of lithium oxide (Li_2O) further enhances the chemical stability modifying the structure of the borate glass matrix into tetrahedral BO_4 entities from three coordinated boron atoms. The insertion of heavy metal oxides like lead and zinc reduces the high phonon energy present in borosilicate glasses, which results in better luminescence efficiency [92,192]. Because of the aforementioned benefits of chemical compounds, we have prepared a glass matrix by the name lithium lead zinc alumino borosilicate glass (LPZABS glass). It is evident from the literature that, any RE ion or transition metal ion can be substituted as dopants at the site of main glass former/transition metal ions [73, 91, 92, 191, 193, 194]. Accordingly, the difference (%) in ionic radius for substituted ion and dopant ion should be less than 30% for better substitution. Lesser the difference of ionic radii, the higher will be the probability for the occupation of a particular ion site. The percentage difference in ionic radii of the doped RE ion with zinc (27.97%) is very less in comparison to that of boron (250.74%). Moreover, the percentage of difference in ionic radius observed for zinc is well below the prescribed upper limit of 30%. This has prompted us to choose ZnO as a suitable substituent site for the doped RE ions in the title glasses.

Among various methods available to prepare glass, in the present work we have opted sudden melt quench method to prepare Sm^{3+}/Eu^{3+} co-doped LPZABS glasses. PL emission and PL decay characteristics were inspected for energy transfer mechanisms involved and utilization of LPZABS glasses for photonic device applications. The energy transfer was probed by Dexter and Reisfeld's approximation and the I-H model using emission spectra and decay profiles respectively. Energy transfer efficiency and CIE chromaticity coordinates were determined,

aiming for generalizing the as-prepared glasses for use in the lighting devices and CuPc based solar cells.

5.2. Materials preparation and characterization

Twelve samples of LPZABS glasses were synthesized via melt quench method having molar composition as represented in Table 5.1. The starting materials were analytical reagent grade Li_2O, PbO, ZnO, Al_2O_3, SiO_2, H_3BO_3, Sm_2O_3, and Eu_2O_3 with high purity. Taking acetone as the wetting medium, the above-mentioned chemicals were ground in an agate mortar for 1 hr. After pouring the mixture into an alumina crucible, it was heated to 1100°C for 2 h in a muffle furnace. Later the melts were poured on a pre-heated brass mold and pressed quickly with another brass mold. The glasses thus prepared were immediately transferred to another furnace for annealing at around 350 °C for about 4 h to eliminate the mechanical and thermal strains produced inside the glasses.

In the present study, XRD measurements for the Sm^{3+} doped, Eu^{3+} doped and Sm^{3+}/Eu^{3+} co-doped glass samples were performed by Bruker D8 Advanced Powder X-ray

diffractometer acquiring Cu-Kα radiation (λ = 1.54Å, 40kV, 40mA), with source angle 2θ having the range of 20-80°. JASCO FP-8300 Spectro-fluorophotometer provided with Xenon flash lamp was used to record PL properties of the samples. PL decay spectral recordings were measured through a Hitachi-F7000 fluorescence spectrofluorometer.

Table 5.1. Abbreviations of LPZABS glasses doped with Sm^{3+}, Eu^{3+} and Sm^{3+}/Eu^{3+} ions.

S.No.	Molar composition	Dopant mol%	Abbreviation Used
1	$10Li_2O–5PbO-(5-x)\ ZnO-10Al_2O_3-10SiO_2-60B_2O_3-xSm_2O_3$	0.1	BSM01
		0.5	BSM05
		1.0	BSM10
		1.5	BSM15
		2.0	BSM20
		2.5	BSM25
2	$10Li_2O–5PbO-(5-x)\ ZnO-10Al_2O_3-10SiO_2-60B_2O_3-xEu_2O_3$	1.0	BEU10
3	$10Li_2O–5PbO-(4-x)\ ZnO-10Al_2O_3-10SiO_2-60B_2O_3-1Sm_2O_3-xEu_2O_3$	0.1	BSEU01
		0.5	BSEU05
		1.0	BSEU10
		1.5	BSEU15
		2.0	BSEU20

5.3 Results and discussions

5.3.1. X-ray diffraction analysis

X-ray diffraction for 1 mol% of Sm^{3+} doped (BSM10), 1 mol% of Eu^{3+} doped (BEU10), and the prepared five sets of Sm^{3+}/Eu^{3+} co-doped borosilicate glass samples (BSEU01, BSEU05, BSEU10, BSEU15, and BSEU20) are shown in Fig. 5.1. The non-existence of any sharp peaks in recorded X-ray diffraction pattern confirms non-crystalline nature of prepared glass samples.

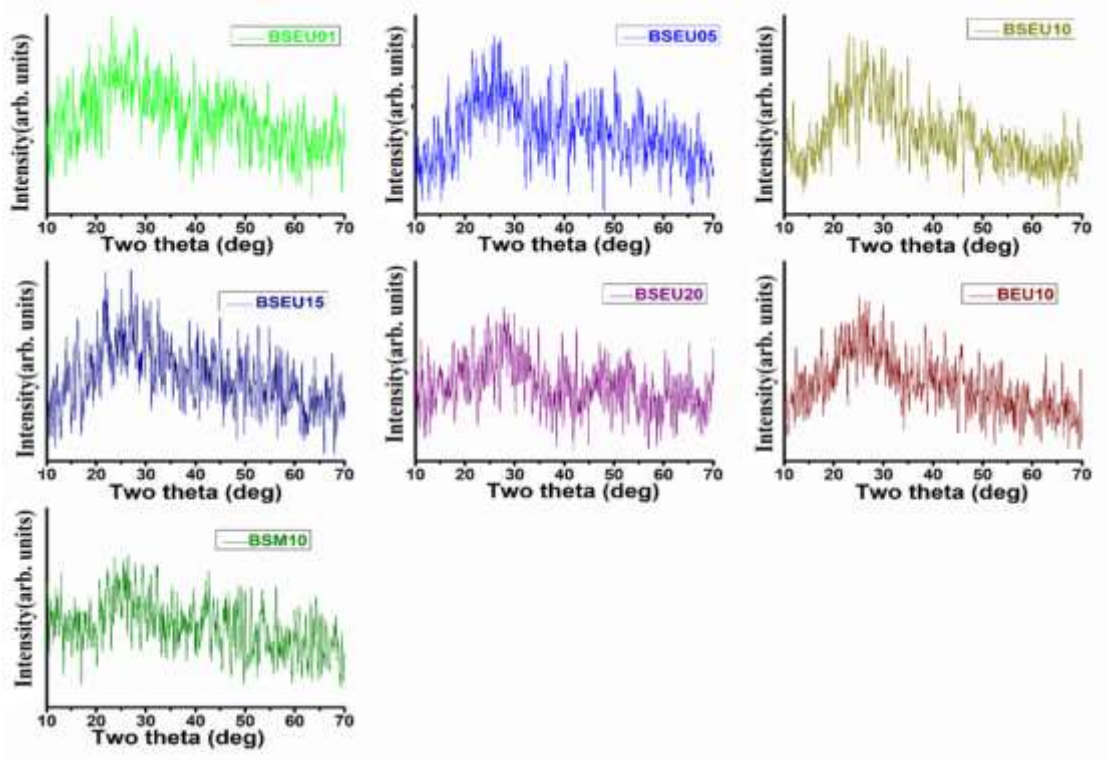

Fig. 5.1. X-ray diffraction patterns of BSM10, BEU10 and BSEU01, BSEU05, BSEU10, BSEU15 and BSEU20 borosilicate glass samples.

5.3.2. PL characteristics of Sm^{3+} ions doped LPZABS glasses

To understand fluorescence properties of Sm^{3+} ions doped LPZABS glasses, the PL excitation and emission spectra were recorded. Fig. 5.2 (a) represents the PL excitation spectra recorded for Sm^{3+} ions doped LPZABS glasses (under 598 nm emission wavelength) with varying concentrations of Sm^{3+} ions (from 0.1 to 2.5 mol% marked as BSM01 to BSM25 respectively) from 320 to 500 nm range. In Fig. 5.2 (a) various transitions can be noticed, emerging from a lower level ($^6H_{5/2}$) to nine exciting levels ($^4H_{9/2}$ at 342 nm, $^4D_{3/2}$ at 358 nm, $^6P_{7/2}$ at 372 nm, $^4L_{15/2}$ at 387 nm, $^4F_{7/2}$ at 401 nm, (^6P, $^4P)_{5/2}$ at 414 nm, $^4G_{9/2}$ at 442 nm, $^4I_{13/2}$ at 460 nm and $^4I_{11/2}$ at 470 nm) of Sm^{3+} ions. Among these transitions, 401 nm is finest [91, 195].

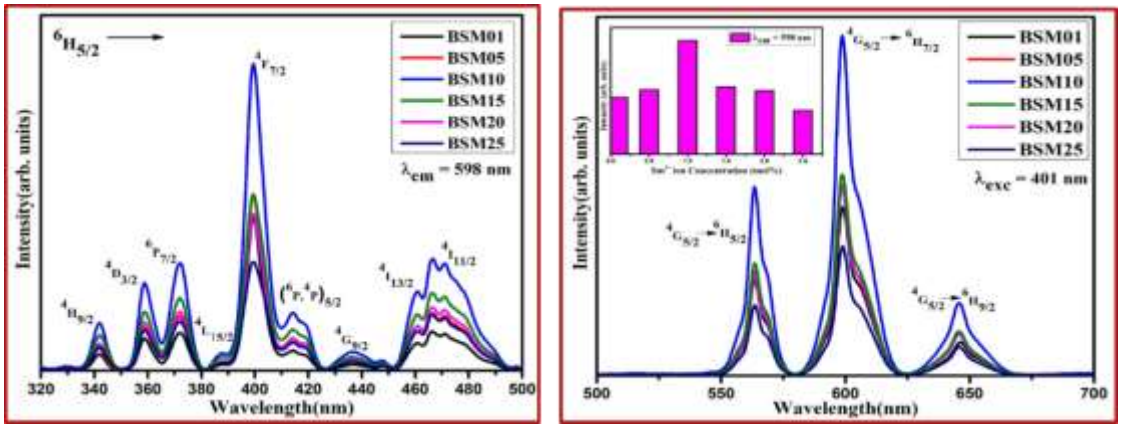

Fig. 5.2. PL **(a)** excitation and **(b)** emission spectra of BSM01, BSM05, BSM10, BSM15, BSM20 and BSM25 glasses. (Inset show intensity variation of PL emission at 598 nm with Sm^{3+} ion concentration).

Fig. 5.2 (b) represents the PL emission spectra of Sm^{3+} ions doped LPZABS glasses (under 401 nm excitation) representing intense emission bands at 562 nm ($^4G_{5/2}\rightarrow{}^6H_{5/2}$), 598 nm ($^4G_{5/2}\rightarrow{}^6H_{7/2}$), and 645 nm ($^4G_{5/2}\rightarrow{}^6H_{9/2}$). Among three emissions, most intense transition is at 598 nm due to the $^4G_{5/2}\rightarrow{}^6H_{7/2}$ transition in the visible orange region. The inset of Fig. 5.2 (b) demonstrates how the intensity of the most intense visible orange transition ($^4G_{5/2}\rightarrow{}^6H_{7/2}$) varying with concentration of Sm^{3+} ions. According to selection rules, $\Delta J = 0, \pm 1$; where J represents angular momentum, the $^4G_{5/2}\rightarrow{}^6H_{5/2}$ transition is MD in nature. On the other hand, another transition $^4G_{5/2}\rightarrow{}^6H_{9/2}$ is ED in nature in accordance with selection rule $\Delta J \leq 6$; $\Delta J = 2$, 4, and 6 if J or J' = 0, while most intense $^4G_{5/2}\rightarrow{}^6H_{7/2}$ transition is attributed has both ED and MD transitions [195-197]. The MD transition does not depend upon the crystal environment while the forced ED transition depends immensely on the crystal field of the ligands and shows hypersensitive nature. The intensity ratio measured for the $^4G_{5/2}\rightarrow{}^6H_{9/2}$ transition to $^4G_{5/2}\rightarrow{}^6H_{5/2}$ transition (ED to MD) is attributed to Sm^{3+} ion's symmetry in the local structure. Intensity of MD transition ($^4G_{5/2}\rightarrow{}^6H_{5/2}$) is relatively more intense than the ED transition ($^4G_{5/2}\rightarrow{}^6H_{9/2}$)

suggesting no deviation from the inversion symmetry. The concentration quenching process observed beyond 1 mol% of Sm^{3+} ions in the title glasses (BSM10) emphasizes the possibility of resonant energy transfer and cross-relaxation movement mechanism among Sm^{3+} ions [197-200]. Finally, the PL excitation and PL emission spectral studies conducted on the title glasses reveal 1 mol% of Sm^{3+} ion concentration as optimum in present study.

5.3.3. PL characteristics of Eu^{3+} ions doped LPZABS glasses

Fig. 5.3 (a) represents the PL excitation spectrum recorded for BEU10 (1 mol% of Eu^{3+} doped LPZABS) glass under 615 nm emission wavelength from 300 to 550 nm. Seven distinct transitions could be observed for transitions arising from $^7F_0 \rightarrow {}^5H_6$ (319 nm), $^5D_4$ (362 nm), $^5L_7$ (374 nm), $^5L_6$ (396 nm), $^5D_3$ (415 nm), $^5D_2$ (464 nm), and $^5D_1$ (531 nm). These bands are identified on account of intra 4f transitions of Eu^{3+} ions in the title glasses [201]. Among all excitation bands, one pertaining to $^7F_0 \rightarrow {}^5L_6$ is relatively is finest and apt for recording PL emission spectra of the title glasses. Fig. 5.3 (b) represents the PL emission spectrum recorded for BEU10 glass under 396 nm excitation wavelength from 550 to 725 nm. It comprises of five prominent peaks pertaining to the transitions $^5D_0 \rightarrow {}^7F_0$ (578 nm), $^5D_0 \rightarrow {}^7F_1$ (591 nm), $^5D_0 \rightarrow {}^7F_2$ (615 nm), $^5D_0 \rightarrow {}^7F_3$ (652 nm) and $^5D_0 \rightarrow {}^7F_4$ (701 nm) [202,203]. Because of Stark effect, emission bands split to a maximum of 2J+1 stark levels. The number of peaks splitting is based on the surrounding atmosphere around the dopant ion. In the present investigation, we could see the $^5D_0 \rightarrow {}^7F_1$ transition splitting into two due to the Stark effect [204]. The $^5D_0 \rightarrow {}^7F_2$ transition observed at 615 nm is most intense and is

attributed to forbidden ED transition while $^5D_0 \rightarrow {}^7F_1$ observed at 591 nm is MD transition.

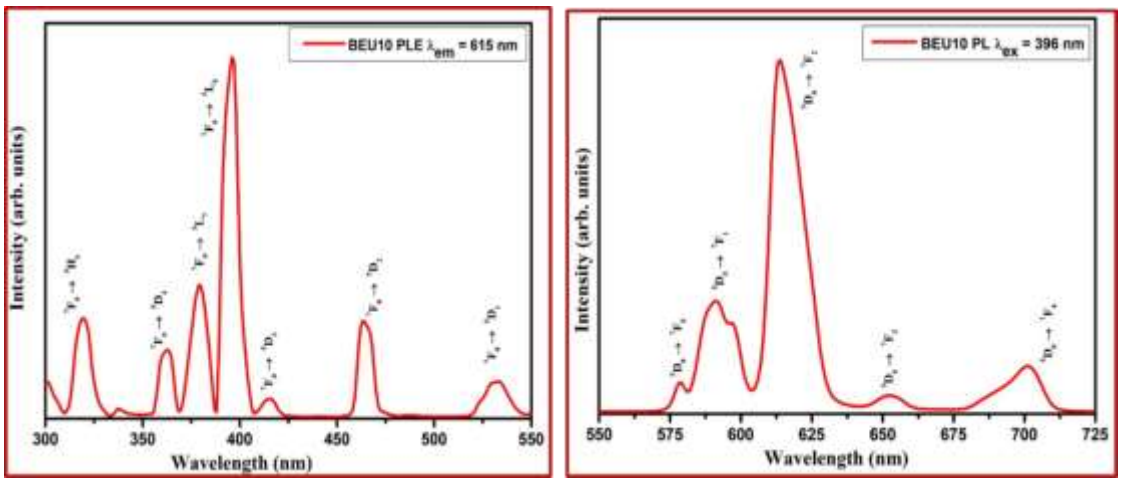

Fig. 5.3. PL **(a)** Excitation and **(b)** emission spectra of BEU10 glasses.

Ligand field environment influences the intensity of ED transitions and doesn't influence the intensity of MD transitions. Eu^{3+} doped LPZABS glass shows that ED transition is more prominent in comparison to MD transition. Here, the asymmetric ratio is the variation in the intensities of ED to MD transitions for Eu^{3+} ions in the network divulging the level of twist from the inversion symmetry. The intense level of covalence and location of Eu^{3+} ions towards lower symmetry sites can be deduced from an asymmetric ratio that is greater than one in the present study [204-206].

5.3.4. PL characteristics of Sm^{3+}/Eu^{3+} co-doped LPZABS glasses

Fig. 5.4 show PL excitation spectra of BSEU10 (1 mol% of Eu^{3+} and 1 mol% of Sm^{3+} co-doped LPZABS glass) glass recorded under 598 nm and 615 nm of emission wavelengths along with PL excitation spectrum recorded for BSM10 & BEU10 glasses recorded under 598 nm & 615 nm emission wavelengths respectively. Among the two excitation spectra recorded for BSEU10 glass, the one pertaining to 615 nm of

emission wavelength is more prominent. As per the representation marked in Fig. 5.4, it may be noted that most of the transitions are due to the Eu^{3+} and a few transitions occur on account of Sm^{3+} ions.

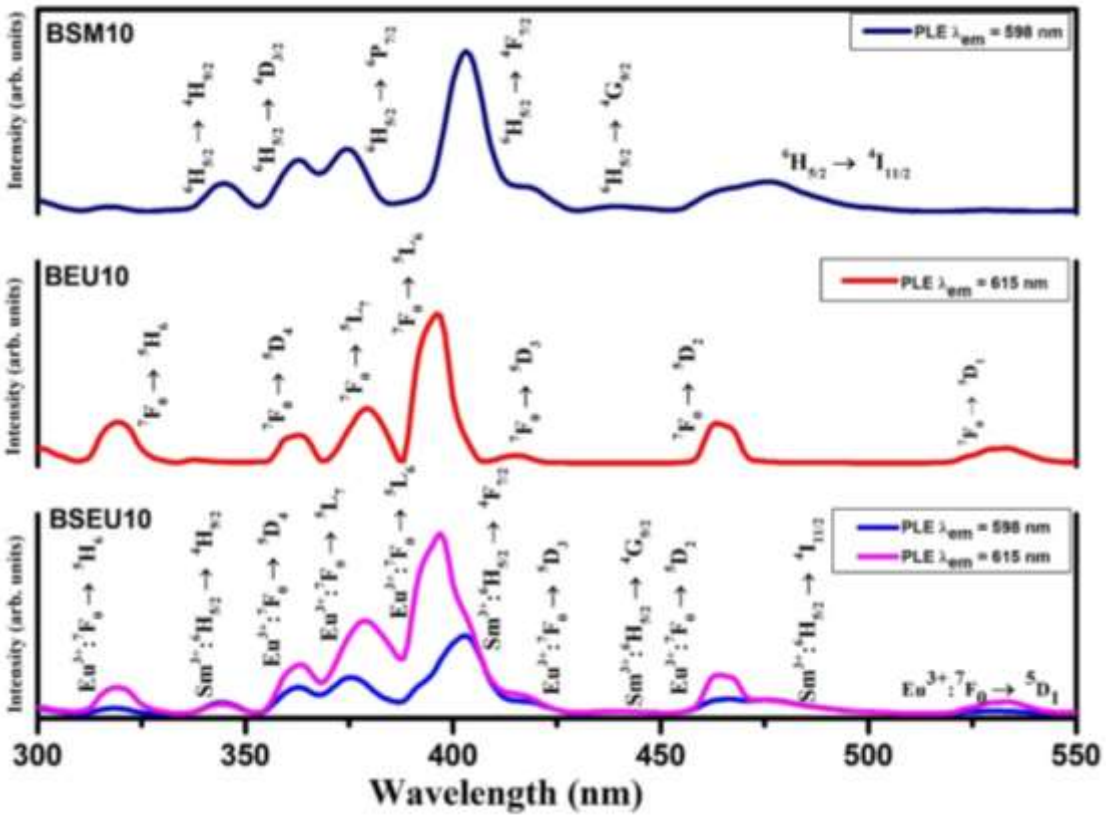

Fig. 5.4. PL Excitation spectra of BSM10 at 598 nm, BEU10 at 615 nm, and BSEU10 at 598 nm and 615 nm emission wavelength.

The bands obtained at 319, 362, 374, 396, 415, 464 and 531 nm corresponding to transitions $^7F_0 \rightarrow {}^5H_6$, $^7F_0 \rightarrow {}^5D_4$, $^7F_0 \rightarrow {}^5L_7$, $^7F_0 \rightarrow {}^5L_6$, $^7F_0 \rightarrow {}^5D_3$, $^7F_0 \rightarrow {}^5D_2$, and $^7F_0 \rightarrow {}^5D_1$ respectively are due to presence of europium ions; while the remaining bands observed at 342, 401, 442 and 477 nm pertaining to $^6H_{5/2} \rightarrow {}^4H_{9/2}$, $^6H_{5/2} \rightarrow {}^4F_{7/2}$, $^6H_{5/2} \rightarrow {}^4G_{9/2}$, $^6H_{5/2} \rightarrow {}^4I_{11/2}$ transitions are due to presence of the Samarium ions. Excitation peak intensity of Eu^{3+} ions gets enlarged by co-doping with Sm^{3+} ions, which implies that the Sm^{3+} ions are able to sensitize Eu^{3+} ions in Sm^{3+}/Eu^{3+} co-doped LPZABS glasses. Based on obtained excitation spectra for Sm^{3+}/Eu^{3+} co-doped

LPZABS glasses, PL emission spectra have been observed under 362, 374, 396, 401, and 442 nm excitation wavelengths [207-209]. Fig. 5.5 (a-e) represents five emission spectra recorded for Sm^{3+}/ Eu^{3+} co-doped LPZABS glasses for the above-specified excitation wavelengths, where Sm^{3+} is fixed at its optimized value i.e., at 1 mol% and Eu^{3+} concentration was varied from 0.1, 0.5, 1.0, 1.5 and 2.0 mol %. PL emission spectra obtained in visible region from 550 to 750 nm, comprising eight prominent emission peaks. Among them, four transitions are on account of Eu^{3+} ions, namely, $^5D_0 \rightarrow {}^7F_0$, $^5D_0 \rightarrow {}^7F_1$, $^5D_0 \rightarrow {}^7F_2$, $^5D_0 \rightarrow {}^7F_3$, and $^5D_0 \rightarrow {}^7F_4$ observed at 578, 591, 615, 654, and 701 nm respectively. Rests three are on account of Sm^{3+} bands $^4G_{5/2} \rightarrow {}^6H_{5/2}$, $^4G_{5/2} \rightarrow {}^6H_{7/2,}$ and $^4G_{5/2} \rightarrow {}^6H_{9/2}$ observed at 563, 598, and 645 nm respectively. The transition from $^5D_0 \rightarrow {}^7F_2$ represents the forced ED transition arising due to the hypersensitive nature of ligand atoms on account of the crystal field such that the emission intensity corresponding to these transitions is highly arisen by crystal field. $^5D_0 \rightarrow {}^7F_1$ transition represents the MD transition not governed by crystal environment. The transition $^5D_0 \rightarrow {}^7F_3$ on account of Eu^{3+} ions at 654 nm and transition $^4G_{5/2} \rightarrow {}^6H_{9/2}$ on account of Sm^{3+} ions at 645 nm seems to be non-distinguishable as they lie in close proximity to each other and amalgamate to form one transition. On perceiving the PL emission spectra shown in Fig. 5.5 (a-e), intensity of Sm^{3+} ions transitions decrease whereas intensity of Eu^{3+} ions transitions is enhancing gradually for increase in Eu^{3+} ions concentration and keeping Sm^{3+} ions concentration fixed. A decrease in intensity of Sm^{3+} ions emission bands with an increase in Eu^{3+} ions concentration in LPZABS glasses due to energy transfer from Sm^{3+} ions to Eu^{3+} ions [2, 210, 211]. The PL emission spectra observed for different excitation wavelengths show transitions at the same location with variations in intensity.

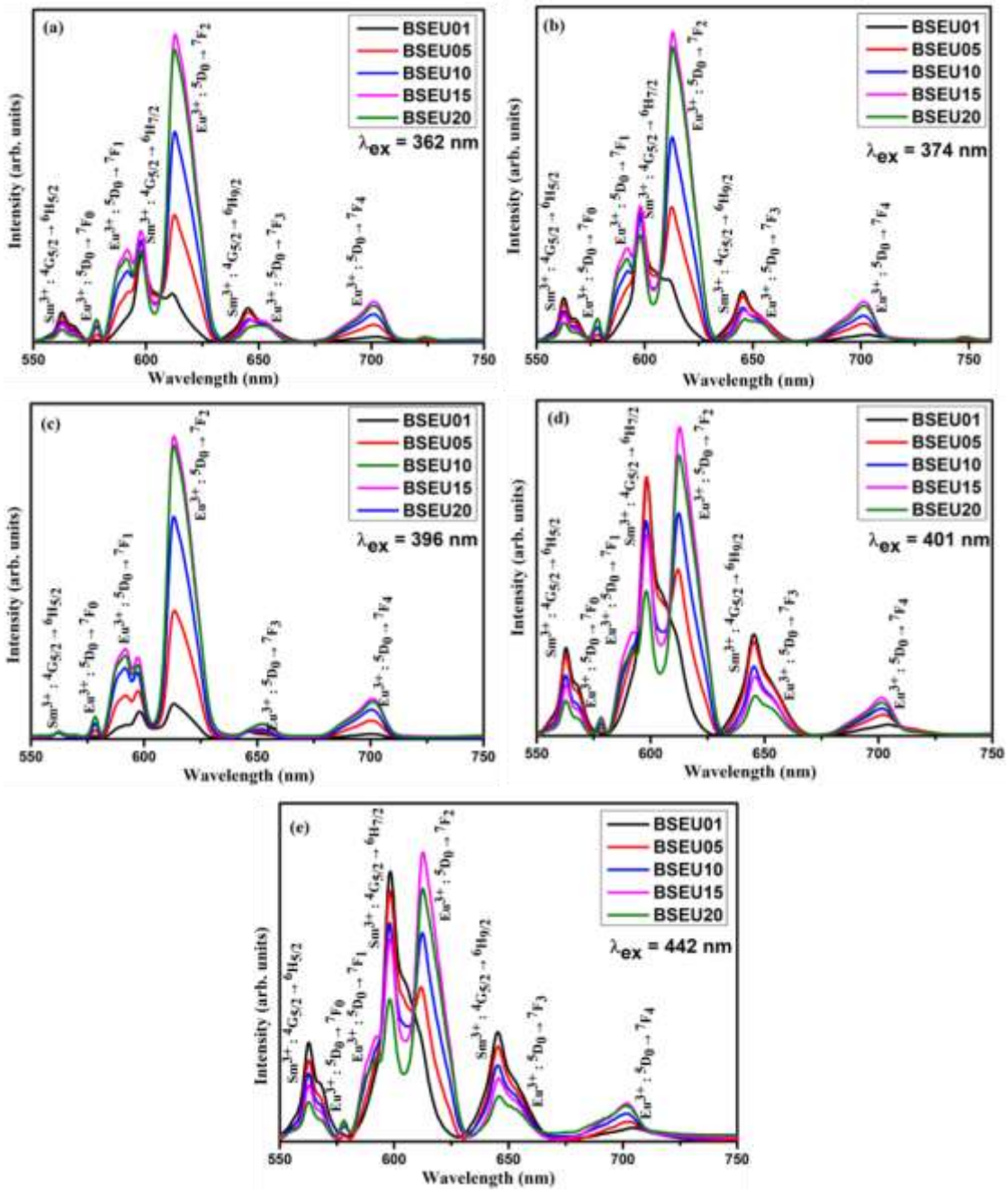

Fig. 5.5. PL emission spectra of BSEU01, BSEU05, BSEU10, BSEU15 and BSEU20 glasses under different excitation wavelengths [λ_{ex} = **(a)** 362 nm, **(b)** 374 nm, **(c)** 396 nm, **(d)** 401 nm and **(e)** 442 nm].

From PL emission spectra in Fig. 5.5 (a and b) under 362 and 374 nm excitation wavelengths, it can be observed that the intensities due to Sm^{3+} peaks are low in comparison to the intensities of Eu^{3+} peaks since the samples are excited at wavelengths corresponding to Eu^{3+} ions. This result allows us to say that these

transitions occur because of both Sm^{3+} and Eu^{3+} ions in co-doped LPZABS glasses. Again from Fig. 5 (c), it is quite noticeable that, under 396 nm excitation wavelength, the PL emission spectra comprise of dominant Eu^{3+} transitions along with weak emission transitions belonging to Sm^{3+}. Also, it is evident that concentration quenching occurs at 1.5 mol% of Eu^{3+} ions in co-doped LPZABS glasses. Lastly, in Fig. 5.5 (d and e), the PL emission spectra under the excitation wavelength of 401 nm and 442 nm comprise of transitions due to both Sm^{3+} and Eu^{3+} ions comparable in terms of intensity since the excitation wavelength lies in the overlap region of the excitation spectra of Sm^{3+} and Eu^{3+} doped glass samples. Such transitions can be assumed on account of Sm^{3+} ions and the observed Eu^{3+} transitions are owing to an energy transfer from Sm^{3+} to Eu^{3+} ions. From same figure, emission peak intensity attributing to Sm^{3+} ion shows a decline whereas the intensity of peaks due to Eu^{3+} ions increase with an increase in Eu^{3+} ions concentration under the constant Sm^{3+} concentration (optimized concentration equal to 1 mol%). The prominent emission transition of Sm^{3+}/ Eu^{3+} co-doped LPZABS glasses lies in absorption region of CuPc based solar cells. Downshifting photons produced by the title glasses (visible reddish-orange region) under n-UV and blue excitation wavelengths are quite useful in enhancing the efficiency of CuPc based solar cells [191]. Sm^{3+}/Eu^{3+} co-doped LPZABS glasses may be used to increase efficiency of the CuPc based solar cells by placing them over CuPc built natural solar cells through down transmutation of n-UV/blue photons.

Exchange interaction and multipolar interaction are two methods of non-radiative energy transfer in between sensitizer/donor and activator/acceptor RE ions. First method arises only if the two ions are at the nearest neighbor locations. Multipolar

interaction between Sm^{3+} and Eu^{3+} ions in the LPZABS glass, multipolar interaction must be explored, based on the concept given by Dexter theory and Reisfeld's approximation using the equation given below [210]:

$$\frac{\eta_0}{\eta} \alpha\ C^{n/3}$$

here, η_0 and η represents luminescence quantum efficiency of Sm^{3+} ions (sensitizer) in lack and availability of Eu^{3+} ions (activator), C represents whole mole percentage of Sm^{3+} ions and Eu^{3+} ions, and data corresponding to n is 6 (dipole-dipole), 8 (dipole-quadrupole) and 10 (quadrupole-quadrupole) defining the type of interaction. Emission intensities can be used to determine the ratio of luminescence quantum efficiencies of sensitizer in lack and availability of activator by the relation:

$$\frac{I_{so}}{I_s} \alpha\ C^{n/3}$$

here, I_{so} and I_s represent the intrinsic emission intensity and emission intensity for hypersensitive transition $^4G_{5/2} \rightarrow {}^6H_{7/2}$ of Sm^{3+} ions in availability of Eu^{3+} ions. Graph between $\frac{I_{so}}{I_s}$ versus $C^{n/3}$ is plotted where n is equal, to 6, 8 and 10 for 401 nm excitation wavelength, in Fig. 5.6. Best linear fit attained for Sm^{3+} and Eu^{3+} co-doped LPZABS glass corresponds to n = 6, emphasizing energy exchange from Sm^{3+} to Eu^{3+} on account of radiation less dipole- dipole mechanism among sensitizer and activator ions. The energy transfer efficiency (η_T) among sensitizer to activator ions could be estimated through the relation:

$$\eta_T = 1 - \frac{I_s}{I_{so}}$$

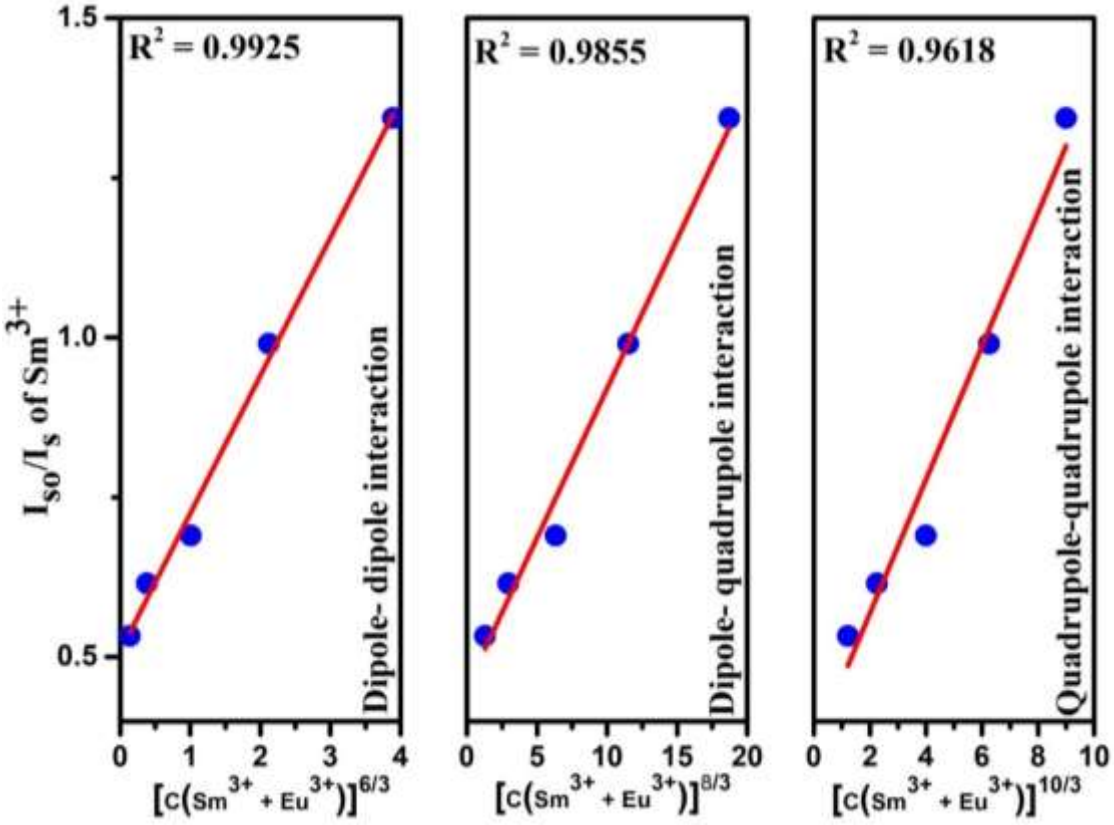

Fig. 5.6. Dependence of $\frac{I_{so}}{I_s}$ of Sm^{3+} on $[C(Sm^{3+} + Eu^{3+})]^{n/3}$ of BSEU01, BSEU05, BSEU10, BSEU15 and BSEU20 glasses for 401 nm excitation.

The calculated data of energy transfer efficiency for BSEU01, BSEU05, BSEU10, BSEU15, and BSEU20 are shown in Table 5.2 and intends towards energy transfer efficiency increases with an increase in Eu^{3+} ion concentration under all five different excitations.

Fig. 5.7 displays the energy level diagram of Sm^{3+} and Eu^{3+} ions in LPZABS glasses along with the energy exchange mechanism involved in the title glasses. The Sm^{3+} and Eu^{3+} ions are raised from a lower state to a higher energy state upon excitation by a suitable energy source.

Table 5.2. Energy transfer efficiency (η_T) for BSEU01, BSEU05, BSEU10, BSEU15 and BSEU20 glasses under different excitation wavelengths.

Excitation wavelength	η_T				
	BSEU01	**BSEU05**	**BSEU10**	**BSEU15**	**BSEU20**
362 nm	37.31	46.59	53.03	63.25	73.67
374 nm	24.24	38.82	42.42	56.62	69.69
396 nm	74.81	78.21	78.40	79.54	83.14
401 nm	23.51	25.25	35.77	40.42	57.05
442 nm	92.99	94.12	94.69	96.02	97.34

Both the ions fall to a lower energy state (Sm^{3+} ions to $^4G_{5/2}$ and Eu^{3+} ions to $^5D_0$) by releasing the energy in the form of non-radiative emission and finally decays to stable lower states (Sm^{3+}: $^6H_{5/2}$, $^6H_{7/2}$ and $^6H_{9/2}$ while that of Eu^{3+}: ^7F_J, J = 0 - 4) in sort of radiative transitions. The energy difference between $^4G_{5/2}$ (17,924 cm^{-1}) and $^5D_0$ level (17,277 cm^{-1}) is approximately 647 cm^{-1} (slight variation in the two levels) confirming that the Sm^{3+} ions transport some part of its energy in the form of radiation less transition to the Eu^{3+} ions, demonstrating that Sm^{3+} behaves like an effective sensitizer for the Eu^{3+} ions [2, 210-211]. This transportation of energy from Sm^{3+} to Eu^{3+} ions results in a decrement of emission intensity of Sm^{3+} ions and increment in intensity of Eu^{3+} ions as shown in Fig. 5.5.

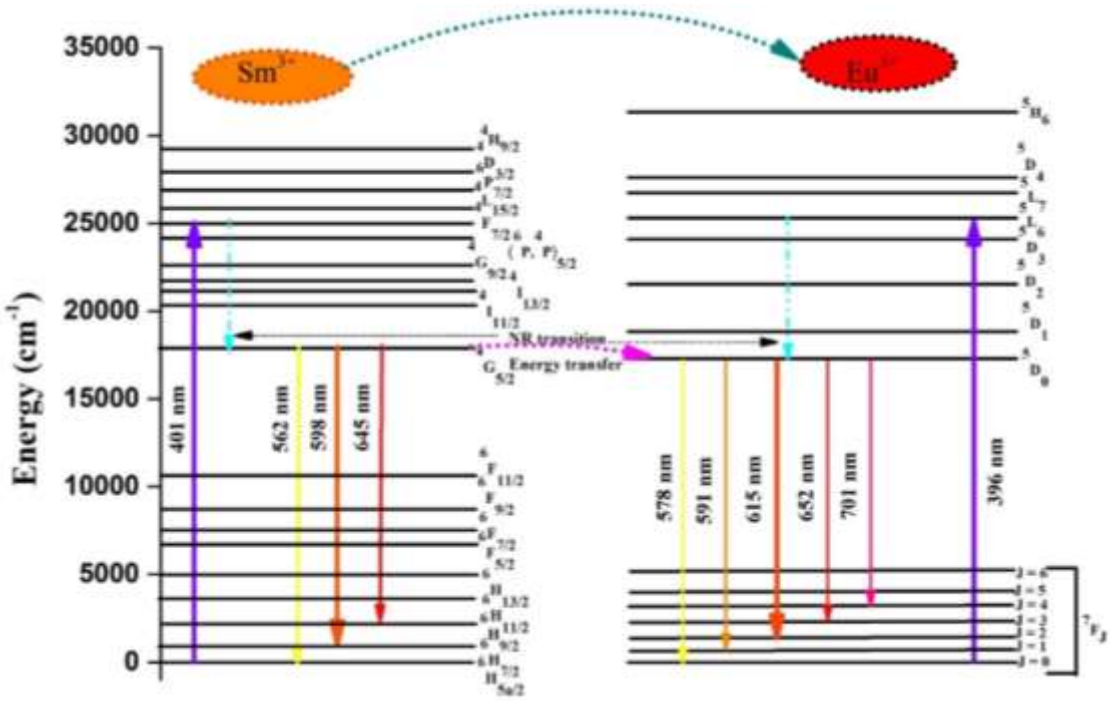

Fig. 5.7. Energy level diagram showing energy transfer involved in the as prepared glasses.

5.3.5. Colorimetric calculations

The colorimetric calculations were conducted on the emission spectral data obtained for Sm^{3+}/Eu^{3+} co-doped LPZABS glasses excited with different excitations wavelengths (362, 374, 396, 401, and 442 nm) and are shown in Fig. 5.8 (a-e). The necessary mathematical equations needed to calculate CIE coordinates and correlated color temperature (CCT) were collected from literature [191]. CIE chromaticity coordinates and corresponding CCT values of Sm^{3+}/Eu^{3+} co-doped LPZABS glasses are shown in Table 5.3 for different excitation wavelengths. From the data represented in Table 5.3, CIE chromaticity coordinates are gradually drifting from the orange region to pure red region with an increase in Eu^{3+} ion concentration.

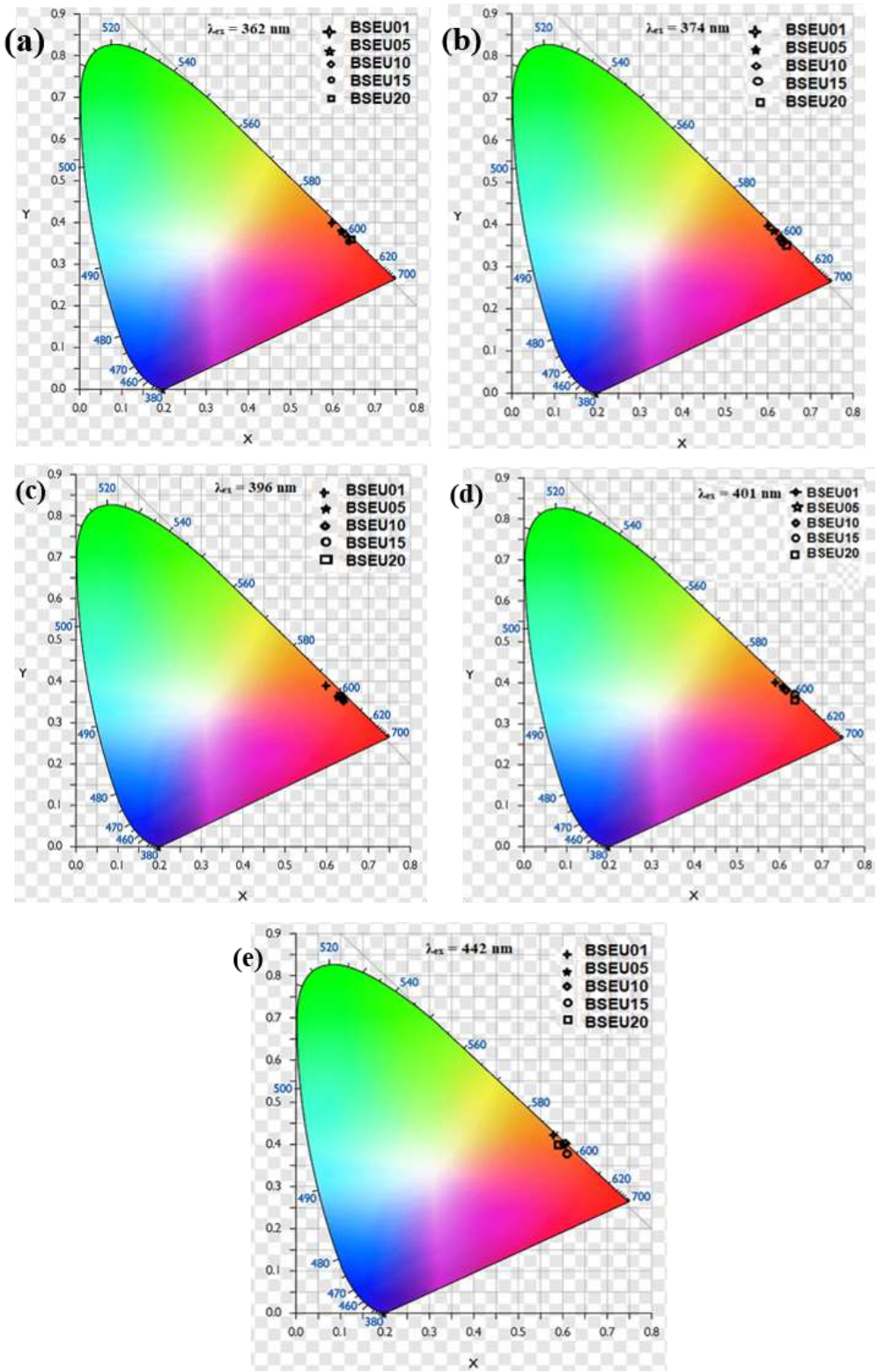

Fig. 5.8. CIE chromaticity diagram of BSEU01, BSEU05, BSEU10, BSEU15 and BSEU20 glasses at excitation wavelength of **(a)** 362 nm, **(b)** 374 nm, **(c)** 396 nm **(d)** 401 nm and **(e)** 442 nm.

Table 5.3. CIE chromaticity coordinates (x, y) and CCT values Sm^{3+}/Eu^{3+} ions in LPZABS glasses under different excitation wavelengths.

Samples	Parameters	Excitation wavelength (nm)				
		362	**374**	**396**	**401**	**442**
BSEU01	**(x,y)**	(0.603,0.396)	(0.602,0.396)	(0.605,0.389)	(0.599,0.399)	(0.579,0.417)
	CCT (K)	1728	1727	1746	1720	1771
BSEU05	**(x,y)**	(0.624,0.374)	(0.623,0.376)	(0.636,0.362)	(0.611,0.387)	(0.601,0.396)
	CCT (K)	1917	1886	2150	1767	1725
BSEU10	**(x,y)**	(0.630,0.368)	(0.627,0.372)	(0.640,0.358)	(0.619,0.378)	(0.596,0.399)
	CCT (K)	2025	1956	2272	1849	1720
BSEU15	**(x,y)**	(0.638,0.359)	(0.637,0.362)	(0.638,0.359)	(0.629,0.369)	(0.610,0.387)
	CCT (K)	2231	2172	2227	2004	1769
BSEU20	**(x,y)**	(0.638,0.360)	(0.639,0.359)	(0.636,0.361)	(0.631,0.366)	(0.591,0.404)
	CCT (K)	2215	2230	2187	2050	1723

CIE chromaticity coordinates obtained for different excitation wavelengths are being in proximity with commercially available red phosphor Y_2O_2S: Eu^{3+} (0.622, 0.351) highlighting the fact that Sm^{3+}/Eu^{3+} co-doped LPZABS glasses are perfect for red fluorescent module needed to construct w-LEDs [2, 204].

5.3.6. PL decay spectral studies

PL luminescence decay curves recorded for $^4G_{5/2} \rightarrow {}^6H_{7/2}$ emission transition (598 nm) of Sm^{3+}/Eu^{3+} co-doped LPZABS glasses under 401 nm excitation wavelength are depicted in Fig. 5.9. Decay curves could possibly be fitted for single, double, or triple exponential functions, according to the equations available in the literature for fluorescent intensity and decay lifetimes:

$$I(t) = I_0 + A_1 \exp\left(-\frac{t}{\tau_1}\right) + \text{-----} A_n \exp\left(-\frac{t}{\tau_n}\right)$$

$$\boldsymbol{\tau} = \left(A_1\tau_1^2 + \text{----} A_n\tau_n^2\right) / \left(A_1\tau_1 + \text{----} A_n\tau_n\right)$$

In these equations, n is 1 for single exponential, 2 for double exponential and 3 for a triple exponential function. I_0 represents primary intensity for t = 0, **τ** represents the duration in which intensity decays to the inverse of exponential to its initial value for single exponential decay expression and A is the fitting constant. The decay curves show exponential fit for lower RE ion concentration and gradually shift to non-exponential fit as concentration of RE ions increases gradually. Herein, increase in Eu^{3+} ion concentration results in a decrease in average lifetimes due to energy transfer from Sm^{3+} to Eu^{3+} ions. The calculated average lifetimes are 2.382, 2.357, 2.303, 2.189, and 2.106 ms for BSEU01, BSEU05, BSEU10, BSEU15, and BSEU20 glasses respectively, and are given in Table 5.4.

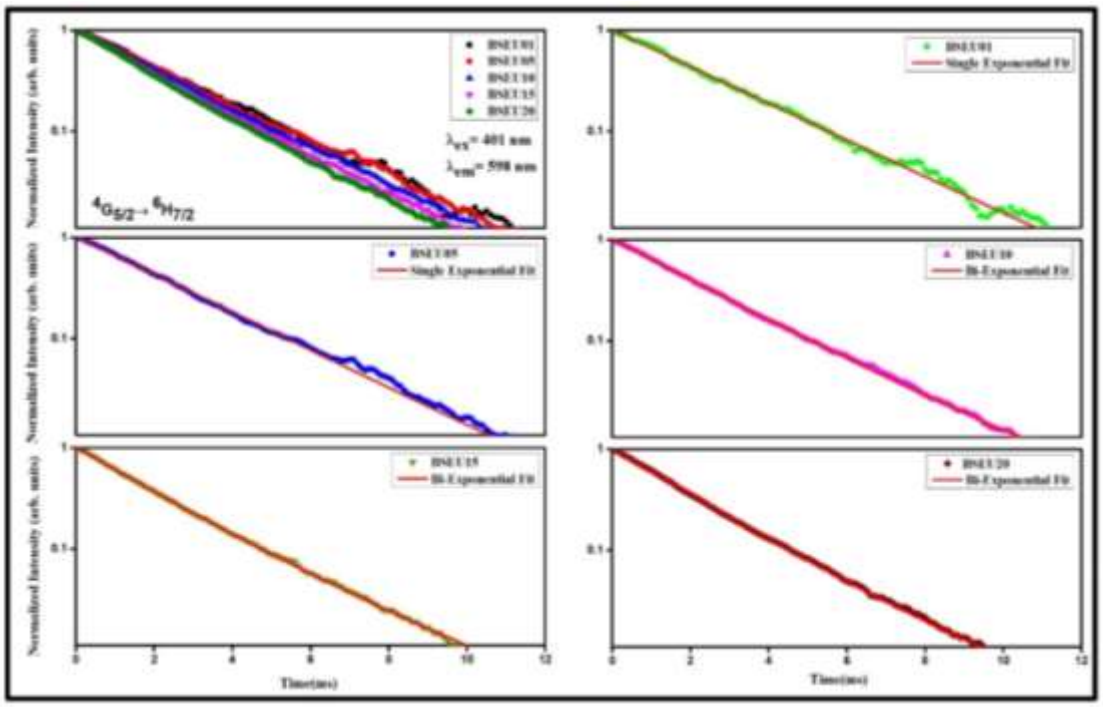

Fig. 5.9. PL decay profiles of BSEU01, BSEU05, BSEU10, BSEU15 and BSEU20 glasses under excitation of 401 nm.

Quantum efficiency can be evaluated through relation [210]:

$$\eta = 1 - \frac{\tau_d}{\tau_{do}}$$

here, τ_d and τ_{do} represent the experimental lifetimes of Sm^{3+} with and without Eu^{3+} ions, respectively, and are given in Table 5.4. The energy transfer probability (P_T) from Sm^{3+} to Eu^{3+} ions due to dipole-dipole interaction can be estimate this equation and are given in Table 5.4:

$$P_T = \frac{1}{\tau_d} - \frac{1}{\tau_{do}}$$

The values obtained for the energy transfer probability enhance with an increase in Eu^{3+} ions concentration in title glasses. Fig. 5.10 depicts the variation of average decay time and quantum efficiency with Eu^{3+} ion concentration.

Table 5.4. Average lifetime (τ_{avg}) (ms), quantum efficiency (η%) and energy transfer probability (P_T) for Sm^{3+}/Eu^{3+} co-doped LPZASB glasses.

Name of sample	τ_{avg}	η (%)	P_T
BSEU01	2.382	20.66	0.0867
BSEU05	2.357	21.48	0.0911
BSEU10	2.303	23.28	0.1011
BSEU15	2.189	27.05	0.1235
BSEU20	2.106	29.83	0.1416

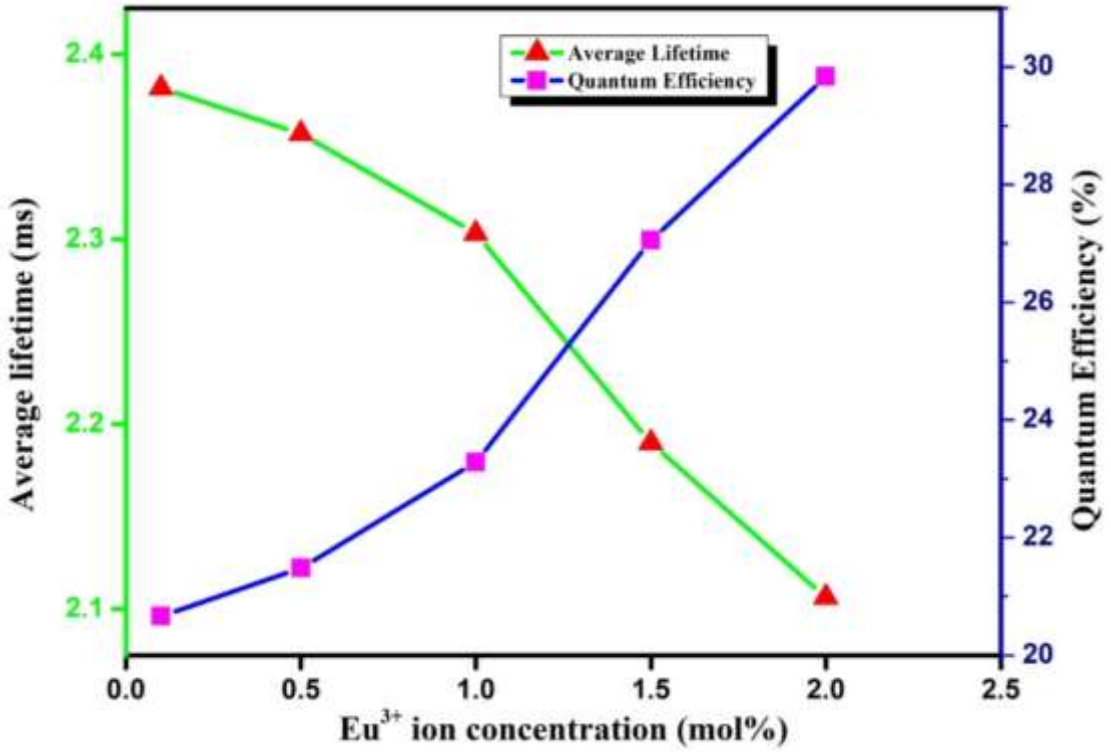

Fig. 5.10. Variation of average lifetime, quantum efficiency of BSEU01, BSEU05, BSEU10, BSEU15 and BSEU20 glasses with Eu^{3+} ion concentration under 401 nm excitation wavelength.

For a better understanding of multipolar interaction responsible for energy transfer process among the doped RE ions, decay curves are subjected to the Inokuti-Hirayama (I-H) model. I-H model provides extensive cognizance of energy exchange methodology for donor to acceptor. According to I-H model, the intensity and time are related as written below [60, 170, 196]:

$$I_t = I_0 \ exp\left\{\frac{-t}{\tau_0} - Q\left(\frac{t}{\tau_0}\right)^{\frac{3}{S}}\right\}$$

here, I_0 is intensity of luminescence when time t = 0, I_t is intensity of luminescence when time t, t being time post excitation, Q represents energy transfer parameter, $\boldsymbol{\tau}_0$ represents intrinsic donor decay time without acceptor. S represents the multipole

index (S = 6, 8 and 10 for dipole-dipole, dipole-quadrupole and quadrupole-quadrupole interaction respectively).

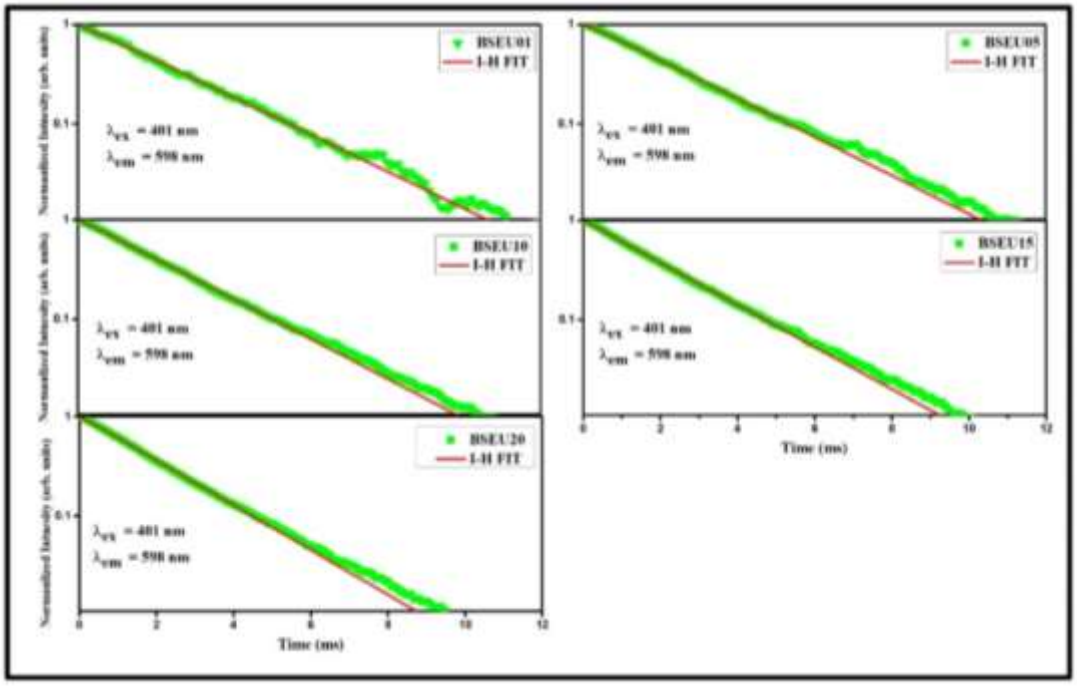

Fig. 5.11. PL decay profiles fitted with I-H model (S = 6) for BSEU01, BSEU05, BSEU10, BSEU15 and BSEU20 glasses.

Decay curves observed for Sm^{3+}/Eu^{3+} co-doped LPZABS glasses were subjected for I-H fitting for various values of S = 6, 8, and 10. The finest fit was procured for S = 6 (i.e., dipole-dipole interaction) as shown in Fig. 5.11. This result obtained from the I-H model is in consonance with the Dexter energy transfer formula and Reisfeld's approximation.

5.4. Conclusions

The melt quenching method is used to prepare Sm^{3+}/Eu^{3+} co-doped LPZABS glasses. Intense emission was observed at 598 nm and 615 nm for Sm^{3+} and Eu^{3+} doped glasses signifying to $^4G_{5/2} \rightarrow {}^6H_{7/2}$ and $^5D_0 \rightarrow {}^7F_2$ bands respectively. The incorporation of Sm^{3+} ions in the form of sensitizer and Eu^{3+} ions as an activator in the host shows

growth in the intensity of excitation spectrum for Sm^{3+}/Eu^{3+} co-doped LPZABS glasses. Under 362 nm and 374 nm excitation, transitions due to Sm^{3+} and Eu^{3+} ions are observable and the intensity for transitions on account of Eu^{3+} increase with an increment of Eu^{3+} ions. Under 401 and 442 nm excitation wavelengths, the emission of Eu^{3+} ions dominate at a higher level of co-doping since the samples were excited with excitation wavelength in the overlapping region. The concentration quenching is noticeable at 1.5 mol% of Eu^{3+} ions in LPZABS glass under 396 nm excitation wavelength of Eu^{3+} ions. The Dexter energy transfer theory-Reisfeld's approximation, the I-H model applied on emission spectra and decay profiles respectively established the mechanism responsible for energy transfer is dipole-dipole in nature. The CIE chromaticity coordinates obtained from PL emission spectra under n-UV excitation shifts from orange to pure red region with an increment in Eu^{3+} ion concentration. All the aforementioned results finally allow us to contemplate that, the Sm^{3+}/Eu^{3+} co-doped LPZABS glasses are quite suitable for the fabrication of CuPc based solar cells as well as w-LEDs under suitable near UV and visible excitation wavelengths.

****

CHAPTER 6

CONCLUSIONS AND FUTURE SCOPE

This chapter contains pertinent conclusions of current research work along with the future scope of the work. The consequence of the current work is aiming the development of borosilicate glasses with potentiality for usage in various photonic device applications. The LPZABS glasses can successfully be prepared and used to develop the optoelectronic device and solar cell applications. We also aim towards investigation of luminescence properties of prepared glasses by altering dopant and host composition.

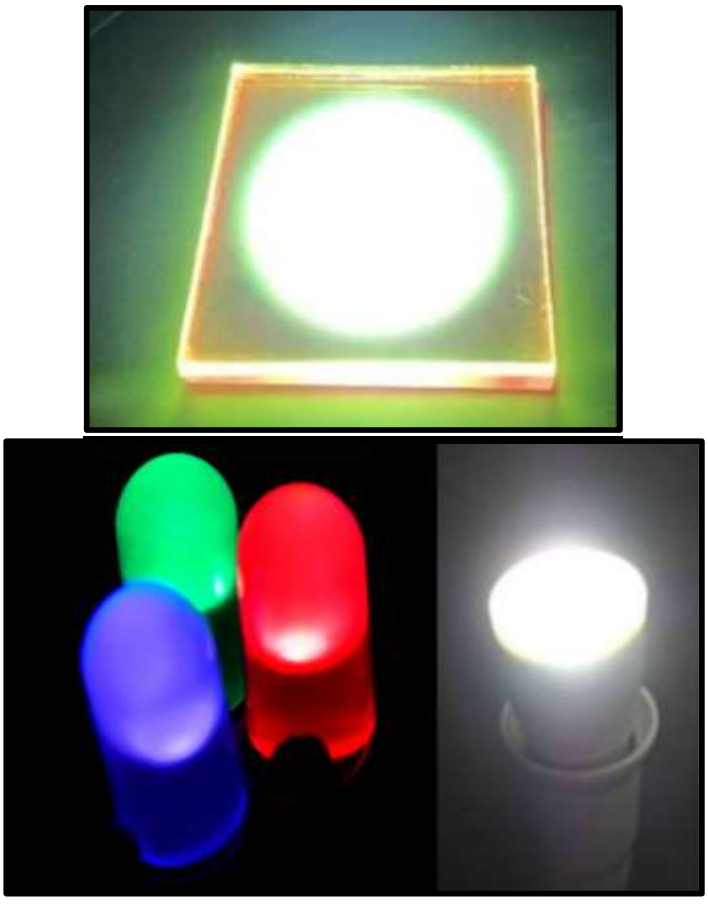

6.1 Conclusions

With the discussion of the objectives of the current work in chapter 1 and preparation of LPZABS glasses by the melt quench technique, resulting in the usage of the LPZABS glasses in the fields of various photonic device applications. In the chapter 2, the preparation technique is discussed in detail with the various characterization techniques to assess structural and optical properties of glasses.

In chapter 3, an intense orange color emitting Sm^{3+} activated LPZABS glasses were fabricated by using sudden quenching method to analyze luminescent assets using spectroscopic methodology like XRD, FT-IR, optical absorption, PL and PL decay measurements. XRD and FT-IR confirms the glassy nature and various functional groups residing in LPZABS host glass. J-O parameters derived from absorption spectra are for estimating various radiative parameters for excited states of Sm^{3+} ions in LPZABS glasses. Under 400 nm excitation, the luminescence spectra in the as prepared glasses exhibit three emission bands that corresponds to $^4G_{5/2}\rightarrow{}^6H_{5/2}$ (563 nm), $^4G_{5/2}\rightarrow{}^6H_{7/2}$ (598 nm) and $^4G_{5/2}\rightarrow{}^6H_{9/2}$ (645 nm) transitions of Sm^{3+} ions. $^4G_{5/2}\rightarrow{}^6H_{9/2}$ transition observed in orange region (598 nm) is relatively more intense and prominent. PL decay curves obtained for $^4G_{5/2}$ fluorescent level exhibit exponential behavior and single exponential fitting is applied to calculate the experimental lifetimes (τ_{exp}). The τ_{exp} values are decreasing with Sm^{3+} ion content as cross-relaxation energy transfer process. The results show that the as prepared Sm^{3+} ion doped LPZABS glasses can be used in preparation of intense visible orange color emitting optoelectronic devices.

In chapter 4, Dy^{3+} ions series of LPZABS glasses was fabricated by melt quench method. Under the spectral analysis, absorption, PLE and PL emission are acquired for Dy^{3+} doped LPZABS glasses. Radiative characteristics were studied by employing the J-O theory on absorption spectral data. 348 nm wavelength is used to record the emission spectra as it is the wavelength which is finest in the excitation spectra obtained at 483 nm for DY01 glass. PL of DY01 to DY25 shows two important peaks in visible region at 483 nm ($^4F_{9/2} \rightarrow {}^6H_{15/2}$) and 575 nm ($^4F_{9/2} \rightarrow {}^6H_{13/2}$). The peak obtained at 483 nm is more intense than the peak obtained at 575 nm. Analyzing the emission data with the radiative properties acquired from absorption spectral feature enable in estimation of emission cross-section, gain band width and optical gain parameters, which in turn gives an insight of LPZABS glasses as photonic devices. White light coordinates of CIE 1931 diagram and calculated coordinates of Dy^{3+} ions doped LPZABS glasses are similar.

In chapter 5, melt quench technique employed for the preparation of Sm^{3+}/Eu^{3+} co-doped LPZABS glasses. Energy transfer method is studied broadly by spectral analysis. XRD of the co-doped series shows the amorphous nature in the series. Elaboration in PLE of Eu^{3+} ions due to sensitizing of it by Sm^{3+} ions in LPZABS glasses. PL of the this co-doped series has bands due to both the ions with increment in intensity on increasing Eu^{3+} ion concentration. Energy transfer confirmation is done by Dexter & Reisfeld's approximation application to PL and I-H model to PL decay profiles. Wherein, d-d interaction among activator and sensitizer is relevant. The CIE chromaticity coordinates obtained from PL emission spectra under n-UV excitation shifts from orange to pure red region with an increment in Eu^{3+} ion concentration. Sm^{3+}/Eu^{3+} co-doped LPZABS glasses are remarkably good for usage for downshifting

of n-UV & blue exciting photons from orange to red photons for copper phthalocyanine (CuPc) solar cell applications.

In a nutshell, major findings and conclusions of the thesis are listed here:

- Successful preparation of LPZABS host glass and doped with Sm^{3+}, Dy^{3+} and Sm^{3+}/Eu^{3+} co-doped ions by melt quench technique.
- XRD and FT-IR data are recorded to study structural characteristic of undoped LPZABS glass.
- Absorption and emission spectra are correlated to study the radiative parameters.
- Application of Dexter and Reisfeld's theory on emission spectra and I-H model on decay curves to predict type of energy transfer interaction among the sensitizer and activator.
- The energy transfer parameters were evaluated through the PL and decay studies.

6.2 Future scope

The current research work is aimed to be extended keeping in mind the various aspects of the luminescent glass. Some areas which are thought upon on working in the future are:

- Optimization of host matrices for diversified photonic device application.
- To improve the luminescence:
  - By altering composition constituents
  - By altering dopant concentration

- By co-doping with suitable RE ions (Nd^{3+}/Yb^{3+})
- By converting the as synthesized glasses into glassy ceramics by heat treating them after recording the DSC and TGA analysis.

- Comparing the efficacy of commercially available materials with the prepared materials.
- To develop efficient RE doped glasses for photonic applications such as laser and w-LEDs.

****

REFERENCES

REFERENCES

[1] S. Hufner, Optical Spectra of Transparent Rare Earth Compounds (Academic press), New York, (1978). https://doi.org/10.1016/B978-0-12-360450-7.X5001-0

[2] M. Kumar, A.S. Rao, S. Kaur, Downshifting analysis of Sm^{3+}/Eu^{3+} co-doped LiBiAlBSi glasses for red emission element of white LEDs, Chem. Phy. Letters, vol 788 (2022) 139303. https://doi.org/10.1016/j.cplett.2021.139303

[3] J. Lucas, Fluoride glasses for modern optics Journal of Fluorine Chemistry, vol. 72 (1995) 177-181. https://doi.org/10.1016/0022-1139(94)00404-4

[4] R.A. Talewar, Sk. Mahamuda, A.S. Rao, S.V. Moharil, Intense infrared emission of Er^{3+} in ZnB_2O_4 phosphors from energy transfer of Bi^{3+} by broadband UV excitation, J. Lumin. Vol. 244, (2022) 118706. https://doi.org/10.1016/j.jlumin.2021.118706

[5] I.Koseva,V.Nikolov,M.Gancheva,L.Aleksandrov,P.Ivanov,P.Petrova,R.Iordanova,R.Tomova, Optical properties of glasses from the system CaO-GeO2-Li2O-B2O3 doped by terbium, Mater. Today. Proc. 61 (2022) 1190-1197. https://doi.org/10.1016/j.matpr.2021.12.118

[6] J.A. Jimenez, S. Lysenko, H. Liu, E. Fachini, C.R. Cabrera, Investigation of the influence of silver and tin on the luminescence of trivalent europium ions in glass, Journal of Luminescence, Vol. 130 (2010) 163-167. https://doi.org/10.1016/j.jlumin.2009.08.007

[7] Y.H. Tsang, D.J. Coleman, T.A. King, High power 1.9μm Tm^{3+}- silica fibre laser pumped at 1.09 μm by a Yb^{3}+-silica fibre laser, Optics Communications, Vol.231 (2004) 357-364. https://doi.org/10.1016/j.optcom.2003.11.072

[8] A. Majchrowski, I.V. Kityk, E. Mandowska, A. Mandowski, J. Ebothe, T. Lukasiewicz, several features of emission spectra of Pr^{3+} ions incorporated into $Li_2B_4O_7$ glass matrices Journal of Applied Physics., vol. 100 (2006) 053101-4. https://doi.org/10.1063/1.2337101

[9] C. Zhu, X. Liang, Y. Yang, G. Chen, Luminescence properties of Tb doped and Tm/Tb/Sm co-doped glasses for LED applications, Journal of Luminescence, Vol. 130 (2010) 74–77. http://dx.doi.org/10.1016/j.jlumin. 2009.07.023

[10] P.R. Ehrmann, J.H. Campbell, Nonradiative energy losses and radiation trapping in neodymium-doped phosphate laser glasses, Journal of the American Ceramic Society, vol. 85 (2002) 1061–1069. https://doi.org/ 10.1111/j.1151-2916.2002.tb00223.x

[11] J. Holsa, H. Jungner, M. Lastuzaari, J. Niittykoski, Persistent luminescence of Eu^{2+} doped alkaline earth aluminates, MAl_2O_4: Eu^{2+}, J. Alloys Compds. Vol. 323 – 324 (2001) 326-330. https://doi.org/10.1016/S0925-8388(01)01084-2

[12] M.F. Joubert, Photon avalanche up conversion in rare earth laser materials, Optical materials, Vol. 11 (1999) 181-203. https://doi.org/10.1016/S0925-3467(98)00043-3

[13] H. Chen, Y. H. Liu, Y.F. Zhou, Z.H. Jiang, Spectroscopic properties of Er^{3+}-doped tellurite glass for 1.55 μm optical amplifier, Journal of Alloys and Compounds, Vol. 397 (2005) 286-290. https://doi.org/10.1016/j.jallcom. 2004.12.051

[14] S. Schweizer, L.W. Hobbs, M. Secu, J.M. Spaeth, A. Edgar, G.V.M. Williams, Photo stimulated luminescence in Eu doped fluorochlorozirconate glass ceramics, Applied Physics Letters, Vol.83 (2003) 449–451. https://doi.org/10.1063/1.1593228

[15] H. Yamauchi, G.S. Murugan, Y. Ohishi, Spectroscopic properties of Tm^{3+} ions in PbO - PbF- $2Bi_2O_3$ - Ga_2O_3 glasses for S-band optical amplifications Journal of Applied Physics, Vol. 96 (2004) 7212-7218. https://doi.org/ 10.1063/1.1814414

[16] S. Sharma, A.S. Rao, K. Kishore, Energy transfer dynamics in thermally stable Sm^{3+}/Eu^{3+} co-doped AEAlBS glasses foe near UV triggered photonic device applications, J. Non. Crys. Solids Vol 580 (2022) 121392. https://doi.org/10.1016/j.jnoncrysol.2021.121392

[17] A.A.Sibirkin, I.G.Fedotova, V.V.Karzanov, Glass forming region and optical properties of TeO_2 -MoO_3-La_2O_3 glasses, J. Non. Cryst. Solids, vol 580 (2022) 121387. https://doi.org/10.1016/j.jnoncrysol.2021.121387

[18] E.González-Suárez, A.Lira, L.Mariscal-Becerra, A.N. Meza-Rocha, U.Caldiño, Phosphor emitting light yellow (laser) and light white through sodium-magnesium-borotellurite glasses activated with Dy^{3+}, Opt. Mat. Vol 123 (2022) 111930. https://doi.org/10.1016/j.optmat.2021.111930

[19] Sk.Mahamuda, P. Sailaja, K. Swapna, M. Venkateswarlu, A.S. Rao, Enhanced red emission in Eu^{3+} ions doped ZnO-Al_2O_3-BaF_2-CaF_2-B_2O_3 glasses for visible laser applications, J. Non. Cryts. Solids, vol 577 (2022) 121306. https://doi.org/10.1016/j.jnoncrysol.2021.121306

[20] Ravita, A.S. Rao, Effective sensitization of Eu^{3+} visible red emission by Sm^{3+} in thermally stable potassium zinc alumino borosilicate glasses for photonic device applications, J. Lumin. Vol 244 (2022) 118689. https://doi.org/10.1016/j.jlumin.2021.118689

[21] P.E. Teresa, M.I. Sayyed, K. Marimuthu, Impact of additives on the structural, elastic, optical and radiation resisting aptitude of the highly dense Sm^{3+} doped multicomponent glasses, Opt. Mater. Vol 122 (2021) 111758. https://doi.org/10.1016/j.optmat.2021.111758

[22] R.H. Doremus, Glass Science, Wiley, 1994.

[23] G.W. Morey, The properties of the Glasses. 2nd edition, Reinhold, N.Y. (1954).

[24] J. E. Stanworth, The ionic structure of glass, Journal Society of Glass Technology Vol. 32 (1948) 366-372.

[25] J. D. Mackenzie (1960-1964) Modern aspects of the vitreous state vol. 1-3, London Butterworths. (1960-1964).

[26] H. Rawson, Inorganic Glass- Forming System academic press, N.Y. (1967).

[27] M. J. Weber, Critical materials problems in energy production Ed. By C. Stein, Academic press, N.Y. (1976).

[28] S.R. Elliott, Physics of amorphous materials, Logman Scientific and Technical, Essex (1990).

[29] D. R. Uhlmann, N.J. Kreidl, Glass, Science and Technology. Volume 4, Academic Press, 1990.

[30] D. Curie, Luminescence in Crystals, John Wiley & Sons Inc, 1963. https://doi.org/10.1107/S0365110X63003352

[31] E.N. Harvey, A History of Luminescence from the Earliest Times until 1900; American Philosophical Society: Philadelphia, 1957. https://doi.org/10.1086/ahr/63.4.937

[32] W.M. Yen, S. Shionoya, H. Yamamoto, Phosphor handbook (2nd. eds, CRC) (2007) 1080. https://doi.org/10.1201/9781315222066

[33] K. Swapna, Sk. Mahamuda, A.S. Rao, M. Jayasimhadri, S. Shakya, G.V. Prakash, Tb^{3+} doped Zinc Alumino Bismuth Borate glasses for green emitting luminescent devices, J. Lumin.156 (2014) 180-187. https://doi.org/10.1016/j.jlumin.2014.08.019

[34] W.H. Brock, The Norton History of Chemistry, 1st American ed., W.W. Norton, New York, 1993.

[35] S. Farooq, Y.M. Reddy, R. Padmasuvarna, V. K. Kummara, C.S. D. Viswanath, Sk. Mahamuda, Structure and photoluminescence of dysprosium doped antimony-magnesium–strontium-oxyfluoroborate glasses, Ceramics Int. 44 (2018) 21303-21308. https://doi.org/10.1016/j.ceramint.2018.08.181

[36] R.A. Talewar, Sk. Mahamuda, K.Swapna, A.S. Rao, Sensitization of Yb^{3+} by Nd^{3+} emission in alkaline-earth chloro borate glasses for laser and fiber amplifier applications, J. Alloys Compd. 771 (2019) 980-986. https://doi.org/10.1016/j.jallcom.2018.08.270

[37] M. Sekita, H. Haneda, S. Shirasaki, T. Yanagitani, Optical spectra of undoped and rare-earth-(=Pr, Nd, Eu, and Er) doped transparent ceramic $Y_3Al_5O_{12}$, J. Appl. Phys. vol 69 (1991) 3709. https://doi.org/10.1063/1.348959

[38] L. J. F. Broer, C. J. Gorter, and J. Hoogschagen, On the intensities and the multipole character in the spectra of the rare earth ions, Physica, vol. 11 (1945) 231-250. https://doi.org/10.1016/S0031-8914(45)80009-5

[39] J. Chrysochoos, and A. Evers, Effect of the primary and secondary solvation spheres of Eu^{3+} upon the electric-quadrupole transitions ($\Delta J=2$), Chemical Physics Letters, vol. 18 (1973) 115-119. https://doi.org/10.1016/0009-2614(73)80353-7

[40] D. M. Gruen, and C. W. Dekock, Absoprtion Spectra of Gaseous $NdBr_3$ and NdI_3, Journal of Chemical Physics, vol. 45 (1966) 455-460. https://doi.org/10.1063/1.1727588

[41] W. F. Krupke, Optical absorption and fluorescence intensities in several rare earth doped Y_2O_3 and LaF_3 single crystals, Physical Review B, vol. 145 (1966) 325-337. https://doi.org/10.1103/PhysRev.145.325

[42] C. K. Jorgensen, and B. R. Judd, Hypersensitive pseudo quadrupole transitions in lanthanides, Molecular Physics, vol. 8 (1964) 281-290. https://doi.org/10.1080/00268976400100321

[43] B. R. Judd, Optical absorption intensities of rare-earth ions, Physical Review, vol. 127 (1962) 750-761. https://doi.org/10.1103/PhysRev.127.750

[44] D. G. Karraker, Hypersensitive transitions of six-, seven-, and eight-coordinate neodymium, holmium, and erbium chelates, Inorganic Chemistry, vol. 5 (1967) 1743-1748. https://doi.org/10.1021/ic50056a022

[45] C. K. Jorgensen, Orbits in Atoms and Molecules, Academic Press, London (1962).

[46] S. P. Sinha, Complexes of Rare Earths, Pergamon Press, Oxford (1966). https://doi.org/10.1016/C2013-0-01952-4

[47] W. T. Carnall, Jr., K.A. Gschneidner, and L. Erying, Handbook on the Physics and Chemistry of Rare Earths, North-Holland, Amsterdam, vol. 3 (1979) p. 171.

[48] R.D. Peacock, Struct. Bond. Berlin 22 (1975) 83-122. http://dx.doi.org/10.1007/BFb0116556

[49] Ch. S. Rao, K. U. Kumar, P. Babu, C.K. Jayasankar, Opt. Mater. 35 (2012) 102-107. https://doi.org/10.1016/j.optmat.2012.07.023

[50] R. Reisfeld, Radiative and nonradiative transition of rare earths in glasses, Structure and Bonding, vol. 22 (1975) 123-175. https://doi.org/10.1007/BFb0116557

[51] E. U. Condon, and G. H. Shortley, The Theory of Atomic Spectra, Cambridge University Press, London (1957).

[52] M. Zahir, R. Olazcuaga, C. Parent, G. Le Flem, and P. Hagenmuller, A structural interpretation of the Pb^{3+}, Eu^{3+} and Nd^{3+} optical spectra in doped sodium borate glasses, Journal of Non-Crystalline Solids, vol. 69, 2-3 (1985) 221-229. https://doi.org/10.1016/0022-3093(85)90024-9

[53] E.W.J.L. Oomen, A. M. A. van Dongen, Europium (III) in oxide glasses: Dependence of the emission spectrum upon glass composition, Journal of Non-Crystalline Solids, vol. 111 2-3 (1989) 205-213. 10.1016/0022-3093(89)90282-2

[54] R. Reisfeld, and C. K. Jorgensen, K. A. Jr. Gschneidner and L. Erying, Handbook on the Physics and Chemistry of Rare Earths North Holland, Amsterdam, vol 9 (1987) p 1.

[55] A. A. Kaminiskii, Laser Crystals, Springer, Berlin. Laser Crystals (1990).

[56] T. Srikumar, M.G. Brik, C.S. Rao, N. Venkatramaiah, Y. Gandhi, N. Veeraiah, Physica B 406 (2011) 3592-3598. https://doi.org/10.1016/j.physb.2011.06.046

[57] Tanabe, S., Ohyagi, T., Soga, N. and Hanada, T., (1992) Compositional dependence of Judd-Ofelt parameters of Er^{3+} ions in alkali-metal borate glasses, Physical Review B, vol. 46 3305-3310. https://doi.org/10.1103/PhysRevB.46.3305

[58] T. Forster, Inter-molecular energy migration and fluorescence, Annalen der Physik, vol. 6 (1948) 55-75. https://doi.org/10.1002/andp.19484370105

[59] D. L. Dexter, A theory of sensitized luminescence in solids, Journal of Chemical Physics, vol. 21 (1953) 836-850. https://doi.org/10.1063/1.1699044

[60] M. Inokuti and F. Hirayama, Influence of energy transfer by the exchange mechanism on donor luminescence, Journal of Chemical Physics, vol. 43, (1965) 1978. https://doi.org/10.1063/1.1697063

[61] E. Fred Schubert, Light-Emitting Diodes, 2nd edition, Cambridge University Press, Chapter 17 (2006)292-298.

[62] M. Shaw, M. Fairchild, Evaluating the 1931 CIE color-matching functions, Color research & application, 27(5) 2002 316-329. https://doi.org/10.1002/col.10077

[63] T.W. Kuo, W. R. Liu, T. M. Chen, High color rendering white light-emitting-diode illuminator using the red-emitting Eu^{2+} activated CaZnOS phosphors excited by blue LED, Opt. Express. 18 (2010) 8187-8192. https://doi.org/10.1364/OE.18.008187

[64] K.V. Krishnaiah, K.U. Kumar, C.K. Jayasankar, Spectroscopic properties of Dy^{3+} doped oxyfluoride glasses for white light emitting diodes, Mater. Express 3 (2013) 61-70. https://doi.org/10.1166/mex.2013.1094

[65] H. M. Yang, J. X. Shi, and M. L. Gong, A novel red emitting phosphor $Ca_2SnO_4:Eu^{3+}$, Solid State Chemistry, vol. 178, 3 (2005) 917-920. https://doi.org/10.1016/j.jssc.2004.12.022

[66] M. Venkateswarlu, M.V.V.K.S. Prasad, K. Swapna, Sk. Mahamuda, A.S. Rao, A. Mohan Babu, D. Haranath, Pr^{3+} doped lead tungsten tellurite glasses for visible red lasers, Ceramics International, vol. 40 (2014) 6261-6269. https://doi.org/10.1016/j.ceramint.2013.11.084

[67] K. Swapna, Sk. Mahamuda, A.S. Rao, M. Jayasimhadri, T. Sasikala, and L.Rama Moorthy, Optical Absorption and luminescence characteristics of Dy^{3+} doped Zinc Alumino Bismuth Boarte glasses for lasing materials and white LEDs, Journal of Luminescence vol. 139 (2013) 119-124. https://doi.org/10.1016/j.jlumin.2013.02.035

[68] K.H. Sun, M.L. Huggins, Energy Additivity in Oxygen-containing Crystals and Glasses, Journal of Physical and Colloid Chemistry, vol.51 (1947) 438–443. https://doi.org/10.1021/j150452a009

[69] S.M. Kaczmark, $Li_2B_4O_7$ glasses doped with Cr, Co, Eu and Dy, Opt. Mater. vol.19 (2002) 189-194. https://doi.org/10.1016/S0925-3467(01)00218-X

[70] R. Bajaj, A.S. Rao, G.V. Prakash, Photoluminescence down-shifting studies of thermally stable Eu^{3+} ions doped borosilicate glasses for visible red photonic device applications, J. Non. Cryst. Solids. Vol 575 (2022) 121184 https://doi.org/10.1016/j.jnoncrysol.2021.121184

[71] N. Deopa, B. Kumar, M. Sahu, P. R. Rani, A.S. Rao, Effect of Sm^{3+} ions concentration on borosilicate glasses for reddish orange luminescent device applications, J. Non. Cryst. Solids. 513 (2019) 152-158. https://doi.org/10.1016/j.jnoncrysol.2019.03.025

[72] M. Monisha, N. Mazumder, G. Lakshminarayana, S. Mandal, S.D. Kamath, Energy transfer and luminescence study of Dy^{3+} doped zinc aluminoborosilicate glasses for white light emission, Ceram. Int. 47 (2021) 598-610. https://doi.org/10.1016/j.ceramint.2020.08.167

[73] K.V. Babu, S. Cole, Luminescence properties of Dy^{3+}-doped alkali lead alumino borosilicate glasses, Ceram. Int. 44 (2018) 9080-9090. https://doi.org/10.1016/j.ceramint.2018.02.115

[74] S. Kaur, A.K. Vishwakarma, N. Deopa, A. Prasad, M. Jayasimhadri, A.S. Rao, Spectroscopic studies of Dy^{3+}doped borate glasses for cool white light generation Mater. Res. Bull. 104 (2018) 77–82, https://doi.org/10.1016/ j.materresbull.2018 04.002

[75] P. Karthikeyan, R. Vijayakumar, K. Marimuthu, Luminescence studies on Dy^{3+} doped calcium boro-tellurite glasses for White light applications, Phys. B Condens. Matter 521 (2017) 347–354, https://doi.org/10.1016/j.physb. 2017.07.018

[76] T.Y. Lim, H. Wagiran, R. Hussin, S. Hashim, M.A. Saeed, Physical and optical properties of dysprosium ion doped strontium borate glasses, Phys. B Condens. Matter 451 (2014) 63–67, https://doi.org/10.1016/j.physb.2014. 06.028

[77] S. Kaur, N. Deopa, A. Prasad, R. Bajaj, A.S. Rao, Intense green emission from Tb^{3+} ions doped zinc lead alumino borate glasses for laser and w-LEDs applications, Opt. Mater. 84 (2018) 318- 323. https://doi.org/10.1016/j.optmat. 2018.07.020

[78] M. Venkateswarlu, S. Mahamuda, K. Swapna, M.V.V.K.S. Prasad, A.S. Rao, A.M. Babu, S. Shakya, G.V. Prakash, Spectroscopic studies of Nd^{3+} doped lead tungsten tellurite glasses for the NIR emission at 1062 nm, Opt. Mater. 39 (2015) 8–15, https://doi.org/10.1016/j.optmat.2014.10.031

[79] R. Sharma, A.S. Rao, N. Deopa, M. Venkateswarlu, M. Jayasimhadri, D. Haranath, G.V. Prakash, Spectroscopic study of Pr^{3+} ions doped Zinc Lead Tungsten Tellurite glasses for visible photonic device applications, Opt. Mater. 78 (2018) 457–464, https://doi.org/10.1016/j.optmat.2018.02.054

[80] W.T. Carnall, K.A. Gschneidner, L. Eyring (Eds.), Hand book of physics and chemistry of rare earths, 1987.

[81] G.S. Ofelt, Intensities of Crystal Spectra of Rare- Earth Ions, J. Chem. Phys. 37 (1962) 511-520. https://doi.org/10.1063/1.1701366

[82] B. Suneetha, S. Sailaja, S.J. Dhoble, B.S. Reddy, Optical analysis of RE^{3+}(RE=Eu, Tb): CdO-PbO-B_2O_3-AlF_3 glasses, Optik 155 (2018) 216–224, https://doi.org/10.1016/j.ijleo.2017.10.155

[83] P. Karthikeyan, S. Arunkumar, K. Annapoorani, K. Marimuthu, Investigations on the spectroscopic properties of Dy^{3+} ions doped Zinc calcium tellurofluoroborate glasses, Spectrochim. Acta Part A Mol. Biomol. Spectrosc 193 (2018) 422–431, https://doi.org/10.1016/j.saa.2017.12.049

[84] C.M. Reddy, G.R. Dillip, B.D.P. Raju, J. Phys. Chem.Solids, 72 (2011) 1436-1441. https://doi.org/10.1016/j.jpcs.2011.08.023

[85] D. Jain, V. Sudharsan, R.K. Vatsa, C.G.S. Pillai, Luminescence studies on ZnO–P_2O_5 glasses doped with Gd_2O_3:Eu nanoparticles and Eu_2O_3, Journal of Luminescence, Vol. 129 (2009) 439–443. 10.1016/j.jlumin.2008.11.011

[86] S. Jiang, T. Luo, M. Myers, J. Myers, J. Lucas, N. Peyghambarian, Phosphate Glasses for High Average Power Lasers, Rare Earth Doped Devices II, SPIE Proceedings Vol. 3280, Photonics West (1998) 2–13. https://doi.org/10.1117/12.305389

[87] C. Hirayama, Properties of aluminoborate glasses of group II metal oxides electrical Properties, Journal of American Ceramic Society, Vol.45 (1962) 288- 293. https://doi.org/10.1111/j.1151-2916.1962.tb11147.x

[88] S.R. Elliott, Physics of Amorphous materials. Longman science and technology Essex section 3, (1984) 53-133.

[89] K. Arai, H. Namikawa, K. Kumata, T. Honda, Y. Ishii, T. Handa, Aluminum or phosphorus co- doping effects on the fluorescence and structural properties of neodymium-doped silica glass, Journal of Applied Mathematics, Vol. 59 (1986) 3430-3436. https://doi.org/10.1063/1.336810

[90] S. Tanabe, Optical transitions of rare earth ions for amplifiers: how the local structure works in glass, Journal of non-crystalline solids, Vol.259 (1999) 1-9. https://doi.org/10.1016/S0022-3093(99)00490-1

[91] Y. Tayal, A.S. Rao, Orange color emitting Sm^{3+} ions doped borosilicate glasses for optoelectronic device applications. Opt. Mat. 107, 110070 (2020). https://doi.org/10.1016/j.optmat.2020.110070

[92] Y. Tayal, A.S. Rao, Spectroscopic analysis of Dy^{3+} ions activated borosilicate glasses for photonic device applications, Opt. Mat. 117 (2021) 111112. https://doi.org/10.1016/j.optmat.2021.111112

[93] R.A. Talewar, Sk. Mahamuda, K. Swapna, M. Venkateswarlu, A.S. Rao, Spectroscopic studies of Sm^{3+} ions doped alkaline–earth chloro borate glasses for visible photonic applications, Mater. Res. Bull. 105 (2018) 45-54. https://doi.org/10.1016/j.materresbull.2018.04.033

[94] S. Kaur, A.S. Rao, M. Jayasimhadri, V.V. Jaiswal, D. Haranath, Tb^{3+} ion induced colour tenability in calcium aluminozincate phosphor for lighting and display devices, J. Alloy. Comp. 826 (2020) 154212. https://doi.org/10.1016/ j.jallcom.2020.154212

[95] X. Chen, H. Zhang, W. Jia, C. Su, Preparation and luminescence properties of Eu_2O_3 doped glass ceramics containing $Na_3Gd(PO_4)_2$, Optik 238 (2021) 166778. https://doi.org/10.1016/j.ijleo.2021.166778

[96] L. Liang, Z. Mo, B. Ju, C. Xia, Z. Hou, G. Zhou, Visible and near-infrared emission properties of Yb_{3+}/Pr_{3+} co-doped lanthanum aluminum silicate glass, J. of Non-Crystalline Solids, 557 (2021) 120578. https://doi.org/10. 1016/j.jnoncrysol.2020.120578

[97] J. Zhang, X. Zhang, H. Yin, Z. Zhang, X. Liu, X. Gong, R. Ding, Nd_{3+}/Yb_{3+} co-doped mid-infrared luminescence fluoroborate glass with energy transfer and zero-thermal quenching IR emission, J. of Rare Earths, 39 (2021) 1049-1055. https://doi.org/10.1016/j.jre.2021.03.003

[98] A. Herrera, F. Londono, N.M. Balzaretti, Structural and optical properties of Nd_{3+} doped GeO_2-PbO glass modified by TiO_2 for applications in laser and fiber amplifier, Opt. Mater., 113 (2021) 110884. https://doi.org/10. 1016/j.optmat.2021.110884

[99] Y. Yan, H. Huo, H. Zhang, T. Zhao, Q. Wang, X. Zou, C. Su, Preparation and luminescence of Dy^{3+} doped glass-ceramics containing $ZnMoO_4$, J. of Non-Cryst. Solids, 569 (2021) 120990. https://doi.org/10.1016/j.jnoncrysol.2021.120990

[100] L.N.L. Silva, A. Torquato, I.N. Assis Jr., M.R. Dousti, Spectroscopic study of Er^{3+}-doped zinc tellurite glass and opaque glass ceramic, Solid State Sciences, 112 (2021) 106444. https://doi.org/10.1016/j.solidstatesciences.2020.106444

[101] M. Mariselvam, J. Liu, Green emission and laser properties of Ho^{3+} doped titano lead borate (TLB) glasses for colour display applications, J. of Solid State Chemistry, 293 (2021) 121793. https://doi.org/10.1016/j.jssc.2020.121793

[102] K.J. Rao, Structural chemistry of glass, Elsevier ltd. 2002.

[103] J.L. Adam, X. Zhang, Chalcogenide glasses, Woodhead publishing, 2013.

[104] L.D. Pye, V. D. Frechette, N.J. Kreidl, Borate Glass Structure, in: Borate Glasses, Structure, Properties, Applications, Material Science Research, Vol.12, 1978 Plenum Press New York, London 11–138.

[105] A.S. Rao, Y.N. Ahammed, R.R. Reddy, T.V.R. Rao, Spectroscopic studies of Nd^{3+}-doped alkali fluoroborophosphate glasses, Optical Mater. Vol 10 (1998) 245-252. https://doi.org/10.1016/S0925-3467(97)00055-4

[106] B. D. Cullity, elements of x-ray diffraction, Addison-wesley publishing company, inc, 1956, 84.

[107] A. Agarwal, V.P. Seth, S. Sanghi, P. Gahlot, D.R. Goyal, Optical band gap studies and estimation of two photon absorption coefficient in alkali bismuth borate glasses, 158 (2003) 793-801. https://doi.org/10.1080/10420150310001618214

[108] M. Altaf, M.A. Chaudhary, M. Zahid, Study of optical band gap of Zinc-borate glasses, J. Res. (Science) 14 (2003) 253–259.

[109] A.S. Rao, R.R. Reddy, T.V.R. Rao, J.L. Rao, Electron Paramagnetic Resonance and optical absorption spectra of Fe^{3+} ions in alkali cadmium borosulphate glasses, Solid State Commun. 96 (9) (1995) 701-705. https://doi.org/10.1016/0038-1098(95)00375-4

[110] K. Li, X. Liu, Y. Zhang, X. Li, H. Lian, J. Lin, Host-Sensitized Luminescence Properties in $CaNb_2O_6$:Ln^{3+} (Ln^{3+} = Eu^{3+}/Tb^{3+}/Dy^{3+}/Sm^{3+}) Phosphors with Abundant Colors, Inorg. Chem. 54 (2015) 323-333. https://doi.org/10.1021/ic502493c

[111] K.A. Kumar, S. Babu, V.R. Prasad, S. Damodaraiah, Y.C. Ratnakaram, Optical response and luminescence characteristics of Sm^{3+} and Tb^{3+}/Sm^{3+} co-doped potassium-fluoro-phosphate glasses for reddish-orange lighting applications, Mater. Res. Bull. 90 (2017) 31-40. https://doi.org/10.1016/j.materresbull.2017.01.046

[112] M. Venkateswarlu, Sk. Mahamuda, K. Swapna, M.V.V.K.S. Prasad, A.S. Rao, Suman Shakya, M. Mohan Babu, G.V.Prakash, Holmium doped lead tungsten tellurite glasses for green luminescent applications, J. Lumin. 163 (2015) 64-71. https://doi.org/10.1016/j.jlumin.2015.02.052

[113] Ch. B Annapurna Devi, K. Swapna, Sk. Mahamuda, M. Venkateswarlu, M.V.V.K.S. Prasad, K.S.R.K. Reddy, N. Deopa, A.S. Rao, Spectroscopic studies and lasing potentialities of Sm^{3+} ions doped single alkali and mixed alkali fluoro tungstentellurite glasses, Optics and Laser Technology 111 (2019) 176-183. https://doi.org/10.1016/j.optlastec.2018.09.051

[114] X. Zhou, G. Ju, T. Dai, Y. Li, H. Wu, Y.Jin, Y. Hu, Strontium substitution enhancing a novel Sm^{3+}-doped barium gallate phosphor with bright and red long persistent luminescence, J. Lumin. 218 (2020) 116820. https://doi.org/10.1016/j.jlumin.2019.116820

[115] P.R. Rani, M. Venkateswarlu, Sk. Mahamuda, K. Swapna, N. Deopa, A.S. Rao, Structural, absorption and photoluminescence studies of Sm^{3+} ions doped barium lead alumino fluoro borate glasses for optoelectronic device applications, Mater. Research Bullitin. 110 (2019) 159-168. https://doi.org/10.1016/j.materresbull.2018.10.033

[116] Sk. Mahamuda, K. Swapna, M. Venkateswarlu, A.S. Rao, S. Shakya, G.V. Prakash, Spectral characterization of Sm^{3+} ions doped Oxy-fluoroborate glasses for visible orange luminescent applications, J. Lumin. 154 (2014) 410-424. https://doi.org/10.1016/j.jlumin.2014.05.017

[117] K.S.R. K. Reddy, K. Swapna, Sk. Mahamuda, M. Venkateswarlu, M.V.V.K. S. Prasad, A.S. Rao, G. V. Prakash, Structural, optical absorption and photoluminescence spectral studies of Sm^{3+} ions in Alkaline-Earth Boro Tellurite glasses, Opt. Mater. 79 (2018) 21-32. https://doi.org/10.1016/ j.optmat.2018.03.005

[118] G. Qian, M. Nikl, J. Bei, J. Pejchal, S. Baccaro, R. Giorgi, A. Cecilia, G. Chen, Temperature dependence of photoluminescence in ZnO-containing glasses, Opt. Mater. 30 (2007) 91-94.https://doi.org/10.1016/j.optmat.2006. 11.054

[119] N. Deopa, S. Saini, S. Kaur, A. Prasad, A.S. Rao, Spectroscopic investigations on Dy^{3+} ions doped zinc lead alumino borate glasses for photonic device applications, J. of Rare Earths. 37 (2019) 52-59. https://doi.org/10.1016/j.jre. 2018.04.013

[120] R.E.de Lamaëstre, H. Bernas, PbS nanocrystal synthesis in Pb-containing silicate glasses, J. Appl. Phys. 98 (2005) 104310. https://doi.org/10.1063/ 1.2132091

[121] L. Ding, Y. Yang, X. Jiang, C. Zhu, G. Chen, Photoluminescence of undoped and B-doped ZnO in silicate glasses, J. of Non-Cryst. Solids 354 (2008) 1382–1385. https://doi.org/10.1016/j.jnoncrysol.2006.10.088

[122] G. Alombert-Goget, N. Gaumer, J. Obriot, A. Rammal, S. Chaussedent, A. Monteil, H. Portales, A. Chiasera, M. Ferrari, Aluminum effect on photoluminescence properties of sol–gel-derived Eu^{3+}-activated silicate glasses, J. Non-Cryst. Solids 351 (2005) 1754–1758. https://doi.org/10.1016/j. jnoncrysol.2005.04.009

[123] L. Koao, H.C. Swart, F. B. Dejene, Effects of aluminum co-doping on photoluminescence properties of Ce^{3+}-doped SiO_2 glasses, Journal of Rare Earths, 28 (2010) 206-210. https://doi.org/10.1016/S1002-0721(10)60368-7

[124] C. F. Song, M. K. Lu, F. Gu, S. W. Liu, S. F. Wang, D. Xu, D. R. Yuan, Effect of Al^{3+} on the photoluminescence properties of Ni^{2+}-doped sol–gel SiO_2 glass, Inorg. Chem. Comm. 6 (2003) 523–526. https://doi.org/10.1016/S1387-7003(03)00019-4

[125] F.H.A. Elbatal, M.M.I. Khalil, N. Nada, S.A. Desouky, Gamma rays interaction with ternary silicate glasses containing mixed CoO+NiO, Mater. Chem. Phys. 82 (2003) 375- 387. https://doi.org/10.1016/S0254-0584(03)00270-0

[126] E.I. Kamitsos, A.P. Patsis, M.A. Karakassides, G.D. Chryssikos, Infrared reflectance spectra of lithium borate glasses, J. Non. Cryst. Solids. 126 (1990) 52-67. https://doi.org/10.1016/0022-3093(90)91023-K

[127] M.S. Gaafar, S.Y. Marzouk, Mechanical and structural studies on sodium borosilicate glasses doped with Er_2O_3 using ultrasonic velocity and FTIR spectroscopy, Physica B: Condens. Matter 388 (2007) 294-302. https://doi.org/10.1016/j.physb.2006.06.132

[128] N. Deopa, A.S. Rao, Spectroscopic studies of Sm^{3+} ions activated lithium lead alumino borate glasses for visible luminescent device applications, Opt. Mater. 72 (2017) 31-39. https://doi.org/10.1016/j.optmat.2017.04.067

[129] W. T. Carnall, K.A. Gschneidner, L. Eyring (Eds.), Handbook on the Physics and Chemistry of Rare- Earths, 26 (1987).

[130] S. Arunkumar, K. Marimuthu, Concentration effect of Sm^{3+} ions in B_2O_3–PbO–PbF_2–Bi_2O_3–ZnO glasses – Structural and luminescence investigations, J. Alloy. Compd. 565 (2013) 104-114. https://doi.org/10.1016/j.jallcom. 2013.02.151

[131] A.S. Rao, B.R.V. Rao, M.V.V.K.S. Prasad, J.V.S. Kumar, M. Jayasimhadri, J.L. Rao, R.P.S. Chakradhar, Spectroscopic and optical properties of Nd^{3+} doped fluorine containing alkali and alkaline earth zinc-aluminophosphate optical glasses, Physica B. 404 (2009) 3717-3721. https://doi.org/10.1016/j.physb.2009.06.114

[132] W.T. Carnall, P. R. Fields, K. Rajnak, Spectral Intensities of the Trivalent Lanthanides and Actinides in Solution. II. Pm^{3+}, Sm^{3+}, Eu^{3+}, Gd^{3+}, Tb^{3+}, Dy^{3+}, and Ho^{3+}, J. Chem. Phys. 49 (1968) 4412-4423. https://doi.org/10.1063/1.1669892

[133] R. Sharma, A. Prasad, S. Kaur, N. Deopa, P. Rekha Rani, M. Venkteswarlu, A.S. Rao, Spectroscopic properties of deep red emitting Tm^{3+} doped ZnPbWTe glasses for optoelectronic and laser applications, J. Non-Cryst. Solids. 516 (2019) 82-88. https://doi.org/10.1016/j.jnoncrysol.2019.04.032

[134] R. Sharma, A.S. Rao, Photoluminescence study of Sm^{3+} doped zinc lead tungsten tellurite glasses for reddish-orange photonic device applications, Opt. Mater. 84 (2018) 375-382. https://doi.org/10.1016/j.optmat.2018.07.035

[135] R. Praveena, V. Venkatramu, P. Babu, C.K. Jayasankar, Fluorescence spectroscopy of Sm^{3+} ions in P_2O_5–PbO–Nb_2O_5 glasses, Physica B 403 (2008) 3527-3534. https://doi.org/10.1016/j.physb.2008.05.027

[136] N. Deopa, A.S. Ro, M. Gupta, G.V. Prakash, Spectroscopic investigations of Nd^{3+} doped lithium lead alumino borate glasses for 1.06 μm laser applications, Optical Mater. 75 (2018) 127-134. https://doi.org/10.1016/j.optmat.2017.09.047

[137] Y.K. Sharma, S.S.L. Surana, R.P. Dubedi, V. Joshi, Spectroscopic and radiative properties of Sm^{3+} doped zinc fluoride borophosphate glasses, Mater. Sci. Eng. B 119 (2005) 131-135. https://doi.org/10.1016/j.mseb.2005.01.016

[138] P. Srivastava, S.B. Rai, D.K. Rai, Optical properties of Sm^{3+} doped calibo glass with addition of lead oxide, Spectrochim. Acta - Part A 60 (2004) 637-642. https://doi.org/10.1016/S1386-1425(03)00273-7

[139] Sk. Mahamuda, K. Swapna, P. Packiyaraj, A.S. Rao, G. V. Prakash, Visible red, NIR and Mid-IR emission studies of Ho^{3+} doped Zinc Alumino Bismuth Borate glasses, Opt. Mater. 36 (2013) 362-371. https://doi.org/10.1016/j.optmat.2013.09.023

[140] K.S.V. Sudhakar, M.S. Reddy, L.S. Rao, N. Veeraiah, Influence of modifier oxide on spectroscopic and thermoluminescence characteristics of Sm^{3+} ion in antimony borate glass system, J. Lumin. 128 (2008) 1791-1798. https://doi.org/10.1016/j.jlumin.2008.04.010

[141] B.C. Jamalaiah, M.V.V. Kumar, K.R. Gopal, Fluorescence properties and energy transfer mechanism of Sm^{3+} ion in lead telluroborate glasses, Opt. Mater. 33 (2011) 1643-1647. https://doi.org/10.1016/j.optmat.2011.04.030

[142] Sk. Mahamuda, K. Swapna, A.S. Rao, T. Sasikala, L.R. Moorthy, Reddish-orange emission from Pr^{3+} doped zinc alumino bismuth borate glasses, Physica B 428 (2013) 36-42. https://doi.org/10.1016/j.physb.2013.07.010

[143] Y. C Ratnakaram, D. T. Naidu, A.V. Kumar, N.O. Gopal, Influence of mixed alkalies on absorption and emission properties of Sm^{3+} ions in borate glasses, Physica B 358 (2005) 296–307. https://doi.org/10.1016/j.physb.2005.01.464

[144] S. Sailaja, C. N. Raju, C. A. Reddy, B. D. P. Raju, Y. Jho, B. S. Reddy, Optical properties of Sm^{3+}-doped cadmium bismuth borate glasses, J. Mol. Struct. 1038 (2013) 29–34. https://doi.org/10.1016/j.molstruc.2013.01.052

[145] C.K. Jayasankar, E. Rukmini, Optical properties of Sm^{3+} ions in zinc and alkali zinc borosulphate glasses, Opt. Mater. 8 (1997) 193-205. https://doi.org/10.1016/S0925-3467(97)00021-9

[146] M.B. Saisudha, J. Ramakrishna, Optical absorption of Nd^{3+}, Sm^{3+} and Dy^{3+} in bismuth borate glasses with large radiative transition probabilities, Opt. Mater. 18 (2002) 403-417. https://doi.org/10.1016/S0925-3467(01)00181-1

[147] I.A. Rayappan, K. Selvaraju, K. Marimuthu, Structural and luminescence investigations on Sm^{3+} doped sodium fluoroborate glasses containing alkali/alkaline earth metal oxides, Physica B 406 (2011) 548-555. https://doi.org/10.1016/j.physb.2010.11.037

[148] L. Boehm, R. Reisfeld, N. Spector, Optical Transitions of Sm^{3+} in Oxide glasses, J. Solid State Chem. 28 (1979) 75-78. https://doi.org/10.1016/0022-4596(79)90060-4

[149] T. Srihari, C.K. Jayasankar, Spectral investigations of Sm^{3+}-doped niobium phosphate glasses, Opt. Mater. 66 (2017) 35-42. https://doi.org/10.1016/j.optmat.2017.01.027

[150] Z. Wu, B. Chen, X. Li, J. Zhang, J. Sun, H. Zhong, H. Zheng, L. Tong, H. Xia, Optical transition properties, energy transfer mechanism and luminescent thermal stability of Sm^{3+} doped silicate glasses, J. Alloys Compd. 663 (2016) 545-551. https://doi.org/10.1016/j.jallcom.2015.12.140

[151] G. Venkataiah, C.K. Jayasankar, K. V. Krishnaiah, P. Dharmaiah, N. Vijaya, Concentration dependent luminescence properties of Sm^{3+}-ions in tellurite-tungsten-zirconium glasses, Opt. Mater. 40 (2015) 26-35. https://doi.org/10.1016/j.optmat.2014.11.042

[152] I.I. Kindrat, B.V. Padlyak, R. Lisiecki, Judd–Ofelt analysis and radiative properties of the Sm^{3+} centres in $Li_2B_4O_7$, CaB_4O_7, and $LiCaBO_3$ glasses, Opt. Mater. 49 (2015) 241-248. https://doi.org/10.1016/j.optmat.2015.09.024

[153] K. Swapna, Sk. Mahamuda, A.S. Rao, T. Sasikala, L. Rama Moorthy, Visible luminescence characteristics of Sm^{3+} doped zinc alumino bismuth borate glasses, J. Lumin. 146 (2014) 288-294. https://doi.org/10.1016/j.jlumin.2013.09.035

[154] A. Kurita, T. Kushida, T. Izumitani, M. Matsukawa, Room-temperature persistent spectral hole burning in Sm^{2+}-doped fluoride glasses, Opt. Lett. 19 (1994) 314-316. https://doi.org/10.1364/OL.19.000314

[155] T. Suhasini, J.S. Kumar, T. Sasikala, K. Jang, H. Sueb, M. Jayasimhadri, J.H. Jeong, S.S. Yi, L.R. Moorthy, Absorption and fluorescence properties of Sm^{3+} ions in fluoride containing phosphate glasses, Opt. Mater. 31 (2009) 1167-1172. https://doi.org/10.1016/j.optmat.2008.12.008

[156] N. Deopa, A.S. Rao, A. Choudhary, S. Saini A. Navhal, M. Jayasimhadri, D. Haranath, G. V. Prakash, Photoluminescence investigations on Sm^{3+} ions doped borate glasses for tricolor w-LEDs and lasers, Mater. Res. Bullitin. 100 (2018) 206-212. https://doi.org/10.1016/j.materresbull.2017.12.019

[157] S. Kaur, A.K. Vishwakarma, N. Deopa, A. Prasad, M. Jayasimhadri, A.S. Rao, Spectroscopic studies of Dy^{3+} doped borate glasses for cool white light generation, Mater. Res. Bull. 104 (2018) 77–82. https://doi.org/10.1016/ j.materresbull.2018.04.002

[158] G. Moulika, S. Sailaja, B.N.K. Reddy, V.S. Reddy, S.J. Dhoble, B.S. Reddy, Optical properties of Eu^{3+} & Tb^{3+} ions doped alkali oxide (Li_2O/ Na_2O/ K_2O) modified boro phosphate glasses for red, green lasers and display device applications, Physica B Condens. Matter 535 (2018) 2–7. https://doi.org/10.1016/j.physb.2017.05.042

[159] J. Juárez-Batalla, A.N. Meza-Rocha, G.H. Muñoz, I. Camarillo, U. Caldiño, Luminescence properties of Tb^{3+}-doped zinc phosphate glasses for green laser application, Opt. Mater. 58 (2016) 406–411. https://doi.org/10.1016 /j.optmat.2016.06.022

[160] F.W. Billmeyer, M. Saltzman Jr., Principles of Colour Technology, Wiley New York, (1981) 240. https://doi.org/10.1002/col.5080070314

[161] A. Bergh, G. Duggal, R. Haitz, Promise and challenge of solid state lighting. Phys. Today 54, 42 (2001). https://doi.org/10.1063/1.1445547

[162] N. Deopa, A.S. Rao, Photoluminescence and energy transfer studies of Dy^{3+} ions doped lithium lead alumino borate glasses for w-LED and laser applications. J. Lumin. 192, 832-841 (2017). https://doi.org/10.1016 /j.jlumin.2017.07.052

[163] K. Jha, A.K. Vishwakarma, M. Jayasimhadri, D. Haranath, Multicolor and white light emitting Tb^{3+}/Sm^{3+} co-doped zinc phosphate barium titanate glasses via energy transfer for optoelectronic device applications. J. Alloy. Compd. 719, 116-124 (2017). https://doi.org/10.1016/j.jallcom.2017.05.076

[164] Z. Ci, Q. Sun, S. Qin, M. Sun, X. Jiang, X. Zhang, Y. Wang, Warm white light generation from a single phase Dy^{3+} doped $Mg_2Al_4Si_5O_{18}$ phosphor for white UV-LEDs. Phys. Chem. Chem. Phys. 16, 11597-11602 (2014). https://doi.org/10.1039/C4CP00357H

[165] C. Zhu, X. Liang, Y. Yang and G. Chen, Luminescence properties of Tb doped and Tm/Tb/Sm co-doped glasses for LED applications. J. Lumin. 130, 74-77 (2010). https://doi.org/10.1016/j.jlumin.2009.07.023

[166] K. Swapna, Sk. Mahamuda, A.S. Rao, M. Jayasimhadri, L.R. Moorthy, Visible fluorescence characteristics of Dy^{3+} doped zinc alumino bismuth borate glasses for optoelectronic devices. Ceram. Int. 39, 8459-8465 (2013). https://doi.org/10.1016/j.ceramint.2013.04.028

[167] S.A. Saleem, B.C. Jamalaiah, M. Jayasimhadri, A.S. Rao, K. Jang, L.R. Moorthy, Luminescent studies of Dy^{3+} ion in alkali lead tellurofluoroborate glasses. J. Quant. Spectrosc. Radiat. Transf. 112, 78-84 (2011). https://doi.org/10.1016/j.jqsrt.2010.08.017

[168] L. Shamshad, G. Rooh, K. Kirdsiri, N. Srisittipokakun, B. Damdee, H.J. Kim, J. Kaewkhao, Photoluminescence and white light generation behavior of lithium gadolinium Silicoborate glasses, J. Alloy Compd, 695 (2017) 2347-2355. https://doi.org/10.1016/j.jallcom.2016.11.105

[169] A.M. Babu, B.C. Jamalaiah, J.S. Kumar, T. Sasikala, L.R. Moorthy, Spectroscopic and photoluminescence properties of Dy^{3+}-doped lead tungsten tellurite glasses for laser materials, J. Alloy Compd. 509 (2011) 457-462. https://doi.org/10.1016/j.jallcom.2010.09.058

[170] C.R. Kesavulu, H.J. Kim, S.W. Lee, J. Kaewkhao, N. Chanthima, Y. Tariwong, Physical, vibrational, optical and luminescence investigations of Dy^{3+} -doped yttrium calcium Silicoborate glasses for cool white LED applications, J. Alloy Compd, 726 (2017) 1062-1071. https://doi.org/10.1016/j.jallcom.2017.08.091

[171] T. Srihari, C.K. Jayasankar, Fluorescence properties and white light generation from Dy^{3+}-doped niobium phosphate glasses, Opt. Mater. 69 (2017) 87-95. https://doi.org/10.1016/j.optmat.2017.04.001

[172] K. Linganna, C.S. Rao, C.K. Jayasankar, Optical properties and generation of white light in Dy^{3+}-doped lead phosphate glasses, J. Quant. Spectrosc. Radiat. Transf. 118 (2013) 40-48. https://doi.org/10.1016/j.jqsrt.2012.12.002

[173] K. Jha, M. Jayasimhadri, Spectroscopic investigation on thermally stable Dy^{3+} doped zinc phosphate glasses for white light emitting diodes. J. Alloys Compds.688, 833-840 (2016). https://doi.org/10.1016/j.jallcom.2016.07.024

[174] W.T. Carnall, P.R. Fields, K. Rajnak, Electronic energy levels in the trivalent lanthanide aquo ions. I. Pr^{3+}, Nd^{3+}, Pm^{3+}, Sm^{3+}, Dy^{3+}, Ho^{3+}, Er^{3+}, and Tm^{3+}. J. Chem. Phys. 49, 4424-4442 (1968). https://doi.org/10.1063/1.1669893

[175] C. Manjunatha, D.V. Sunitha, H. Nagabhushana, B.M. Nagabhushana, S.C. Sharma, R.P.S. Chakradhar, Combustion synthesis, structural characterization, thermo and photoluminescence studies of $CdSiO_3$: Dy^{3+} nanophosphor, Spectrochim. Acta Part A 93 (2012) 140-148. https://doi.org/10.1016/j.saa.2012.02.094

[176] P. Chimalawong, K. Kirdsiri, J. Kaewkhao, P. Limsuwan, Investigation on the Physical and Optical Properties of Dy^{3+} doped Soda-Lime-Silicate Glasses, Procedia Engineering 32 (2012) 690-698. https://doi.org/10.1016/j.proeng.2012.01.1328

[177] K.V. Rao, S. Babu, G. Venkataiah, Y.C. Ratnakaram, Optical spectroscopy of Dy^{3+} doped borate glasses for luminescence Applications, J. Mol. Struct. 1094 (2015) 274-280. https://doi.org/10.1016/j.molstruc.2015.04.015

[178] E.A. Davis, N.F. Mott, Conduction in non-crystalline systems V. Conductivity, optical absorption and photoconductivity in amorphous semiconductors, Philos. Mag. 22 (1970) 903-922. https://doi.org/10.1080/14786 437008221061

[179] Y. Ananta Lakshmi, K. Swapna, K.S.R.K. Reddy, Sk. Mahamuda, M. Venkateswarlu, A.S. Rao, Concentration dependent photoluminescence studies of Dy^{3+} doped Bismuth Boro-tellurite glasses for lasers and w-LEDs, Opt. Mater. 109 (2020) 110328. https://doi.org/10.1016/j.optmat.2020.110328

[180] A.K. Vishwakarma, K. Jha, M. Jayasimhadri, B. Sivaiah, B. Gahtori, D. Haranath, Emerging cool white light emission from Dy^{3+} doped single phase alkaline earth niobate phosphors for indoor lighting applications, Dalton Trans. 44 (2015) 17166-17174. https://doi.org/10.1039/C5DT02436F

[181] A.A. Reddy, M.C. Sekhar, K. Pradeesh, S.S. Babu, G.V. Prakash, Optical properties of Dy^{3+}-doped sodium–aluminum–phosphate glasses, J. Mater. Sci. 46 (2011) 2018-2023. https://doi.org/10.1007/s10853-010-4851-3

[182] P. Du, X. Huang, J.S. Yu, Facile synthesis of bifunctional Eu^{3+}-activated $NaBiF_4$ red-emitting nanoparticles for simultaneous white light-emitting diodes and field emission displays, Chem. Eng. J. 337 (2018) 91-100. https://doi.org/10.1016/j.cej.2017.12.063

[183] B.H. Babu, V.V.R.K. Kumar, White light generation in Ce^{3+} - Tb^{3+} - Sm^{3+} codoped oxyfluoroborate glasses, J. Lumin 154 (2014) 334-338. https://doi.org/10.1016/j.jlumin.2014.05.010

[184] M. Kumar, H. Nagabhushana, Y.C. Ratnakaram, Influence of alkali and alkaline earths on structural and luminescence properties of Sm^{3+} doped lithium fluoro phosphate glasses and different (Na, Mg, K, Ca and Sr) glass ceramics, J. Non-Cryst, Solids 573 (2021) 121146. https://doi.org/10.1016/ j.jnoncrysol.2021.121146

[185] A.N. Meza-Rocha, A. Speghini, M. Bettinelli, U. Caldiño, Orange and reddish – orange light emitting phosphors: Sm^{3+} and Sm^{3+}/Eu^{3+} doped zinc phosphate glasses, J. Lumin. 167 (2015) 305–309. https://doi.org/10.1016/j.jlumin. 2015.06.050

[186] X. Min, Z. Huang, M. Fang, Y.-G. Liu, C. Tang, X. Wu, Energy transfer from Sm^{3+} to Eu^{3+} in red-emitting phosphor $LaMgAl_{11}O_{19}$: Sm^{3+}, Eu^{3+} for solar cells and near-ultraviolet white light-emitting diodes, Inorg. Chem. 53 (2014) 6060–6065. https://doi.org/10.1021/ic500412r

[187] M.A.K. Elfayoumi, M. Farouk, M.G. Brik, M.M. Elokr, Spectroscopic studies of Sm^{3+} and Eu^{3+} co-doped lithium borate glass, J. Alloy. Comp. 492 (2010) 712–716, https://doi.org/10.1016/j.jallcom.2009.12.024.

[188] Y. Dwivedi, S.N. Thakur, S.B. Rai, Study of frequency upconversion in Yb^{3+}/Eu^{3+} by cooperative energy transfer in oxyfluoraborate glass matrix, Appl. Phys. B Laser Opt. 89 (2007) 45–51, https://doi.org/10.1007/s00340-007-2747-y.

[189] H. Lin, D. Yang, G. Liu, T. Ma, B. Zhai, Q. An, J. Yu, X. Wang, X. Liu, E. Yue-Bun Pun, Optical absorption and photoluminescence in Sm^{3+} - and Eu^{3+} - doped rare-earth borate glasses, J. Lumin. 113 (2005) 121–128, https://doi.org/10.1016/j. jlumin.2004.09.115.

[190] A. Langar, C. Bouzidi, H. Elhouichet, B. Gelloz, M. Ferid, Investigation of spectroscopic properties of Sm-Eu codoped phosphate glasses, Displays 48 (2017) 61-67. https://doi.org/10.1016/j.displa.2017.03.004

[191] K. Jha, M. Jayasimhadri, Effective sensitization of Eu^{3+} and energy transfer in Sm^{3+}/Eu^{3+} co-doped ZPBT glasses for CuPc based solar cell and w-LED applicatiobs, J. Lumin. 194 (2018) 102-107. http://dx.doi.org/10.1016 /j.jlumin.2017.09.049

[192] G. Lakshminarayana, S. Buddhudu, Physica B 373 (2006) 100-106. https://doi.org/10.1016/j.physb.2005.11.143

[193] M.Y. Hassaan, H.M. Osman, H.H. Hassaan, A.S. El-Deeb, M.A. Helal, Optical and electrical studies of borosilicate glass containing vanadium and cobalt ions for smart windows applications, Ceram. Int. 43, (2017) 1795-1801. https://doi.org/10.1016/j.ceramint.2016.10.137

[194] Ravita, A.S. Rao, Effective energy transfer from Dy^{3+} to Tb^{3+} ions in thermally stable KZABS glasses for intense green emitting device applications, J. Lumin. 239 (2021) 118325. https://doi.org/10.1016/j.jlumin.2021.118325

[195] A. Thulasiramudu, S. Buddhudu, Optical characterization of Sm^{3+} and Dy^{3+}:ZnO-PbO-B_2O_3 glasses, Spectrochim. Acta - Part A Mol. Biomol. Spectrosc. 67 (2007) 802–807. https://doi.org/10.1016/j.saa.2006.08.036

[196] S.N. Rasool, L.R. Moorthy, C.K. Jayasankar, Spectroscopic Investigation of Sm^{3+} doped phosphate based glasses for reddish-orange emission, Opt. Commun. 311 (2013) 156–162. https://doi.org/10.1016/j.optcom.2013.08.035

[197] E. Kaewnuam, H.J. Kim, C.K. Jayasankar, N. Chanthima, J. Kaewkhao, The photoluminescence, optical and physical properties of Sm^{3+}-doped lithium yttrium borate glasses, Phys. Chem. Glas. Eur. J. Glas. Sci. Technol. Part B 57 (2016) 85–89. https://doi.org/10.13036/17533562.57.2.036

[198] P. Meejitpaisan, S. Insiripong, C. Kedkaew, H.J. Kim, J. Kaewkhao Radiat. Radioluminescence and optical studies of gadolinium calcium phosphate oxyfluoride glasses doped with Sm^{3+}, Phys. Chem. 137 (2017) 62–67. https://doi.org/10.1016/j.radphyschem.2016.01.043

[199] F. Zaman, J. Kaewkhao, G. Rooh, N. Srisittipokakun, H.J. Kim, Optical and luminescence properties of Li_2O-Gd_2O_3-MO-B_2O_3-Sm_2O_3 (MO = Bi_2O_3, BaO) glasses, J. Alloy. Compd. 676 (2016) 275–285. https://doi.org/10.1016/j.jallcom.2016.03.176

[200] N. Wantana, S. Kaewjaeng, S. Kothan, H.J. Kim, J. Kaewkhao, Energy transfer from Gd3+ to Sm3+ and luminescence characteristics of CaO–Gd_2O_3–SiO_2–B_2O_3 scintilating glasses, J. Lumin. 181 (2017) 382–386. https://doi.org/10.1016/j.jlumin.2016.09.050

[201] Y. Wang, W. Zheng, Y. Lu, P. Li, S. Xu, J. Zhang, Effect of alkaline earth metals on luminescence characteristic in Eu-doped oxynitride phosphate glasses, J. of Lumin. 237 (2021) 118152. https://doi.org/10.1016/j.jlumin.2021.118152

[202] W. Zhang, S. Ouyang, Z. Zhang, Y. Zhang, H. Xia, Luminescent properties of Eu^{3+}- doped glass ceramics containing $BaGdF_5$ nanocrystals under NUV-excitation for W-LEDS, Ceram. Int. 41 (2015) 14035–14040. https://doi.org/10.1016/j.ceramint.2015.07.017

[203] V.R.L. Constantino, M.A. Bizeto, H.F. Brito, Photoluminescence study of layered niobates intercalated with Eu^{3+} ions, J. Alloy Compd. 278 (1998) 142-148. https://doi.org/10.1016/S0925-8388(98)00588-X

[204] I.I. Kindrat, B.V. Padlyak, Luminescence properties and quantum efficiency of the Eu-doped borate glasses, Opt. Mater. 77 (2018) 93-103. https://doi.org/10.1016/j.optmat.2018.01.019

[205] J. Rajagukguk, J. Kaewkhao, M. Djamal, R. Hidayat, Suprijadi, Y. Ruangtaweep Structural and optical characteristics of Eu^{3+} ions in sodium-lead-zinc-lithium borate glass system, J. Mol. Struct. 1121 (2016) 180–187. https://doi.org/10.1016/j.molstruc.2016.05.048

[206] J. Kaewkhao, K. Boonin, P. Yasaka, H.J. Kim, Optical and luminescence characteristics of Eu^{3+} doped zinc bismuth borate (ZBB) glasses for red emitting device, Mater. Res. Bull. 71 (2015) 37–41. https://doi.org/10.1016/j.materresbull.2015.07.002

[207] Y. Jin, Z. Hao, X. Zhang, Y. Luo, X. Wang, J. Zhang, Dynamical processes of energy transfer in red emitting phosphor $CaMoO_4:Sm^{3+}$, Eu^{3+}, Opt. Mater. 33 (2011) 1591–1594. https://doi.org/10.1016/j.optmat.2011.04.009

[208] Z. Wang, P. Li, Z. Yang, Q. Guo, Luminescence and energy transfer of Sm^{3+} and Eu^{3+} in Ca_2PO_4Cl, J. Lumin. 151 (2014) 170–175. https://doi.org/10.1016/j.jlumin.2014.02.030

[209] H.-Y. Lin, Y.-C. Fang, S.-Y. Chu, Energy transfer $Sm^{3+}\rightarrow Eu^{3+}$ in potential red phosphor $(Ca, Ba)_3(VO_4)_2:Sm^{3+}$, Eu^{3+} for use in organic solar cells and white light emitting diodes, J. Am. Ceram. Soc. 93 (2010) 3850–3856. https://doi.org/10.1111/j.1551-2916.2010.03957.x

[210] Suzanny Lima Brito, Thiago Augusto Lodi, Robson Ferrari Muniz, Alysson Steimacher, Franciana Pedrochi, Energy transfer investigation of Sm^{3+}/Eu^{3+} CaBAl glasses, J. Lumin. 219 (2020) 116947. https://doi.org/10.1016/j.jlumin. 2019.116947

[211] M.K. Sahu, M. Jayasimhadri, K. Jha, B. Sivaiah, A.S. Rao, D. Haranath, Synthesis and enhancement of photoluminescence properties in spherical shaped Sm^{3+}/Eu^{3+} co-doped $NaCaPO_4$ phosphor particles for w-LEDs, J. Lumin.202 (2018) 475-483. https://doi.org/10.1016/j.jlumin.2018.06.002

****

Optical Materials 107 (2020) 110070

Contents lists available at ScienceDirect

Optical Materials

journal homepage: http://www.elsevier.com/locate/optmat

Orange color emitting Sm^{3+} ions doped borosilicate glasses for optoelectronic device applications

Yasha Tayal, A.S. Rao *

Department of Applied Physics, Delhi Technological University, Bawana Road, New Delhi, 110042, India

ARTICLE INFO

Keywords:
Glasses
Photoluminescence
J-O parameters
CIE coordinates
Emission cross-sections
Quantum efficiency

ABSTRACT

An intense orange color emitting Sm^{3+} activated Li_2O–PbO–ZnO–Al_2O_3–B_2O_3–SiO_2 (LPZABS) glasses were propitiously fabricated by using sudden quenching method to study the luminescent potentiality using spectroscopic techniques such as XRD, FT-IR, optical absorption, photoluminescence (PL) and PL decay. XRD and FT-IR reveals the glassy nature and various functional groups present in LPZABS host glass respectively. Judd-Ofelt parameters derived from absorption spectra are used to estimate various radiative parameters for the excited states of Sm^{3+} ions in LPZABS glasses. Under 400 nm excitation, the luminescence spectra in the as prepared glasses exhibit three emission bands that corresponds to $^4G_{5/2} \rightarrow {}^6H_{5/2}$ (562 nm), $^4G_{5/2} \rightarrow {}^6H_{7/2}$ (598 nm) and $^4G_{5/2} \rightarrow {}^6H_{9/2}$ (645 nm) transitions of Sm^{3+} ions. Among these three, $^4G_{5/2} \rightarrow {}^6H_{9/2}$ transition observed in orange region (598 nm) is relatively more intense and prominent. The PL decay curves recorded for $^4G_{5/2}$ fluorescent level reveal exponential behavior and single exponential fitting is applied to evaluate the experimental lifetimes (τ_{exp}). The τ_{exp} values are found to be decreasing with Sm^{3+} ion content due to cross-relaxation energy transfer process. The results reveal that the as prepared glasses can be effectively used in fabricating intense visible orange color emitting optoelectronic devices.

1. Introduction

The attention for research related to rare earth (RE)/transition metal (Tm) ions doped materials has been increasing since few decades because of their applications in diversified fields such as up & down-conversion lasers, fiber amplifiers and solid state lighting (SSL) devices [1–4]. In order to get maximum output and optimized properties of RE based glasses, two methods are mostly used: (a) by altering the composition of the host material/concentration of active ions (RE ions) and, (b) by changing the geometrical structure around RE ion by applying external pressure [5]. In the present report, the first approach was used to study the photoluminescent (PL) properties of silicoborate glasses added with network modifiers & intermediates (Li_2O, PbO, ZnO and Al_2O_3) and doped with Sm^{3+} ions in varying concentrations. The increasing demand for optoelectronic devices capable of emitting light in visible regions made researches to investigate and develop variety of glass matrix doped with different RE ions i.e., Dy^{3+}, Sm^{3+}, Er^{3+}, Tb^{3+}, Ho^{3+}, Tm^{3+} etc. [2–4,6]. Apart from various RE ions, Sm^{3+} ions are very efficient in producing visible orange-red light emitters in various glass/crystal hosts giving strong fluorescence and radiative properties which makes them important for high power fiber lasers and optoelectronic devices [7–9].

Glasses are an eminent group of materials with important constituents as a former, modifier and intermediates which results in distinct attributes of a specific glass. Glass formers like silicates and borates have excellent thermal and chemical stability with high field strength that makes them pertinent material for the development of corrosion free laboratory equipment's, thermo resistant cooking equipment's, immobilization of radioactive waste, piping to fiber composites, LEDs and LCDs etc. [10–12]. Furthermore, B_2O_3 and SiO_2 merge to build an attractive silicoborate glass network having properties like lower melting temperatures, low thermal expansion coefficient ($\sim 3 \times 10^{-6}$ K^{-1} at 293.15 K), highly resistant to corrosion, high thermal stability and transition of ultraviolet radiation down to 180 nm [10–12]. Glasses containing B_2O_3 despite having so many excellent qualities, will encounter a major setback due to their high phonon energies. Such redundant phonon energies can reduce radiative emission capacity of a host glass. Normally such unwanted and redundant high phonon energies of B_2O_3 containing glasses can be drastically reduced by adding heavy metal oxides like lead oxide (PbO). On the other hand, PbO added

* Corresponding author.
E-mail address: drsrallam@gmail.com (A.S. Rao).

https://doi.org/10.1016/j.optmat.2020.110070
Received 30 March 2020; Received in revised form 17 May 2020; Accepted 25 May 2020
Available online 20 June 2020

Optical Materials 117 (2021) 111112

Contents lists available at ScienceDirect

Optical Materials

journal homepage: www.elsevier.com/locate/optmat

Spectroscopic analysis of Dy^{3+} ions activated borosilicate glasses for photonic device applications

Yasha Tayal [a,b], A.S. Rao [a,*]

[a] Department of Applied Physics, Delhi Technological University, Bawana Road, New Delhi, 110042, India
[b] ABES Engineering College, Ghaziabad, Uttar Pradesh, 201009, India

ARTICLE INFO

Keywords:
Glasses
Photoluminescence
J-O parameters
CIE coordinates
Emission cross-sections

ABSTRACT

A new series of optically translucent borosilicate glasses activated with varying concentrations of Dy^{3+} ions were fabricated by employing melt quenching method. Spectral investigations were conducted by recording the absorption, photoluminescent (PL) excitation and PL emission for Dy^{3+} activated borosilicate glasses. The absorption spectral information was exposed to Judd-Ofelt (J-O) analysis to calculate various radiative properties such as transition probability, total transition probability, branching ratios and radiative lifetimes of the as synthesized glasses. The excitation spectrum recorded under 483 nm emission wavelength possess a sharp peak at 348 nm in 0.1 mol% of Dy^{3+} ions doped borosilicate glass. Emission spectra recorded for all the Dy^{3+} ions activated borosilicate glasses under 348 nm intense excitation wavelength exhibit two potential peaks in visible region at 483 nm ($^4F_{9/2} \rightarrow {}^6H_{15/2}$) and 575 nm ($^4F_{9/2} \rightarrow {}^6H_{13/2}$). The emission centered at 483 nm is most prominent. Radiative properties measured from the absorption spectral feature were correlated with emission spectral information to estimate emission cross-section, gain bandwidth and optical gain parameters to understand the utility of the as synthesized glasses as photonic devices. The CIE coordinates measured for all the titled glasses are in good proximity with the white light coordinates of CIE 1931 diagram.

1. Introduction

From the history of various lighting tools, solid state lighting (SSL) devices are most notable. SSL devices are not only known for environmentally friendly by producing lesser carbon emissions, but also save electrical energy by taking relatively very less amount of power for their operation. There are number of SSL devices used nowadays like white light emitting diodes (w-LEDs), cellular phone illumination, automotive displays, traffic signals, full color displays, etc. Usage of SSL devices for all the aforementioned applications show cost effectiveness, durability and performance over previously used conventional lighting devices. Apart from being more durable, the SSL devices are compact in size, better transparencies, longer lifespan, more reliable, shock resistance and can be designed to greater extent [1–3]. The w-LEDs are prepared by two techniques commercially; first one phosphor based white light emitting diodes (pc w-LEDs) consists of a consolidation of blue LED (InGaN) and a yellow phosphor (YAG: Ce^{3+}). Next method consists of phosphors comprising of three prominent colors red, green and blue, excited with ultraviolet (UV) chip. First method shows high brightness with less production cost. However, it suffers from mediocre color rendering index (CRI) equal to 70–80 and larger color corelated temperature (CCT) equal to 7750K in addition to halo effect. Second method has better CRI but still it bears low luminescent efficiency as blue light gets absorbed in the process. In addition to the above-mentioned individual draw backs, both the methods are suffering with a common problem of using epoxy resin to encapsulate the phosphors. The epoxy resin has some serious draw backs like cracking and delamination. In addition to this, with time, its surface turns into pale yellow color and starts hampering the quality of the output LEDs [4–7]. Rare earth (RE) doped glasses can be thought of a best alternative for the preparation of LEDs in place of phosphor-based LEDs for the prime reason of not using any epoxy resin in their fabrication. Nevertheless, RE doped glasses are superior than phosphors for the fabrication of LEDs from many perspectives such as intense emission in visible & infrared regions, simple to manufacture, low production cost and more durable [8–11].

The usage of borosilicate glasses for general as well as scientific purposes has been existing dates back for various scientific patronages offered by the combination of borates and silicates. The combination of borates with silicates results in reducing melting point, enhances chemical & thermal stability, reduces phonon energies and improves

* Corresponding author.
E-mail address: drsrallam@dce.ac.in (A.S. Rao).

https://doi.org/10.1016/j.optmat.2021.111112
Received 13 March 2021; Received in revised form 5 April 2021; Accepted 19 April 2021
Available online 3 May 2021

Solid State Sciences 125 (2022) 106834

Contents lists available at ScienceDirect

Solid State Sciences

journal homepage: www.elsevier.com/locate/ssscie

Photoluminescence characteristics of Sm^{3+}/Eu^{3+} co-doped LPZABS glasses for solar cell applications

Yasha Tayal [a,b], A.S. Rao [a,*], Sumandeep Kaur [a]

[a] Department of Applied Physics, Delhi Technological University, Bawana Road, New Delhi, 110042, India
[b] ABES Engineering College, Ghaziabad, Uttar Pradesh, 201009, India

ARTICLE INFO

Keywords:
Glasses
Photoluminescence
CIE chromaticity coordinates
Energy transfer
Decay curves

ABSTRACT

A series of Sm^{3+}/Eu^{3+} co-doped LPZABS (lithium lead zinc alumino borosilicate) transparent glasses were synthesized by the melt quench method. Fluorescent characteristics and energy transfer mechanisms were analyzed thoroughly. The amorphous nature of the glasses was confirmed from the observed X-ray diffraction patterns. An expansion in photoluminescence (PL) excitation of Eu^{3+} ions was observed on sensitizing it with Sm^{3+} ions in the title compounds. The PL emission spectra obtained for different excitations show bands due to Sm^{3+} and Eu^{3+} ions with increment in intensity on increasing Eu^{3+} ion concentration. On implementing the Dexter energy transfer formula & Reisfeld's approximation to PL emission spectra and the Inokuti-Hirayama (I–H) model to PL decay profiles, the dipole-dipole interaction among activator and sensitizer is revealed. Chromaticity coordinates (CIE) gradually relocate from the orange to the red region on increasing Eu^{3+} ion concentration in Sm^{3+}/Eu^{3+} co-doped LPZABS glasses. The Sm^{3+}/Eu^{3+} co-doped LPZABS glasses have the potential for downshifting of *n*-UV & blue exciting photons into visible red color photons which make it useful for copper phthalocyanine (CuPc) solar cell applications.

1. Introduction

In neoteric years, a substantial number of investigations have been done on rare earth (RE) doped glasses, owing to their incredible optical and spectroscopic properties and applications. They act as excellent luminescent centers on account of their electronic configuration of 4f and 5d-4f shells which are further concealed by $5s^25p^6$ electrons, enabling them for light-emitting diodes (LEDs), sensors, solar control devices, lasers, and many more applications [1,2]. It is well known that, Y_2O_2S: Eu^{3+} and CaS: Eu^{2+} phosphors are widely used red light-emitting devices. However, these two sulfide-based phosphors suffer from some drawbacks like generation of poisonous gas, poor chemical and thermal stability, scanty lifetime under ultraviolet (UV) light excitation, etc. These setbacks have prompted a number of researchers in search of alternatives leading to exploration of different luminescent materials doped with RE ions, like Sm^{3+} and Eu^{3+} on account of their application in white LEDs and CuPc based solar cells [3,4]. Moreover, there is a need for encapsulating phosphor materials with an organic material that deteriorates with temperature. To avoid coating with organic material, one can make use of RE doped glasses as visible emitters in display and lighting devices. Both Sm^{3+} and Eu^{3+} ions are having certain similarities like having ionic radii in proximity and being capable of showing visible luminescence in orange & red regions. This has prompted the use of Sm^{3+} (sensitizer) and Eu^{3+} (activator) in glass matrices for enhancing the excitation wavelength range and enhancing visible red emission. The $^5D_0 \rightarrow {}^7F_2$ transition from the Eu^{3+} ion (activator) is highly sensitive to the crystal field environment which leads to high efficiencies when co-doped with Sm^{3+} ions (sensitizer) by increasing absorption around 400 nm [5,6]. These two RE ions have energy levels in proximity, which adds to energy transfer activity among Sm^{3+} to Eu^{3+} ions by enhancing emission for Eu^{3+} ions. A strategic energy transfer from electromagnetic radiation to red photons using non-utilized photons is found in the absorption range of the natural absorber substance CuPc. Hence, Sm^{3+}/Eu^{3+} co-doped glasses find a key role in the development of display devices, UV-sensors, optoelectronic devices, lighting devices, and solar cells [5,7–9].

From the various glass systems produced, alumino borosilicate glasses emerge as an excellent choice owing to their excellent transparency from visible to near infra-red (NIR), good chemical and thermal stability [10,11]. The addition of lithium oxide (Li_2O) further enhances the chemical stability modifying the structure of the borate glass matrix into tetrahedral BO_4 entities from three coordinated boron atoms. The

* Corresponding author.
E-mail address: drsrallam@gmail.com (A.S. Rao).

https://doi.org/10.1016/j.solidstatesciences.2022.106834
Received 24 April 2021; Received in revised form 12 January 2022; Accepted 24 January 2022
Available online 26 January 2022